

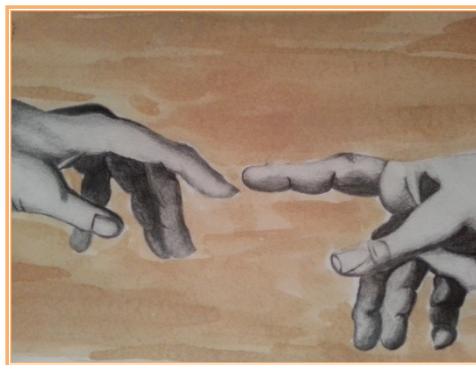


UNIVERSITA' DEGLI STUDI DI CATANIA

DIPARTIMENTO DI SCIENZE CHIMICHE
DOTTORATO DI RICERCA IN SCIENZA E TECNOLOGIA DEI MATERIALI
XXVII CICLO

Fabiola Spitaleri

*Synthesis, characterization and thermal properties of polymers based
composites materials for High Power Electronic Packaging Applications*



TESI DI DOTTORATO DI RICERCA

Tutor: Chiar.mo Prof. Placido G. Mineo

Coordinatore: Chiar.ma Prof.ssa Maria G. Grimaldi

DICEMBRE 2014

Ad Amata.

“... il mondo, la vita, la morte, il presente, il futuro:
tutto è vostro!
Ma voi siete di Dio”

- 1 Cor 3, 22-23 -

In copertina:
Stefania Spitaleri,
“Particolare della Creazione”, Michelangelo.
Collezione privata, 2012.

1. A look on power	7
1.1 High Power Electronic Packaging	7
1.1.1 Packaging Technology	8
1.1.2 Integrated Circuit Packaging	13
1.2 Semiconductor Power Devices	16
2. Aim of research	22
2.1 State of the art	25
2.2 Know how	27
3. Polymeric Matrix	33
3.1 Epoxy resins synthesis	40
3.2 Epoxy resins characterizations	46
4. Fillers	53
4.1 Polyamidic fillers	54
4.1.1 Synthesis and characterization of Poly(meta-phenylene isophthalamide)	55
4.1.2 Synthesis and characterization of Poly(p-phenylene terephthalamide)	64
4.1.3 Characterization of Kelin 130	73
4.2 Polyimidic filler	77
4.2.1 Synthesis and characterization of Poly(para-phenylen pyromellitimide)	79
4.3 Graphenoxidic filler	87

5. Composites	90
5.1 Synthesis of composites	90
5.2 Composites Characterization	92
5.2.1 TGA and DTA analysis of "NOM.10" type composites	92
5.2.2 FT-IR analysis of NOM.10 composites	96
5.2.3 TGA and DTA analysis of NOM.33 and KEV.33 composites	98
5.2.4 FT-IR analysis of NOM.33 and KEV.33 composites	101
5.2.5 TGA and DTA analysis of SIL.33 composite	102
5.2.6 FT-IR analysis of SIL.33 composite	104
5.2.7 TGA analysis of "KAP.33" composite	105
5.2.8 FT-IR analysis of KAP.33	109
5.2.9 Thermal Characterization of GO.33 composite	111
5.2.10 Thermal Characterization of KEL.33 composite	113
5.3 Indirect Thermal Conductivity determination	115
5.4 Finite Element Method	120
5.4.1 Virtual Prototyping	121
5.5 Direct Thermal Conductivity measurements	125
5.6 Prototypes	131
6. Conclusions and future perspectives	134
<i>Appendix</i>	140
<i>Research products</i>	161
<i>Acknowledgments</i>	164

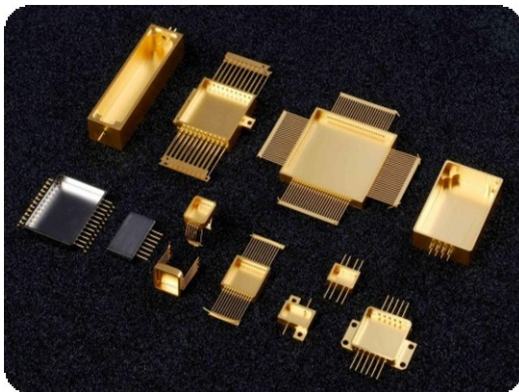


1. A look on power

Power electronics deals with electric energy conversion trying to perform this transformation by minimizing the power dissipated. Electronic devices and power modules are key components of several power systems for the storage, conversion and conditioning of electromagnetic energy.

The package provides mechanical, chemical and electromagnetic protection to electronic devices; it also dissipates heat and allows the interconnection with other component.

1.1 High Power Electronic Packaging



Package starts at the interface with chip and includes the interconnection of chip itself to the substrate and its encapsulation.

First, the power package must be able to manage increases of power and current by several orders of magnitude (this requires a wide area for interconnections). Secondly the voltage, according to several applications, can reach several kilovolts (it requires high voltages breakdown). Finally, because these devices operate at high frequencies and density power, electrical conduction must be reduced to minimized parasitic noise and dissipation heat must be optimized¹.

¹ S. Wen and G. Q. Lu, “Finite-element modeling of thermal and thermomechanical behavior for three-dimensional packaging of power electronics modules” Proceeding of the 7th Intersociety Conference on Thermal and Thermomechanical Phenomena in Electronic Systems, Vol. II, Las Vegas, Nevada, May, 2000, pp. 303-309.



1. A look on power

1.1.1 Packaging Technology

Nowadays packaging of devices and semiconductor power modules can be built by following several technologies: flip-chip, wire-bonding, MIPPS, POL, DAI, EP, press pack.

Flip-chip technology

This package technology is also known as “C4” (Controlled Collapse Chip Connection) is a method for the interconnection of semiconductor devices, such as integrated circuits and Micro-Electro-Mechanical Systems (MEMS). Electrical connections between chip and substrate were provided by solder bumps: chips is upside down and mounted on a suitable substrate.²

Device assembled with flip chip technology is much smaller than a traditional system: the chip is allocated directly on the printed circuit, and it is much smaller both in surface that height. Short links reduce inductance, allowing the exchange of information faster and greater heat dissipation.³

Flip-chip flex is an extension of flip-chip technology on flex circuits.⁴

Solder bumps connects chip to a flexible substrate (figure 1) ; the module is then encapsulated by a polymeric material capable of reducing the thermo-mechanical stresses imposed on the solder joints.

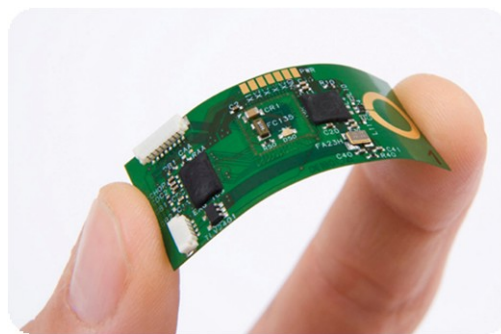


Figure 1: Flip-chip flex technology

² J. H. Hua, “*Flip Chip Technologies*”, New York: McGraw Hill, 1995

³ R. R. Tummala, E. J. Rymaszewski, and A. G. Klopfenstein, “*Microelectronics, Packaging Handbook*”, New York: Chapman & Hall, 1999.

⁴ J. Bai, G. Q. Lu, and X. Liu, “*Flip-chip on flex integrated power electronics modules for high-density power integration*” IEEE Transactions on Advanced Packaging, vol. 26, no. 1, pp. 54-59, Feb. 2003



1. A look on power

Wire Bonding

Wire bonding is the interconnection technology chip nowadays more common for the power electronics. Thin wires connects chip with the respective pins on the package. Chips are soldered to copper heat sink and the source and gate terminals are connected by metal wires to heat sink (Figure 2); generally these wires are made of gold, aluminum or copper.

Wires diameters can reach several hundred microns for high power applications.⁵

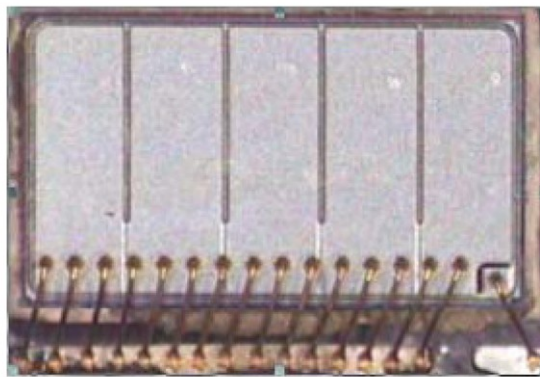


Figure 2: wire bonding packaging⁶

Top of chips and bonding wires are encapsulated with insulating material, typically epoxy resins or ceramic.

The connections can be realized in two ways: Ball bonding or Wedge bonding (figure 3).

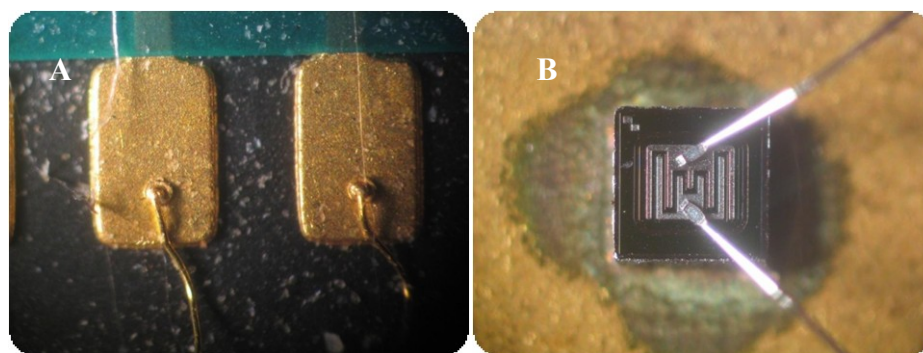


Figure 3: Ball bonding (A) e Wedge bonding (B).

⁵ R. R. Tummala, "Fundamentals of Microsystems Packaging", McGRAW Hill, 2001, pp.346-347

⁶ "New packaging concepts for low voltage power MOSFETs lead to performance improvemnet in advanced DC-DC converters", ST Microelectronics Application Note AN2066, Nov. 2004.



1. A look on power

Wire Bonding process have many advantages: it is highly flexible and performing, a lot of industries have infrastructure suited to this technology, there is a rapid advances in equipment, tools and materials for this package technology.

The disadvantages include slower speed interconnection due to presence of wire bonds, length of chip-to-package interconnection, and limited heat dissipation.

MPiPPs (Metal-Posts Interconnected Parallel Plates) Technology

This packaging technique uses metal pins bonded directly to the die⁷ (Figure 4).

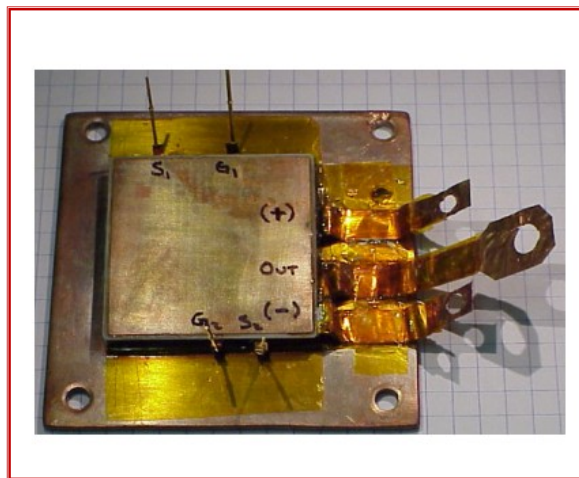


Figure 4: MPiPPs Technology

At the top of DBC there is an aluminum nitride substrate (AlN) and chips are directly connected by solder. The copper pins, having different sizes, are soldered on top of devices and connecting them to AlN substrate.

This technology has parasitic currents lower than the conventional wire bonding, but requires solderable devices.

POL (Power Overlay) Technology

POL technology eliminates wires bonding through the use of Cu/polyimide interconnections⁸, this reduce parasitic currents and improve thermal dissipation (due to

⁷ S. Haque, K. Xing, R. Lin, C. T. A Suchicital, G. Q. Lu, D. J. Nelson, D. Boroyevic, and F. C. Lee, “An innovative technique for packaging power electronics building blocks using metal posts interconnected parallel plates structure”, IEEE Transactions on Advanced Packaging, vol. 22, no. 2, pp. 136-144, May, 1999.



1. A look on power

reduced number of thermal interfaces). Semiconductor devices are upside down and soldered to heat sink DBC, a thin layer of polyimide is deposited over the die and the interconnections are obtained with laser or with mechanical perforation. All upper surface is copper plated.

DAI (Dimple Array Interconnect) Technology

Electrical interconnection is established by the formation of solder bumps between device electrode and matrix, consisting of a metal foil with dimples as shown in figure 5⁹. The result is a planar interconnection fits for the multi-layer integration with other components.

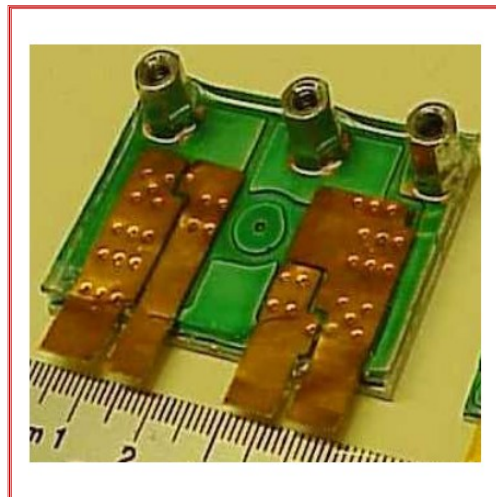


Figure 5: DAI technology

This technique reduces parasitic currents interconnection and increases thermal capacity of packaging; however, the mismatch in thermal expansion coefficients between copper foil and silicon dimples can cause thermo-mechanical problems.

⁸ R. Fisher, R. Filion, J. Burgess, and W. Hennessy, “High frequency, low cost, power packaging using thin film power overlay technology” Proc. of the 10th Applied Power Electronics Conference and Exposition (APEC), Dallas, TX, Mar. 1995, pp. 12-17

⁹ Wen, D. Huff, and G. Q. Lu, “Dimple-array interconnect technique for packaging power semiconductor devices and modules”, Proc. of the 13th International Symposium on Power Semiconductor Devices and ICs (ISPSD), Osaka, Japan, Jun. 2001, pp. 69-74



1. A look on power

EP (Embedded Power) technology

EP packaging technology concerns the construction of a planar power devices, embedded in a ceramic matrix; it presents a multi-layer structure: ceramic substrates, printable and sealing dielectric materials for encapsulating power device.

Power devices are mounted in special holes on ceramic substrate and surrounded by an adhesive polymer. Dielectric materials is printed with circuital pattern, copper layer is above deposited to give electrical connection. Copper layer can be thickened by an electro-deposition process.

Press Pack Technology

Press pack is a bonding wireless technology. The press pack structure has evolved to a sandwiched structure and involves Molybdenum strain buffers, gate connection and insulation, Copper (Cu) pole-piece and a ceramic ring.¹⁰

At the collector there is a cylindrical structure in copper and molybdenum in a wide disc connected to all of chips; at the emitter, instead, each die is in contact with a multi-column copper structure through a thin layer of molybdenum. The whole is enclosed by a ceramic ring, figure 6.

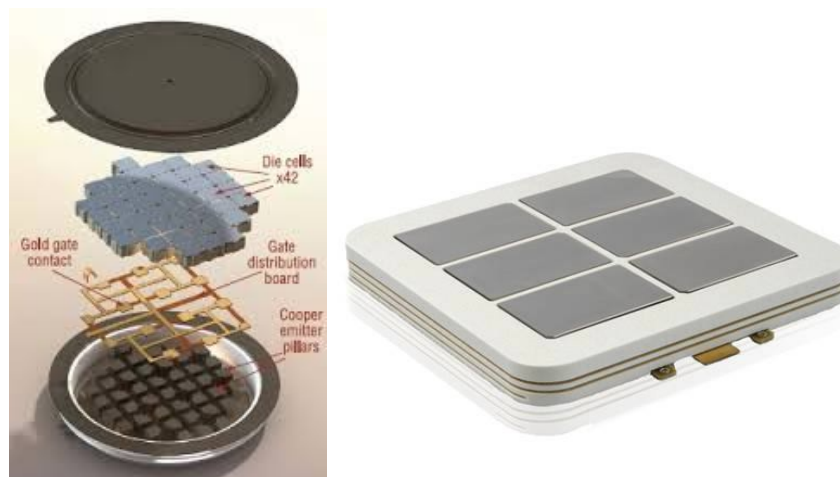


Figure 6: Press-Pack Technology

¹⁰ S. Eicher, M. Rahimo, E. Tsyplakov, D. Schneider, A. Kopta, U. Schlapbach, and E. Carroll, “4.5 kV press pack IGBT designed for ruggedness and reliability,” Proc. of the 39th Industry Applications Conference (IAS), Seattle, Washington, Oct. 2004, pp. 1534-1539



1. A look on power

Press-pack packages reaches high reliability for wide ranges of temperature and power applications. Disadvantages concern high costs of production and need to keep pressure in various parts of the package.

1.1.2 Integrated Circuit Packaging

The first integrated circuit appeared in 1958 and had only one transistor, today there are more than one million transistors on each one. As devices evolve, must do so also the hardware and interconnections of circuits. High power density devices, or with multiple dies, are calling for several new packaging technologies.

Packaging of Integrated Circuits can be divided into the following categories¹¹:

- ✚ Surface mount package (in plastic or ceramic materials);
- ✚ Chip-scale package;
- ✚ Bare die;
- ✚ Through-hole package.

Surface mount package

Package obtained with this technique allows to have a small, lightweight device and able to withstand shocks; it is also economical because the manufacturing process takes place in a single stage. The case, usually plastic, is molded around the main frame of device; they are still in study new materials for this purpose, such as polyimides that could solve problems related to hermeticity and mismatch of expansion coefficients between chip and package. Plastic packages are hygroscopic and absorb moisture depending on the environment that surrounds them. Moisture can be removed with a quick warm-up, with the risk of package cracking (known as “popcorn effect”), and subsequent entry of contaminants that can corrode circuit.¹²

For special applications (eg. aerospace and military) are used hermetic packages such as flat pack or CLCCs: Flat Pack (Figure 7a) is a square or rectangular package, it was born in 1962¹³ as an improvement of the existing package in heat dissipation and

¹¹ Meeldijk, V. “*Integrated Circuit Packages*” ,The Electronic Packaging Handbook, Ed. Blackwell, G.R. Boca Raton: CRC Press LLC, 2000

¹² DA Burkhart, MM Chau: “*Materials for semiconductor device assemblies*”, US Patent 5,855,821, 1999.

¹³ Dummer, G.W.A., “*Electronic Inventions and Discoveries*” 2nd ed. Pergamon Press



1. A look on power

number of chips inside circuits. Flat Packs can be made of glass, ceramic or metal and are hermetic.

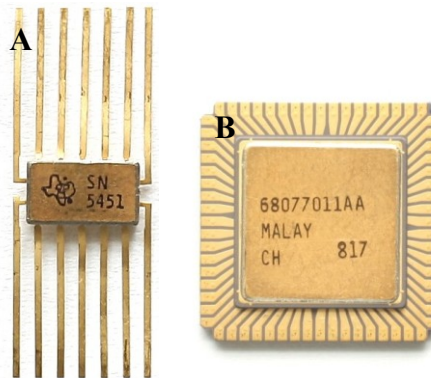


Figure 7: Package Flat Pack (A) e CLCCs (B)

CLCCs (ceramic leadless chip carrier) don't have wires, but are surrounded by pins along edges (Figure 7b). For simple applications can be realized in plastic.

Bare die

The use of bare die (figure 8) is increasing: the aim is to reduce both the size and the weight of the final product. The use of bare die eliminates delays (caused by inductance and parasitic capacitance): for static RAMs, there was a 20% improvement in access time¹⁴. The use of bare die has some problems: at this time, it is more costly for vendors to handle and ship bare die than packaged if compared to encapsulated devices and therefore this technology is still evolving.

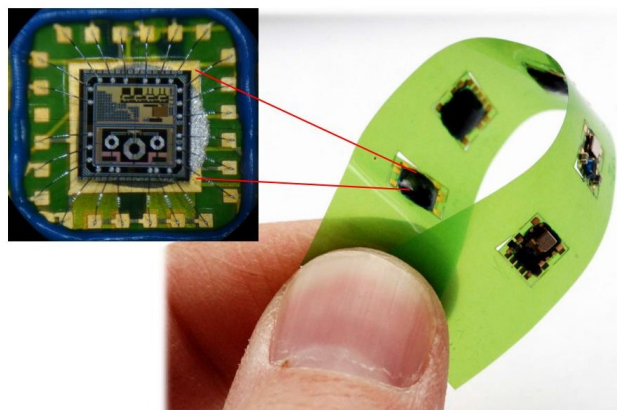


Figure 8: bare dies

¹⁴ Meeldijk, V. "Integrated Circuit Packages" ,The Electronic Packaging Handbook, Ed. Blackwell, G.R. Boca Raton: CRC Press LLC, 2000



Chip-Scale Packaging

This packaging technique is designed to obtain size and performance of bare die but with the handling and controllability of encapsulated devices: the size of the package does not exceed more than 1.2 times the bare die.

Through-hole package

This technique involves assembly of the package in holes, generally plated metal, on printed circuit board.

The choice of packaging technique to apply to a certain device or power module can already improve the properties for what concerns parasitic noise, hermeticity, heat dissipation, handling, cost of production, etc ...

Material component package may implement these properties even more: there are below a list of the main materials, depending on the type of microelectronic packaging¹⁵.

- ⇒ Plastic Packages: epoxy resins, silicone resins, polyurethanes;
- ⇒ Metallic Packages: Kovar¹⁶(that is a nickel–cobalt ferrous alloy with 25% Ni, 17% Co, 0.3% Mn, 0.2% Si and C<0.01%), aluminum, steel;
- ⇒ Ceramic Packages: (Al₂O₃, glass, SiO₂, ZrO₂);
- ⇒ Composite Packages: reinforced glass fiber, G200 (a high quality potassium/sodium/calcium aluminum silicate ground to 200 mesh¹⁷), FR4¹⁸ (woven of glass fibers in a epoxy resin matrix), Kapton¹⁹ (polyimide film), polyamides, Teflon.

¹⁵ <http://www.optoi.com/it/servizi/packaging>

¹⁶USPTO United States Patent and Trademark Office (1993). "Trademark Assignment Abstract": <http://assignments.uspto.gov/assignments/q?db=tm&sno=71367381>

¹⁷ <http://www.standardceramic.com/G200Changes.pdf>

¹⁸ <https://www.nema.org/Standards/ComplimentaryDocuments/LI1.pdf>

¹⁹<http://www.dupont.com/content/dam/assets/products-and-services/membranes-films/assets/DEC-Kapton-general-specs.pdf>

1.2 Semiconductor Power Devices

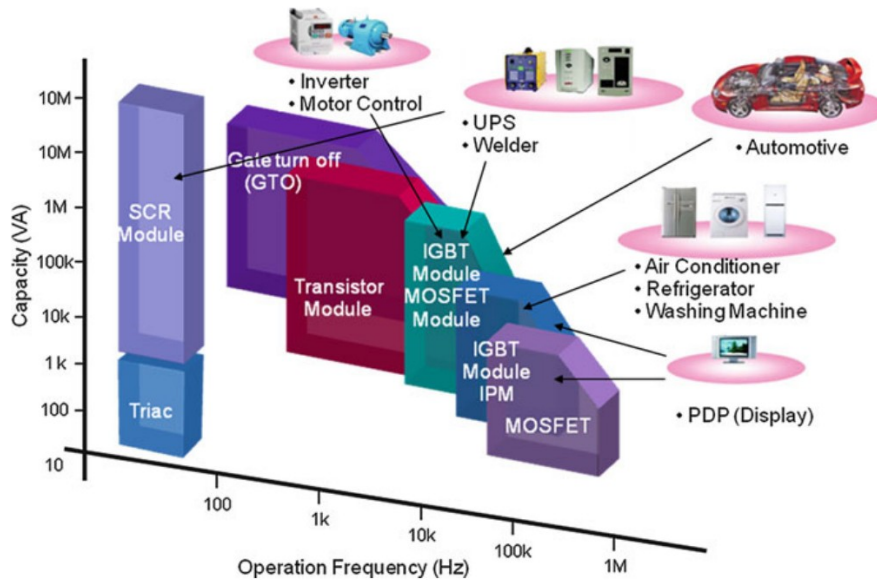
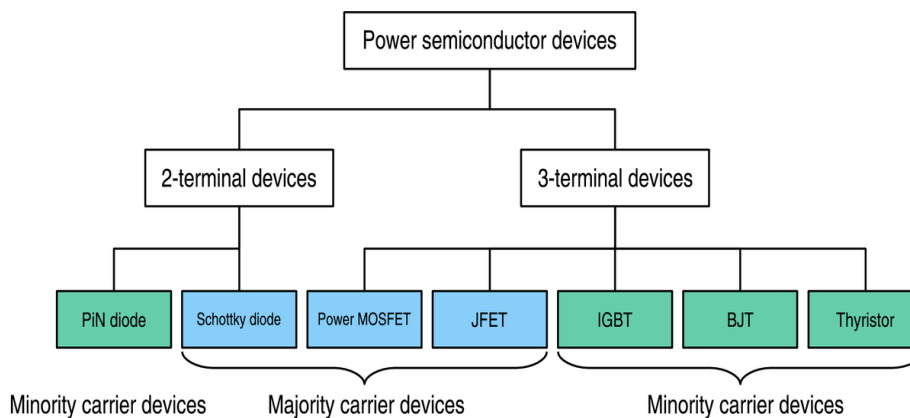


Figure 9: Power devices applications

A power semiconductor device, used as a switch or rectifier in the power electronics, is often called power device or, if used in an integrated circuit, IC power. The most common power devices are diode, SCR, MOSFET and IGBT.

The power devices can be classified as follows (Scheme 1):

- ✘ two-terminal devices (diode), dependent on the external power circuit to which it is connected;
- ✘ three terminal devices, whose state depends also by the signal on gate.



Scheme 1: power devices classification



1. A look on power

Another classification concerns the device performance:

- ✗ majority carrier devices (Schottky diode, MOSFET, etc.);
- ✗ minority carrier devices (SCR, bipolar transistor, IGBT, etc.), they use both majority and minority charge carriers (ie electrons and holes).

Diode

Diode is a non-linear bipole in which the terminals are anode and cathode. When diode is polarized with a negative voltage anode-cathode, it behaves like an open circuit and it is said polarized in reverse region. Instead, when the current flows from anode to cathode, the diode behaves as a short circuit: it is polarized in direct region.

A **semiconductor PN diode** (Figure 10) is based upon the p-n junction: it conducts current in only one direction, and it is made by joining a p-type semiconducting layer to an n-type semiconducting layer.²⁰ Semiconductor diodes have multiple uses including rectification of alternating current to direct current, detection of radio signals, emitting light and detecting light.

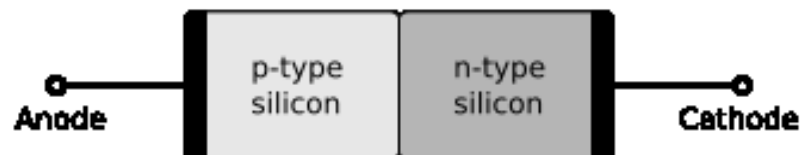


Figure 10: P-N diode structure

Schottky diode²¹ and PIN diode have also great application in electronics.

Particularly, Schottky diode have a low potential drop between terminals that allows to have high switching speed and a better efficiency. Instead of a pn junction, it's formed a Schottky barrier (Figure 11). Metal generally used are: Mo, Pt, W or Cr, and sometimes PtSi or PdSi and semiconductor is n-type silicon. The metal layer constitutes anode of diode, while the n-type semiconductor is cathode.

²⁰ John Sparkes (1994). Semiconductor Devices (2nd ed ed.). CRC Press.

²¹ <http://powerelectronics.com/SchottkyDiodes.pdf>



1. A look on power

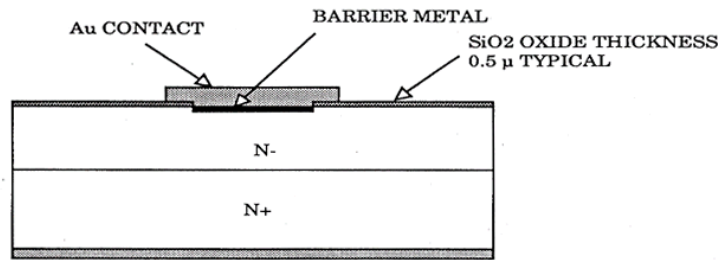


Figure 11: Schottky diode

A **PIN diode**²² (P-type, Intrinsic, N-type) is a diode with a large region of intrinsic semiconductor material contained between a p-type and a n-type semiconductors. A PIN diode shows an increase of electrical conductivity as a function of amplitude, wavelength and the rate of modulation of incident radiation; for this reason many photo-sensors include at least one PIN diode, such as PIN photodiodes or phototransistors.

JFET (Junction gate Field Effect Transistor)

The JFET transistors are unipolar : they only have n-type current or p-type current²³. JFETs can have an n-type or p-type channel. In the n-type, if the voltage applied to the gate is less than that applied to the source, the current will be reduced (similarly in the p-type, the voltage applied to the gate is greater than that applied to the source).

BJT (Bipolar Junction Transistor)

A bipolar junction transistor is based on contact of two types of semiconductors, generally based on silicon. The BJTs are generally used as switches or amplifiers, both as individual components as part of integrated circuits²⁴.

²² Doherty, Bill: "PIN Diode Fundamentals", Watertown, MA: Microsemi Corp., MicroNote Series 701.

²³D. Chattopadhyay: "Junction field-effect transistor (JFET)". Electronics (fundamentals and applications). New Age International, 2006. pp. 269 ff.

²⁴ Peter Ashburn: "SiGe Heterojunction Bipolar Transistors". New York: Wiley. 2003, Chapter 10.



1. A look on power

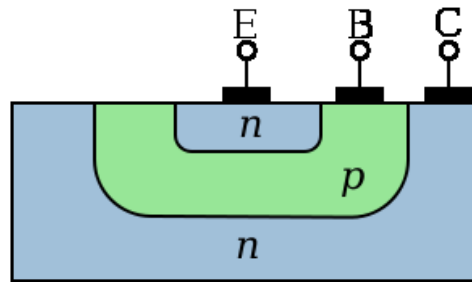


Figure 12: Cross-section of BJT n-p-n

They are composed of three layers of doped semiconductor material in which the central layer has doping opposite to the other two, so as to form a double pn junction (Figure 12).

MOSFET (Metal Oxide Semiconductor Field Effect Transistor)

The ideal physical structure of MOSFET is constitute of a monocrystalline substrate of p-type where are realized two junctions of n^{+25} type, with two terminals of drain and source composed of semiconductor, doped in opposite way: if the substrate has a p-type, two terminals have n-type doping, and vice versa. In the area between drain and source is grown a layer of silicon dioxide (thickness less than 0.01 mm), which is an excellent insulator. The gate electrode is made of polycrystalline silicon.

There is also a fourth terminal connected to the bulk. The area between the drain and source is said channel.

Depending on the voltage applied to the substrate under the gate (MOS capacitor) the channel can be full of gaps, empty, or electrons.

Thyristors

Thyristors are semiconductor devices with PNPN junctions: they are used for high currents and high voltages control. For example SCR is able to control thousands of amperes and kV.

SCR (Silicon Controlled Rectifier, figure 13) is a controlled rectifier in silicon so as to stop the normal flow current as long as a small signal applied to a third electrode (gate).

²⁵ Semiconductor doping concentration higher than that of a normal n-type.

The current flow can be interrupted only by applying a reverse voltage or opening anode circuit.



Figure 13: SCR device

The bulk of SCR is a weakly doped n-type Si with hundreds of μm thickness. On sides is carried out a diffusion of p-type Si, forming a wafer PNP. Subsequently, boron is diffused on both sides to obtain a thin p^{+26} layer.

SCRs are often employed in inverter and chopper.

TRIAC (Triod AC) can be considered as two antiparallel SCR: they can conduct or stop current flow in two directions. A lot of TRIAC applications concerns appliances.

GTO (Gate turn-off thyristor)

Thyristors are not completely controllable: they conduct (ON) by applying an appropriate voltage to gate electrode, but can not be stopped (OFF) using the same electrode. The thyristors remain in the ON state even the gate signal is removed. To return to the OFF state it requires that the current flowing below a certain limit value known as holding current. Unlike the SCR, the GTO can be turned on or off carrying respectively a positive or negative signal to the gate electrode. GTOs have long interval of time in which a residual current continues to flow until all the remaining charge is eliminated from the device. This limits the maximum operating frequency of about 1 kHz; however, if compared with SCR is ten times smaller²⁷.

²⁶ Semiconductor doping concentration higher than that of a normal p-type.

²⁷ <http://www.circuitstoday.com/gate-turn-off-switch>



1. A look on power

IGBT (Insulated Gate Bipolar Transistor)

IGBT is a semiconductor device used as electronic switch in high power applications. It can be shown schematically as the connection of a BJT and a MOSFET²⁸. The IGBT today have assumed great importance for all applications of high voltages and currents power such as industrial inverter or photovoltaic. They are key components in electric and hybrid cars, which are the only solution for small engine control unit, powerful and efficient: the Toyota Prius uses a 50KW inverter based on IGBT which controls two motors connected to the batteries²⁹.

An IGBT device is similar to a power MOSFET, with the difference that the drain n^+ is replaced with a layer p^+ (figure 14), thus forming a vertical PNP bipolar junction transistor.

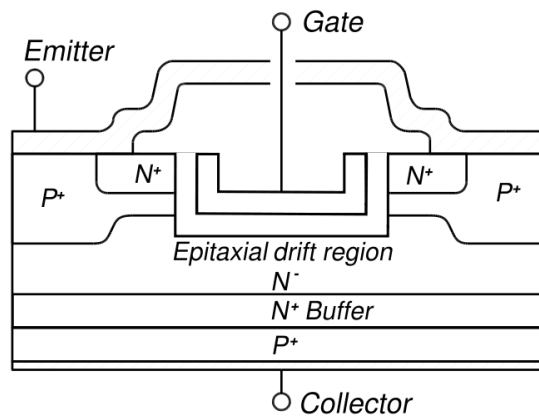


Figure 14: IGBT device

²⁸ B. J. Baliga, "Fast-switching insulated gate transistors", IEEE Electron Device Letters, Vol. EDL-4, pp. 452-454, 1983.

²⁹ <http://www.turbo-electric.com/PriusResearch.php>



2. Aim of research

Thermal dissipation plays an important role in integrated circuits: temperature is a critical parameter for the good performance of any electronic device. Temperature increases a series of device failure mechanisms, such as leakage current, electromigration, "hot electrons"³⁰, etc...

When electricity passes through a power module, generates a temperature increase due to Joule effect; this increase may damage device according to Dakin-Arrhenius equation³¹:

$$L = A(\epsilon^{bT} - 1) \quad \text{Equation 1}$$

with L length of device life, A and b are constants depending on material and stress, T is temperature and ϵ is emissivity.

The temperature of a device increases when it dissipates power according to:

$$\theta J_A \cdot P_d + T_A < T_{j-max} \quad \text{Equation 2}$$

With T_A temperature of contact between device and surrounding environment, T_{j-max} is temperature that generates device break, P_d is dissipated power and θJ_A is thermal resistance.

Each device has a maximum operability temperature, T_{j-max} correlated to a maximum dissipated power, P_{max} . If there isn't a good heat transfer from device to outside, when $T = T_{max}$, a further power and temperature increase breaks device.

From *Equation 2*, by varying the temperature, it is possible to draw a derating curve (Figure 15) for each device.³²

³⁰ "Hot electrons": it's a phenomenon occurs when electrons device reach so high kinetic energies as to generate a charge space that can cause device degradation.

³¹ DAKIN, T.W.: 'Electrical insulation deterioration treated as a chemical rate phenomenon', AIEE Trans., 1948,67, pp. 113–122

³² R.K. Singh, Ashish Dixit: "Basic Electronics Engineering & Devices", LAXMI publication 2007, pp. 612 ss.



2. Aim of research

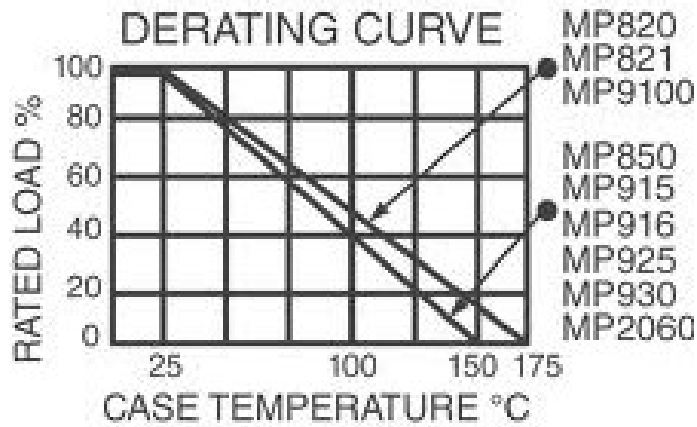


Figure 15: Derating curves for some devices

Derating curves shows how it is possible to enhance power dissipated improving package thermal efficiency. Because all surrounding chip constitutes package (soldering, gel insulation, heat sink, package case, Figure 16), it is possible to act on each of these components.

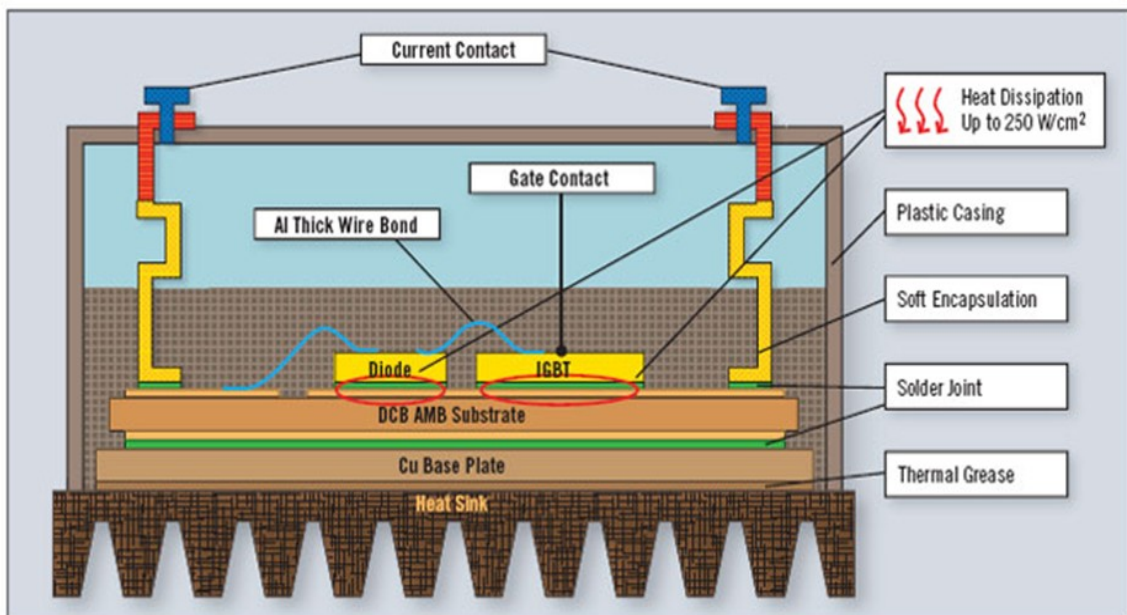


Figure 16: Power module components

Therefore there are different levels on which act in order to improve package thermal properties: we focused on *case* thermal efficiency which depends both on materials and geometry. In particular, degradation temperature and thermal conductivity are related to



material forming package, while ability to transfer heat to the cooling fluid regards its geometry.

Considering that heat dissipation propagates in three different modes: conduction, convection and radiation, package thermal efficiency depends on:

- material and contact with die (thermal conductivity);
- material and dimensions (thermal resistance);
- geometry, ventilation conditions and mounting position (cooler fluid convection);
- color (effect of "black body" and irradiance efficiency);
- ability to electrically isolate die.

2.1 State of the art

Commonly, chips are packaged in epoxy molding compounds filled with silica powder.³³ As previously it was seen, only for some special uses are applied metal or ceramic package.

Furthermore, marketing needs to obtain devices more and more advanced, able to work at higher power densities, frequency, current and voltage. Particularly, due to the limit of silicon power device at high voltage level (600–700 V), the technological advancement has pushed the development of new materials for power devices, such as SiC, gallium nitride (GaN), and other semiconductor materials³⁴.

Silicon carbide (SiC) is having enormous interest for applications in high power density devices which require high temperature resistance. In Table 1 is reported a comparison between silicon (Si) and 4H-SiC properties.³⁵

Table 1: Comparison between SiC and Si properties

PROPERTIES OF SILICON AND 4H-SiC		
Property	Si	4H-SiC
Bandgap, E_g (eV)	1.12	3.26
Electron mobility, μ_n (cm ² /Vs)	1400	800
Hole mobility, μ_p (cm ² /Vs)	450	140
Intrinsic carrier concentration, n_i (cm ⁻³) at 300 K	1.5×10^{10}	5×10^{-9}
Electron saturated velocity, v_{nsat} ($\times 10^7$ cm/s)	1.0	2.0
Critical breakdown electric field, E_{crit} (kV/mm)	25	220
Thermal conductivity, Θ (W/cm·K)	1.5	3.0-3.8
Dielectric constant	11.8	9.8

³³ National Research Council (U.S.): “*Materials for high-density electronic packaging and interconnection*”, Washington, D.C, National Academy Press; 1990, p.18

³⁴ Yong Liu “*Power Electronic Packaging Design, Assembly Process, Reliability and Modeling*”, New York, Springer, 2012, p. 5

³⁵ A. K. Agarwal, R. Singh, S. H. Ryu, J. T. Richmond, D. C. Capell, S. Schwas, B. Moore, and J. W. Palmour, “*600 V, 1-40 A, schottky diodes in SiC and their applications*” available: <http://www.cree.com/products/pdf/PWRTechnicalPaper1.pdf>

The high value of electrical breakdown makes SiC well suited to the development of high-voltage (HV) devices: we report recent examples of PIN diodes and MOSFETs in SiC with a blocking voltage of 10 kV^{36 37}.

Furthermore, the very high thermal conductivity of SiC reduces the thermal resistance of the device die.

The incremental use of SiC requires significant improvements in packaging properties: low resistance interconnections, less noise, less parasitic oscillations, increased reliability, insulation capacity of HV and improved thermal management because the encapsulated itself is more capable of dissipating (SiC has higher thermal conductivity than Si)³⁸.

An example of new package materials to support heat transfer and electrical performance are thermosetting composites containing nano-silica particles as filler³⁹ in order to dissipate heat quickly.

At present, a lot of semi-conductor devices encapsulants are based on thermosetting epoxy resin and sealings, currently, are PbSnAg alloys or sometimes without Pb⁴⁰: the choice to use various materials is mainly based on their thermal stability⁴¹. Moreover, in some devices it is also necessary the presence of an electrically insulating gel, usually based on silicones⁴².

³⁶ R. Singh, K. G. Irvine, D. C. Capell, J. T. Richmond, D. Berning, A. R. Hefner, and J. W. Palmour, "Large area, ultra-high voltage 4H-SiC p-i-n rectifiers," IEEE Transactions on Electron Devices, 2002, pp. 2308-2316 (vol. 49, no. 12)

³⁷ T. H. Duong, A. Rivera-Lopez, A. R. Hefner, and J. M. Ortiz-Rodriguez, "Circuit simulation model for a 100 A, 10 kV half-bridge SiC-MOSFET/JBS power module," Proc. of the 23th Applied Power Electronics Conference and Exposition (APEC), Austin, Texas, 2008, pp. 913-917.

³⁸ R. R. Tummala, E. J. Rymaszewski and A. G. Klopfenstein, "Microelectronics Packaging Handbook", Part II, Semiconductor Packaging, Chapman & Hall, 1996, p. 12.

³⁹ Sun, Yangyang; Zhang, Zhuqing; Wong, C. P. "Influence of nanosilica on composite underfill properties in flip chip packaging" Proceedings - International Symposium on Advanced Packaging Materials: Processes, Properties and Interfaces, 9th, Atlanta, GA, United States, Mar.24-26, 2004, pp 253-259

⁴⁰ Kim, Hyoung Il; Tian, Jun; Gupta, Vijay: "In-situ measurement of solder joint strength in board-mounted chip-scale packages using a quantitative laser spallation technique", Journal of Adhesion Science and Technology (2013), 27(7), 719-730

⁴¹ Bolannos M.A: "Semiconductor IC packaging technology challenges". In: EMAP 2005, Tokyo, Japan

⁴² M. T. Do, J.-L. Auge, O. Lesaint: "Partial discharges in silicon gel in the temperature range 20-150°C" From Annual Report - Conference on Electrical Insulation and Dielectric Phenomena 2006, pp. 590-593 (Vol. 2)



2.2 Know-how

For a preliminary check on polymeric materials currently used for package of commercial electronic devices, and the type and amount of filler (often patented), it was initially designed, within activity of doctorate, an investigation on some commercial package transistors (BD139 and BD791).

In particular, thermogravimetric analysis has highlighted the presence of inorganic and organic residual, whose chemical nature is clarified by FT-IR spectrophotometry. These analysis were conducted both in air or nitrogen atmosphere.

Thermograms of BD139 and BD791 packages, are reported respectively in Figure 17 and 18, the relevant data are shown in Table 2.



2. Aim of research

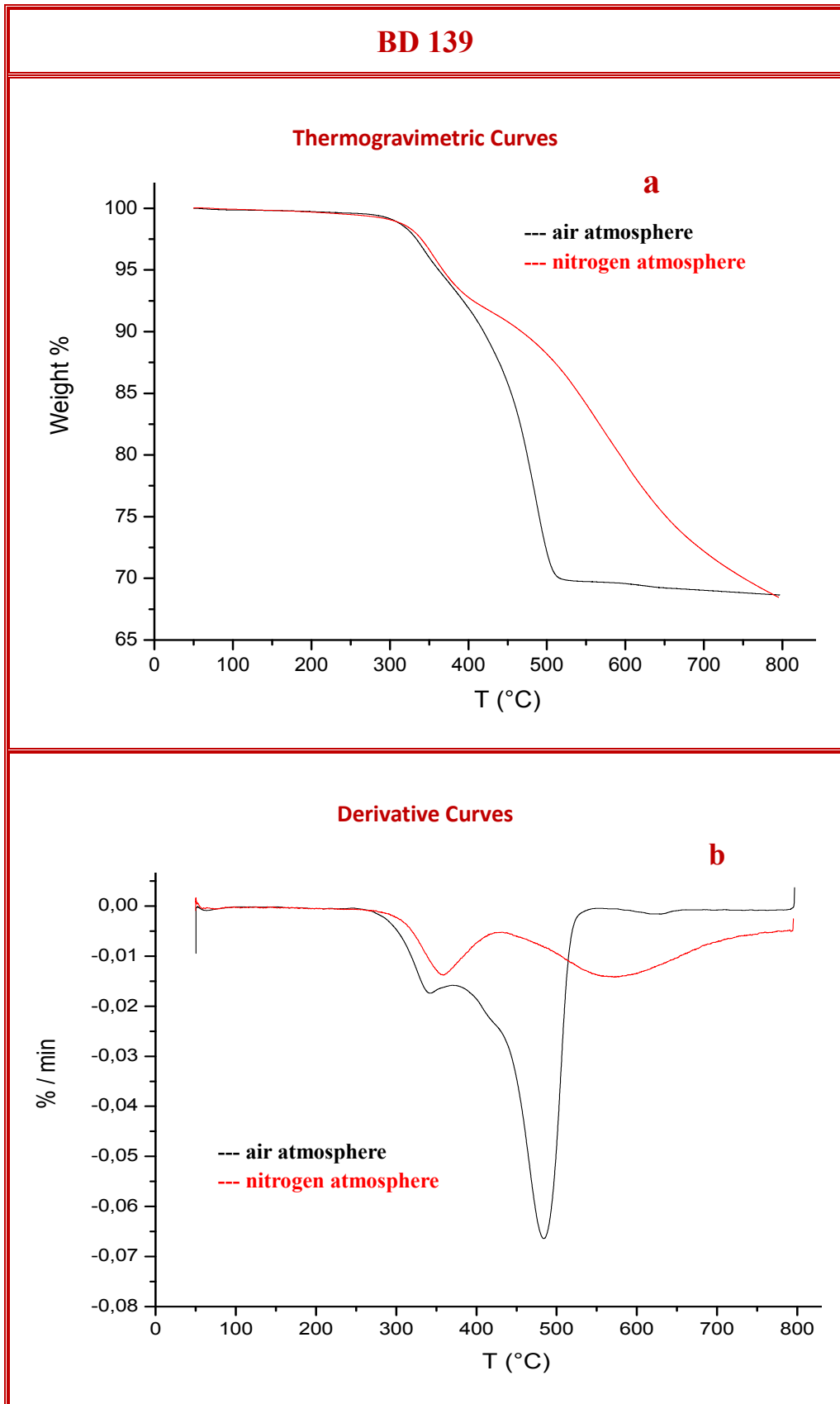


Figure 17: Thermogravimetric curves (a) and derivative curves (b) of BD139



2. Aim of research

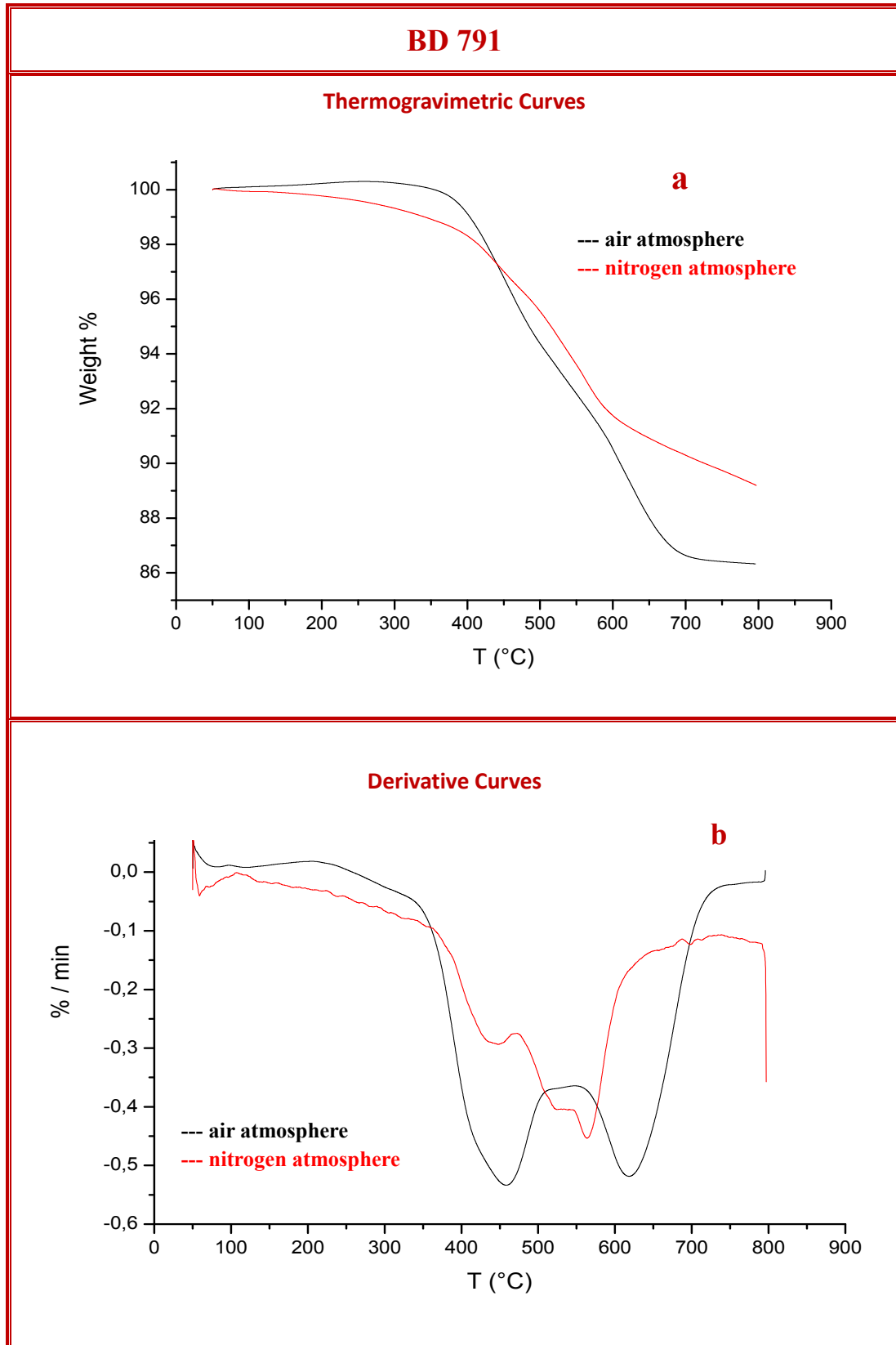


Figure 18: Thermogravimetric curves (a) and derivative curves (b) of BD791

Table 2: Data relative to thermogravimetric analysis shown in figure 17 and 18.

Samples	T _{onset} (°C)	PDT (°C)	Residue (%)
BD139 air	311,4	341,9	68,5
BD139 N ₂	320,8	358,3	68,5
BD791 air	384,3	457,9	86,3
BD791 N ₂	388,8	439,7	89,2

In particular, analysis conducted in air flow are useful to know content of inorganic residue, corresponding to amount of package filler.

Data reported shows that the package of BD139 begins to degrade in air at about 311.4 °C, ie at a lower temperature than in a nitrogen atmosphere (320.8 °C); also the residual percentage is the same both in air and in nitrogen, therefore it is principally of inorganic nature. BD791 package has similar behavior: it begins to degrade in air at 384.3 °C, while in a nitrogen atmosphere at 388.8 °C. These systems reach a maximum degradation rate between 350 °C and 500 °C.

At the end of air thermal treatment, sample residues appear essentially white in color.

These composites were analyzed by means of FT-IR analysis, shown in Figure 19, the signals are indicated in Table 3.



2. Aim of research

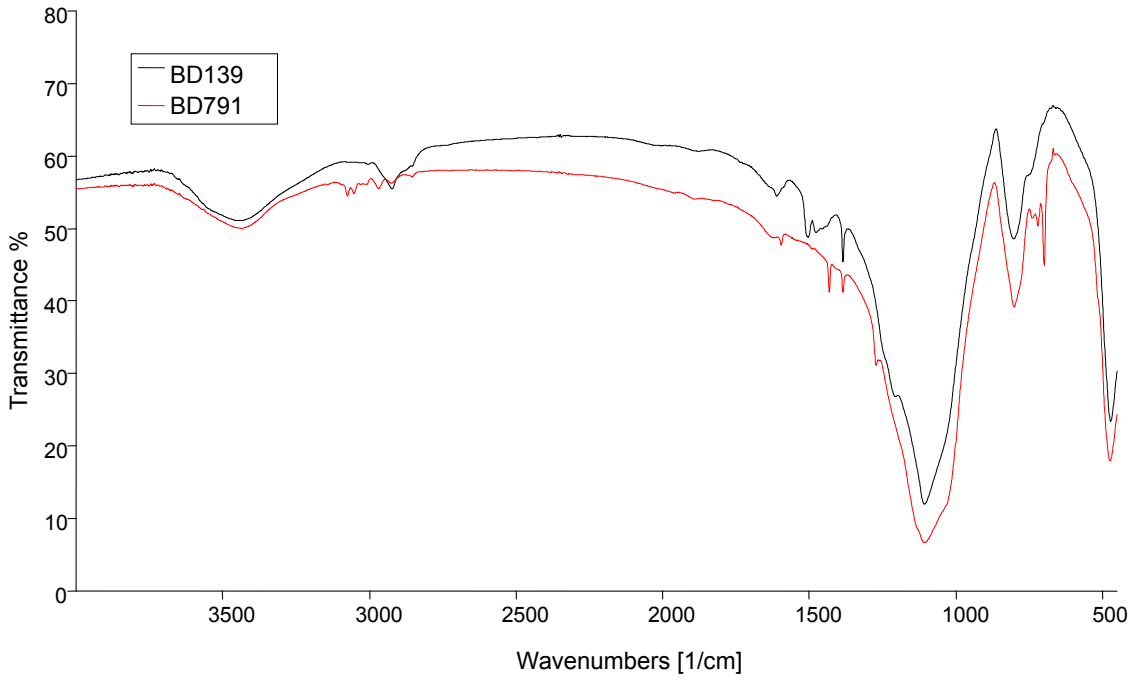


Figure 19: FT-IR spectra of BD139 and BD791

Table 3: FT-IR signals of BD391 and BD791 packages (s = strong signal; m = medium; w = weak; sh = sharp; br = broad)

Bond	Bd139 (cm ⁻¹)	Bd791 (cm ⁻¹)
Aryl C-H (stretching)	—	3074.07 w (a)
Aryl C-H aryl (bending)	—	697.97 w sh (a')
Alkyl CH (stretching)	2922.1 w (b) 1384.4 w (b')	2967.80 w (c) 1430.94 w (c')
O-H (stretching)	3436.1 w br (d)	3436.78 w br (e)
Si-O (stretching)	1106.5 s br (f)	1106.9 s br (g)

It's possible to observe the strong Si-O signal, confirming the presence of silica-based inorganic fillers in both samples, and CH aromatic and aliphatic signals.

In the end, FT-IR spectrum of packages residues after thermogravimetric analysis until 800°C, in air flow (figure 20), points out silica signals:

- O-H bond stretching: 3447 cm⁻¹;
- Si-O stretching: 1093 cm⁻¹.



2. Aim of research

Spectra shows characteristic Si-O and OH bonds stretching of silanol groups; furthermore, by a comparison with the spectra in Figure 19, there is the disappearance of aliphatic and aromatic signals.

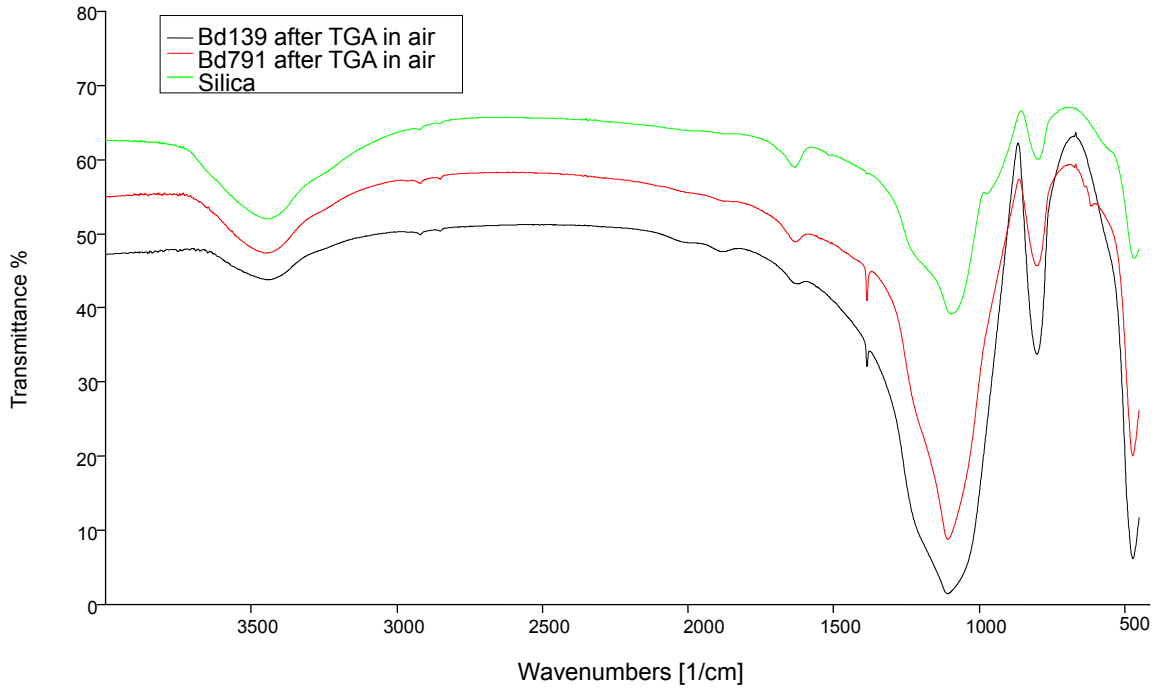


Figure 20: spectra of BD139 and BD791 after thermogravimetric analysis in air flow

Evaluations on commercial packages have allowed us to get a background on which to design research, concerning synthesis of new composite materials; ie the choice of polymeric matrix and type and percentage of filler used for final composites.

In particular, we focused on new materials suitable for power packaging and capable of dissipate heat better than commercial package. At the beginning, as upon described, research activity was investigation on actual materials used for commercial package, then move on to testing of new composite materials based on polymeric matrix properly filled and/or functionalized.

3. Polymeric Matrix

Composites matrix used was a thermosetting polymers based on epoxy resins⁴³; they are cross-linked polymers having high rigidity due to the large number of crosslinking points, generated by bonds formation between chains. They differ from other polymer systems cause impossibility of changing its shape once obtained, because their irreversible chemical modifications due to bonds formation between chains of prepolymers. Prepolymers are usually organic compounds with low molecular weight, multifunctional and chemically active. Prepolymers react trough a polyaddition obtaining three-dimensional cross-linked structures insoluble in solvents, infusible and degradable only at very high temperatures. In order to crosslink the resin at least one of comonomers must have than of two functional groups (hardening agent); crosslinking event may also occur with UV radiation⁴⁴. Crosslinking reaction begins with chains oligomeric formation which immediately begin to ramify. With the progress of polymerization, molecular weight and molecular size increase, until is obtained a complex network as a result of covalent bonds between chains.

During initial step of synthesis (Figure 21), oligomeric chains interact with each other by Van der Waals forces: it forms an elastic soluble gel (gelation), from which depend three-dimensional network structure.



Figure 21: Cross-link Beginning

⁴³ Associazione Italiana di Scienza e Tecnologia delle Macromolecole A.I.M. , “Macromolecole. Scienza e Tecnologia”, 2007

⁴⁴ Hyun-Sung Do1, Jin-Hee Park, Hyun-Joong Kim “UV-curing behavior and adhesion performance of polymeric photoinitiators blended with hydrogenated rosin epoxy methacrylate for UV-crosslinkable acrylic pressure sensitive adhesives”, European Polymer Journal Volume 44, Issue 11, November 2008, Pages 3871–3882.

With reaction progress covalent bonds are formed (Figure 22): now it is formed a covalent gel. When curing events end it is formed a three-dimensional structure.

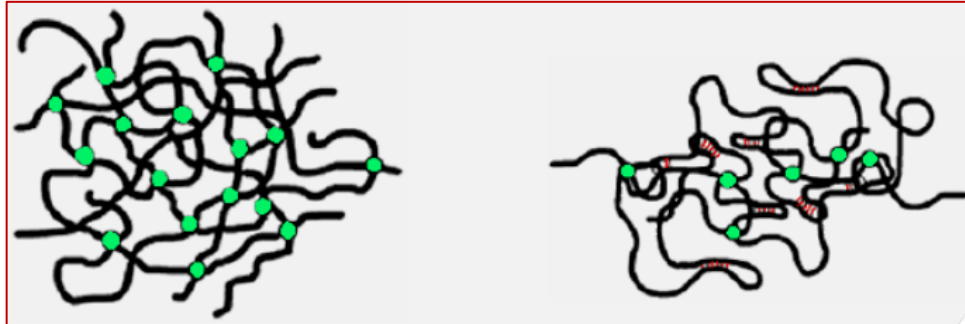
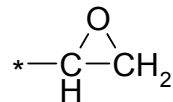


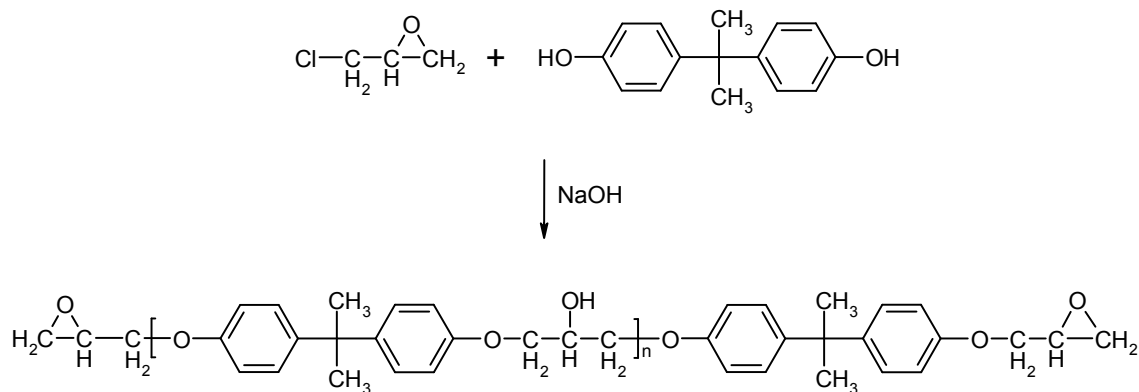
Figure 22: Curing events

Epoxy resins⁴⁵ may be defined as those materials in which chain extension and cross-linking occurs through reactions of the epoxy group (Scheme 2):



Scheme 2: Epoxy group

These resins were first developed in the 1940s and, although a number of different types are now commercially available, the major share of the market is still held by systems based upon the reaction products of epichlorhydrin and 2,2-bis(4'-hydroxyphenyl)propane (Bisphenol-A)⁴⁶:



Scheme 3: Reaction between epichlorhydrin and Bisphenol-A, where n = 0 to 12.

⁴⁵ P.M. Hergenrother, H.H. Levine, Journal of Polymer Science Part A / 5 (1967) p.1453.

⁴⁶ J. P. Critchley, G. J. Knight, W.W. Wright, "Heat-Resistant Polymers", Plenum Press New York, 1983, p 44.

Depending upon the value of n , the resins are either liquids or low-melting-point solids. The products with low values of n are the most widely used because, as n increases, melt viscosity also increases and solubility decreases, thus making processing more difficult. Cross-linking under the influence of heat alone is not sufficiently rapid, and hence a curing agent must be added: the epoxy system is very versatile and various types of curing agent may be used.⁴⁷

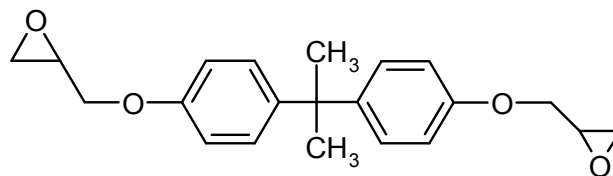
The properties of epoxy resin are very much governed by the curing agent used; but generally they have some common peculiarity⁴⁸:

- ✳ Mechanical and thermal resistance.
- ✳ Good flexibility.
- ✳ Chemical inertia.
- ✳ High adhesion.
- ✳ Waterproofing.

All these properties make epoxy resins an excellent polymer matrix for composites to be used in microelectronic packaging (cf. chap. 2).

Thermal resistance of resins depends on type of curing agent: in general amines give thermal resistance above 250 °C in air⁴⁹. This is acceptable, whereas the maximum operating temperatures of the power module are approximately 150 °C.

Epoxy resin chosen as polymer matrix for composites of this research, is obtained by crosslinking of DGEBA (Di-Glycidyl Ether of Bisphenol-A, Scheme 4), with different types of aliphatic or aromatic amines⁵⁰.



Scheme 4: DGEBA structure

⁴⁷ J. P. Critchley, G. J. Knight, W.W. Wright, "Heat-Resistant Polymers", Plenum Press New York, 1983, p 44.

⁴⁸ Pascault, J.P., Sautereau, H., Verdu, J., Williams, R.J.J.: "Chemistry of Crosslinked Polymer Synthesis", CRC Press, 2002, Chapter 2.

⁴⁹ J. P. Critchley, G. J. Knight, W.W. Wright, "Heat-Resistant Polymers", Plenum Press New York, 1983, p 47.

⁵⁰ Marcel Dekker, "Epoxy Resins Chemistry and technology", 1988, pp 54 to 63.

DGEBA Characterization

DGEBA is often used as precursor (prepolymer) because allows to obtain a wide range of polymers. Polymerization mechanism is based on the addition reactions involving epoxy rings, especially reactive due to the tension ring⁵¹, by the hardeners. DGEBA was characterized by means of FT-IR Spectrophotometry, ¹H-NMR spectroscopy and MALDI-TOF(+) mass spectrometry.

FT-IR spectrum is shown in Figure 23 and characteristic signals are shown in Table 4.

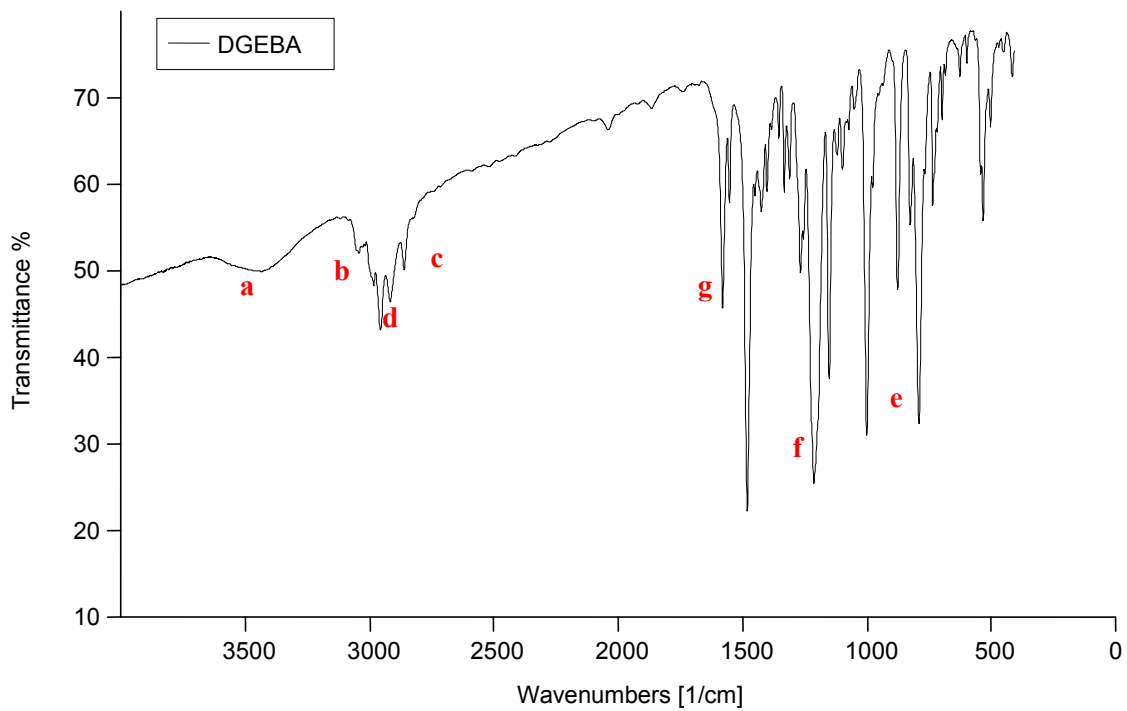
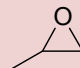


Figure 23: DGEBA FT-IR spectrum

⁵¹ Antonio Moroni, Jovan Mijovic, Eli M. Pearce, Cheu Ching Foun: “Cure kinetics of epoxy resins and aromatic diamines”, 1986, Journal of Applied Polymer Science, Vol. 32, pages 3761–3773.

Table 4: DGEBA FT-IR signals
(s = strong signal; m = medium; w = weak; sh = sharp; br = broad)

Bond	Wavenumbers (cm ⁻¹)
Methyl C-H (asymmetric stretching)	2967 w sh (b)
Methyl C-H (symmetric stretching)	2873 w sh (c)
Methylen C-H (asymmetric stretching)	2928 w sh (d)
Epoxy ring  (asymmetric stretching)	828 s sh (e)
(symmetric stretching)	1246 s sh (f)
Aromatic C-C (stretching)	1608 m sh (g)
Aromatic C-H (stretching)	3063-2997
Aromatic CH (bending)	866-724
Bonded OH (stretching)	3445 w br (a)

To confirm DGEBA chemical structure, methyl (2873-2967 cm⁻¹) and methylene aliphatic (2928 cm⁻¹), aromatic (866-724 cm⁻¹), hydroxyl group (3445 cm⁻¹) and epoxy ring (828, 1246 cm⁻¹) FT-IR signals are evident.

DGEBA ¹H-NMR spectrum is shown in Figure 24 with relative chemical structure.

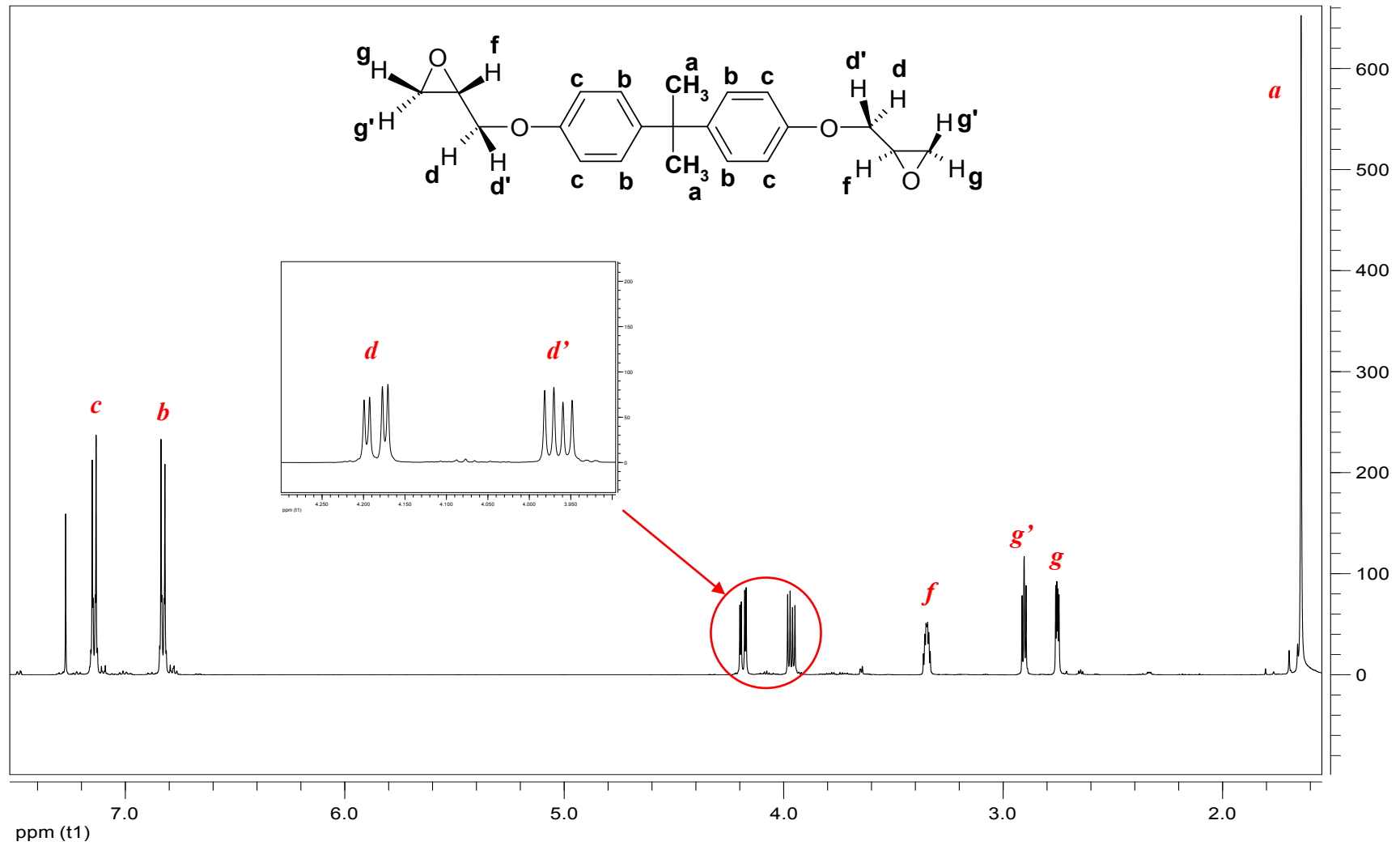


Figure 24: DEGBA $^1\text{H-NMR}$ spectrum and relative signals (Solvent CH_2Cl_2)

Figure 25 shows DGEBA MALDI-TOF (+) mass spectrum, which shows characteristic signal at $m/z = 341$ (DGEBA molecular peaks: MH^+).

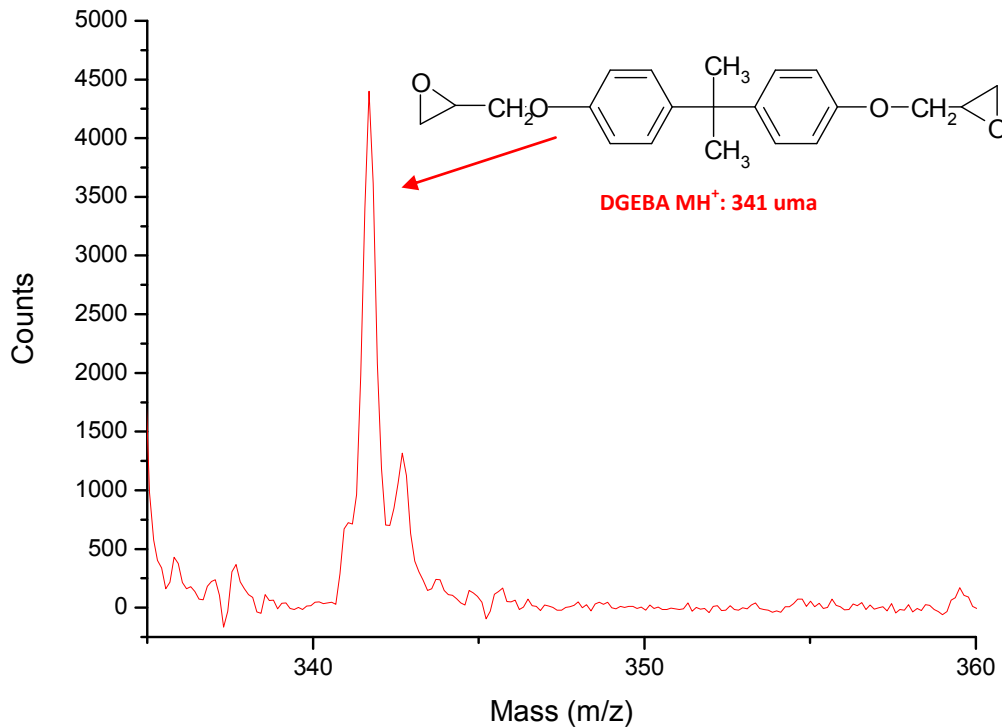


Figure 25: DGEBA MALDI-TOF (+) mass spectrum; Matrix: IAA, Solvent: THF.

Curing Agents

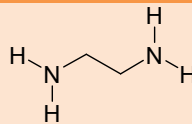
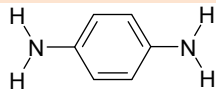
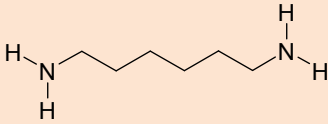
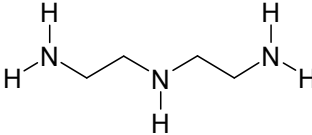
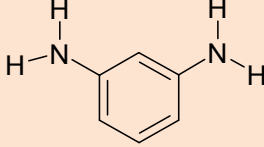
As curing agent, was used several aliphatic and aromatic amines. In general, they must have more than three active hydrogen atoms and two amino groups in a molecule so that the cured resin becomes crosslinked polymer.

Aliphatic amine rapidly reacts with epoxy prepolymer, is a representative room-temperature curing agent. Resins that have been cured using aliphatic amines are strong, and are excellent in bonding properties. They have resistance to alkalis and some inorganic acids, and have good resistance to water and solvents, but they are not so good to many organic solvents.

Aromatic amine has weaker basicity than aliphatic amine and slowly cures: normally, the curing of aromatic amine requires higher temperature than aliphatic.⁵²

Table 5 shows amines used as curing agents for epoxy resins.

Table 5: Curing agents used

Reagenti	Formula di Struttura
Ethylene-diamine	
Paraphenylene-diamine	
Hexamethylene-diamine	
Diethylene-triamine (DETA)	
Metaphenylene-diamine	

3.1 Epoxy resins synthesis

Resins produced are:

- ✓ DGEBA + Diethylene triamine (DETA);
- ✓ DGEBA + Ethylenediamine;
- ✓ DGEBA + Hexamethylenediamine;
- ✓ DGEBA + Para-phenylene diamine;
- ✓ DGEBA + Meta-phenylene diamine

In order to understand best conditions in which to operate for the synthesis of resins and composites (following described), was synthesized a resin model DGEBA: DETA (3: 2) by means of DTA (Differential Thermal Analysis), obtaining curve shown in Figure 26.

⁵² <https://www.threebond.co.jp/en/technical/technicalnews/pdf/tech32.pdf>

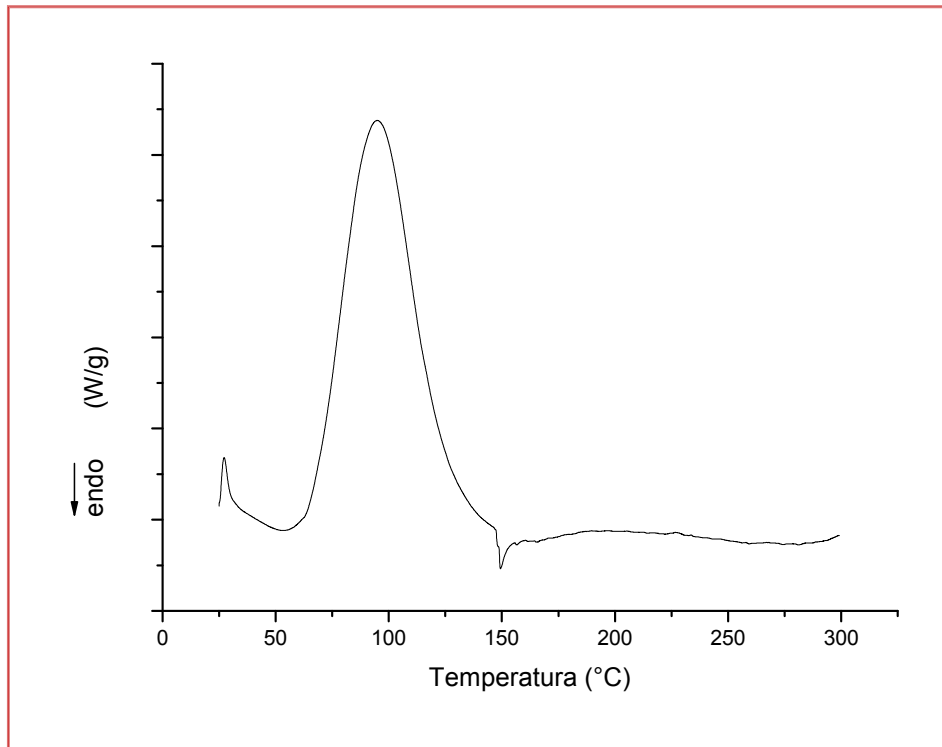


Figure 26: DTA curve of resin model DGEBA: DETA 3:2.

DTA curve shows that branching takes place with heating, in fact it is an exothermic peak. Branching event finish at a temperature of 145 °C. Referring to this analysis, all resin polymerizations are conducted at 150 °C, to ensure the end of crosslinking.

To obtain 1 g of these resins, it is always operated in the same way: DGEBA was weighed, stored in a vial and weakly heated. Later was added amine, shaking and flushing with nitrogen (to limit amine groups oxidation). Then vial is inserted in a thermoblock (figure 27) at 150 °C, for 2 hours.



Figure 27: Thermoblock used to cure resins

Molar ratio between DGEBA and amines was 3:2, to maximize crosslinks.

All obtained resins are infusible and insoluble.

Table 6 shows molar quantities of reagents.

Table 6: Obtained resins

Resins	DGEBA	Amines
DGEBA:DETA	<i>0,8021g (0,00235 mol)</i>	DETA: <i>166,52 μl (0,00154 mol)</i>
DGEBA:Ethylen diamine	<i>1,0082g (0,00290 mol)</i>	Ethylen diamine: <i>120,31 μl (0,00193 mol)</i>
DGEBA: Hexamethylen diamine	<i>0,9077g (0,00261 mol)</i>	Hexamethylen diamine: <i>0,1887 g (0,00162 mol)</i>
DGEBA: Para-phenylen diamine	<i>0,8067g (0,00232 mol)</i>	Para-phenylen diamine: <i>0,1557 g (0,00144 mol)</i>
DGEBA:Meta-phenylen diamine	<i>0,8242g (0,00237 mol)</i>	Meta-phenylen diamine: <i>0,1766 g (0,00163 mol)</i>

A Molecular Model

In addition to resins described above, it was prepared a model system DGEBA: DETA (1: 1) in order to study the progress of the branching by means of MALDI-TOF (+). It was used 0.49316 g (1.42 mmol) of DGEBA placing in a vial, heated weakly until melting point (40-44 °C). Later were added 153.10 μ l (1,42 mmol) of DETA, stirring. Finally, mixture was put on a Teflon mold for 24 hours, and was obtained a gluey liquid system.

It was verified sample solubility in THF (Tetrahydrofuran) and proceeded with MALDI-TOF(+) analysis, obtaining mass spectrum shown in Figure 28; structural assignment is reported in Table 7.

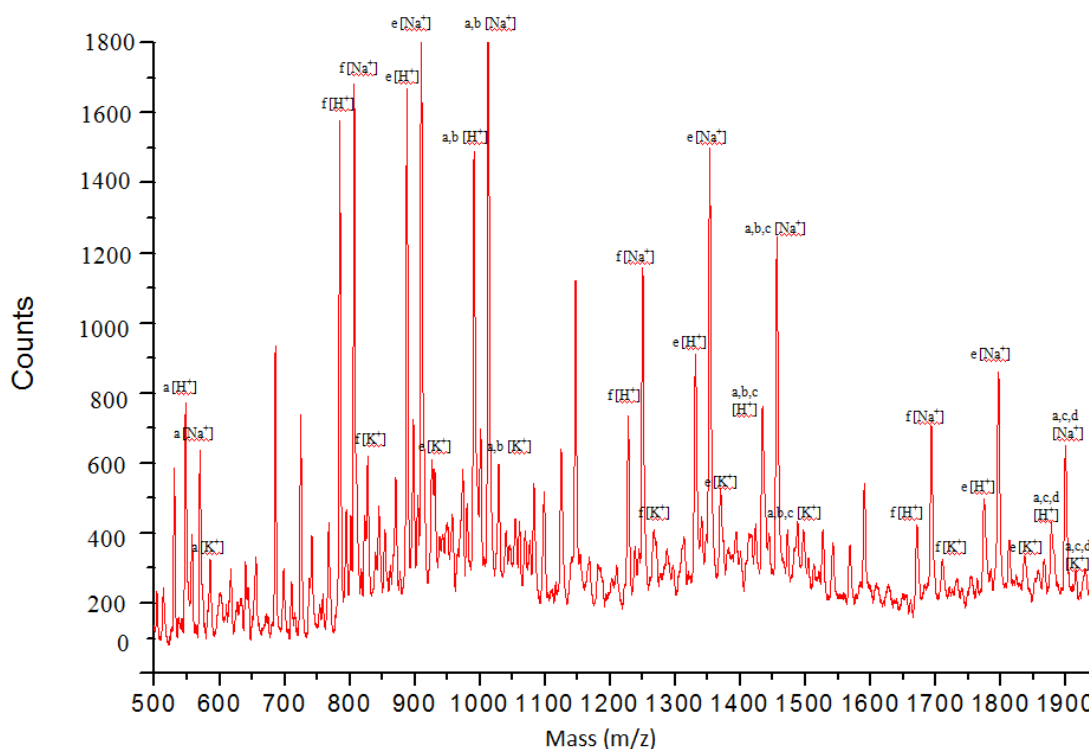
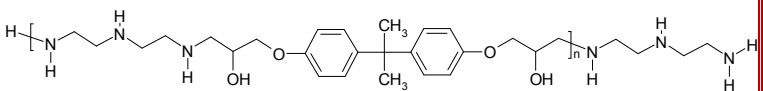
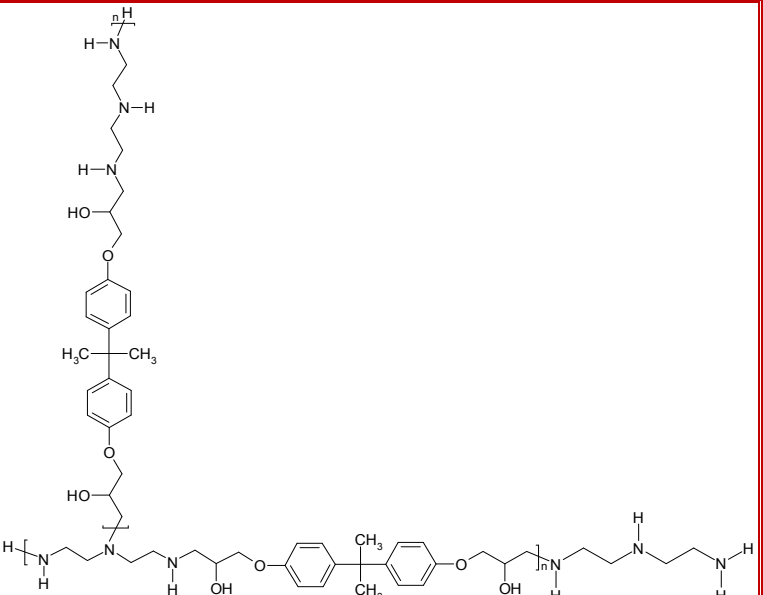
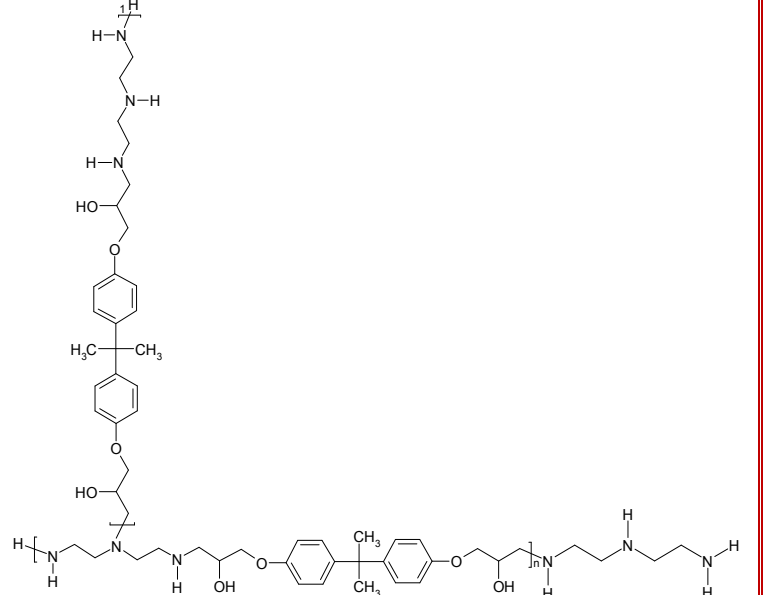
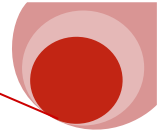


Figure 28: MALDI-TOF spectrum of molecular model DGEBA/DETA (1:1).
Matrix: IAA, Solvent: THF

Table 7: Structural peak assignment relative to mass secum in fig.28

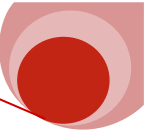
Series	Oligomeric Structures	H ⁺ (n)	Na ⁺ (n)	K ⁺ (n)
a		546 (1) 989 (2) 1431 (3) 1874 (4)	568 (1) 1011 (2) 1453 (3) 1896 (4)	584 (1) 1027 (2) 1469 (3) 1912 (4)
b		989 (1) 1431 (2)	1011 (1) 1453 (2)	1027 (1) 1469 (2)
c		1431 (2) 1873 (3)	1453 (2) 1895 (3)	1469 (2) 1911 (3)



d		1873 (1)	1895 (1)	1911 (1)
e		885 (1) 1327 (2) 1769 (3)	907 (1) 1349 (2) 1792 (3)	923 (2) 1365 (3) 1808 (3)
f		782 (0) 1224 (1) 1666 (2)	804 (0) 1246 (1) 1688 (2)	820 (0) 1262 (1) 1704 (2)

In mass spectrum can be observed:

- ⊕ The presence of an oligomeric distribution with 1 to 4 number of repeating units, centered on dimer.
- ⊕ Both linear and branched oligomers.
- ⊕ The presence of terminal epoxy and amino groups.



3.2 Epoxy resins characterizations

Thermal Analysis

Thermogravimetric analysis of synthesized resins were conducted in air or nitrogen atmosphere. Thermograms are shown in Figures 29-30 and relative data in Table 8.

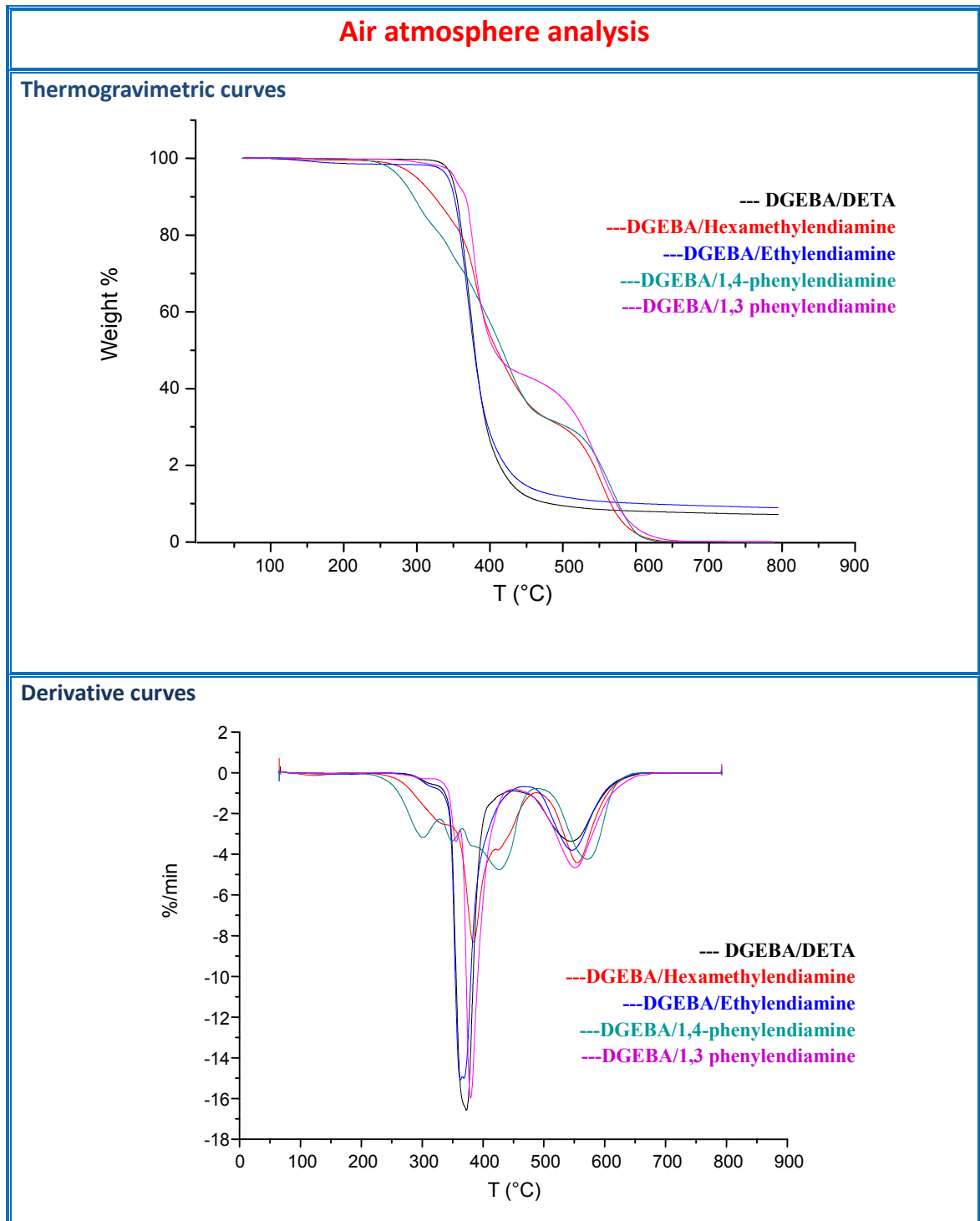


Figure 29: thermograms and relative derivative curves in air atmosphere

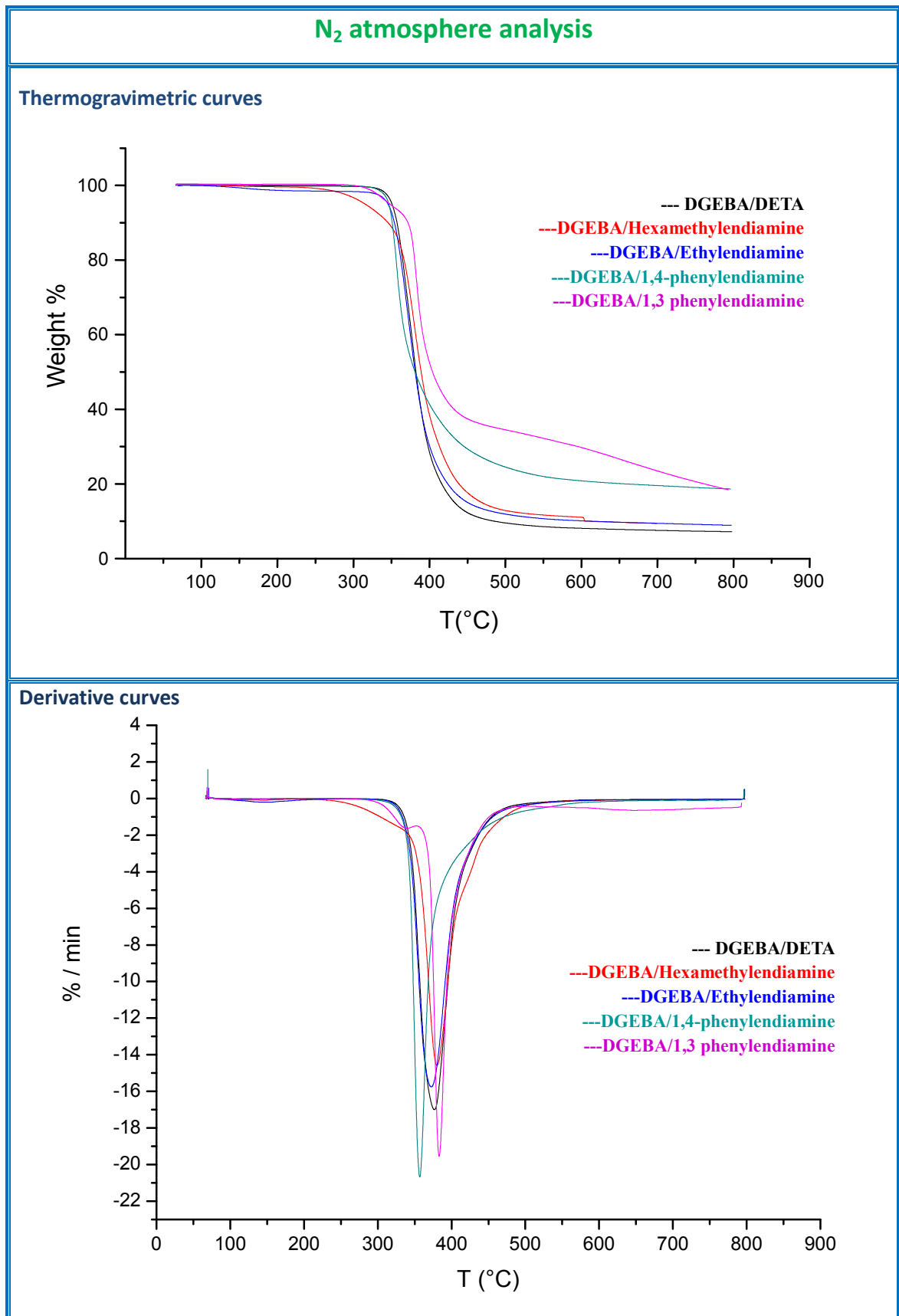
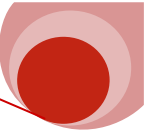


Table 8: Datasheet concerning resins thermogravimetric analysis

Resins	Atmosphere	T _{onset} (°C)	PDT (°C)	%Char
3 DGEBA + 2 DETA	air	349,6	372,8	7,2
	nitrogen	353	376,8	7,2
3 DGEBA + 2 Hexamethylenediamine	air	346,2	384,8	0,2
	nitrogen	360,5	380,3	11,6
3 DGEBA + 2 Etylendiamine	air	348,9	363	0
	nitrogen	350,6	372,6	9,1
3 DGEBA + 2 1,4-phenylenediamine	air	342,5	355	1,2
	nitrogen	346,7	356,7	18,5
3 DGEBA + 2 1,3-phenylenediamine	air	368,2	379,6	0,3
	nitrogen	370,6	383,1	18,6

Thermogravimetric analysis shows that resins, in air, begin to degrade at 342.5 °C to 368.2 °C; while in nitrogen between 346.7 °C to 370.6 °C. In air, cause oxidative events, they tend to degrade at lower temperature. These resins also reach the maximum degradation rate at temperatures between 355 °C and 385 °C. In general their decomposition temperature would permit the use such as packages in power devices, where temperatures, generally, are lower than 275 °C⁵³.

In addition to the thermogravimetric analysis, were performed DTA characterizations; obtained graphs are shown in Figure 31.

⁵³ <http://www.precisionresistor.com/SM063-.5W-Wire-Wound-Precision-Power-Axial Resistor.html>

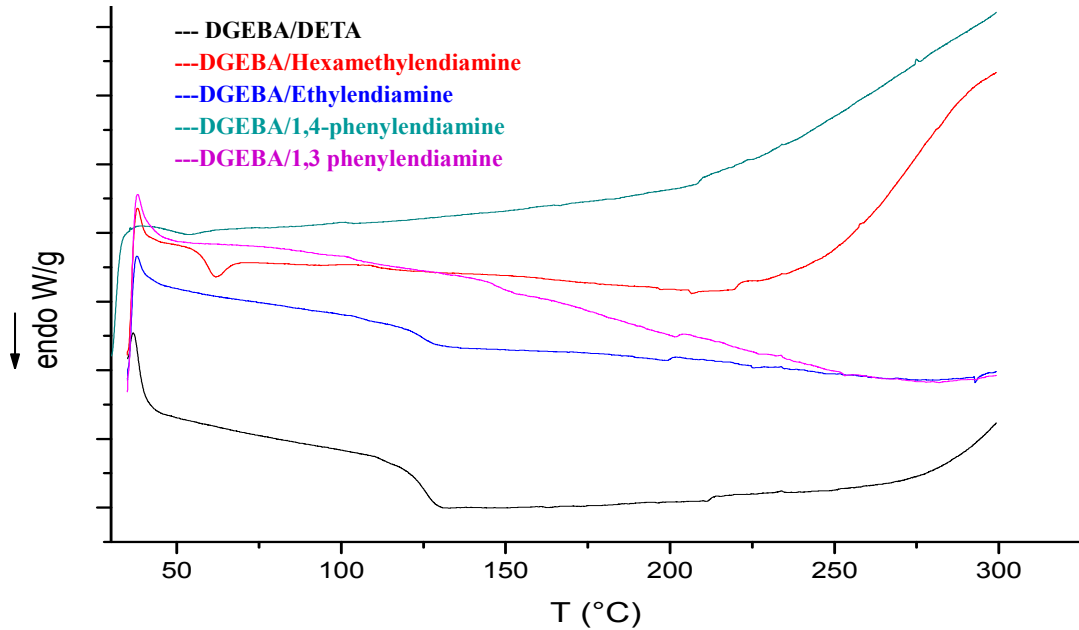


Figure 31: DTA thermograms of resins

DTA curves of resins do not show particular events, with the exception of those related to DGEBA:DETA (3:2) and DGEBA:ethylenediamine (3: 2), in which glass transitions (T_g) are observed.

During the curing process (discussed at the beginning of this chapter) may be that macromolecular structure contains amounts of oligomers, free or aggregates, and soluble branched molecules. The system, therefore, is defined as a biphasic system sol-gel. In the course of the reaction may occur another phenomenon, the vitrification: conversion process of a viscous liquid or an elastic gel in a glassy solid. This phenomenon is characterized by the variation of the kinetics of reaction mechanism, passing from chemical to diffusive type: in fact, the increase of density, due to the presence of cross-links between the chains, the monomer reactivity will be lower and dependent on diffusion through the polymer mass.

The follow diagram (figure 32), called TTT (Time-Temperature-Transformation) diagram, describes chemical-physical phenomena during crosslinking reaction.

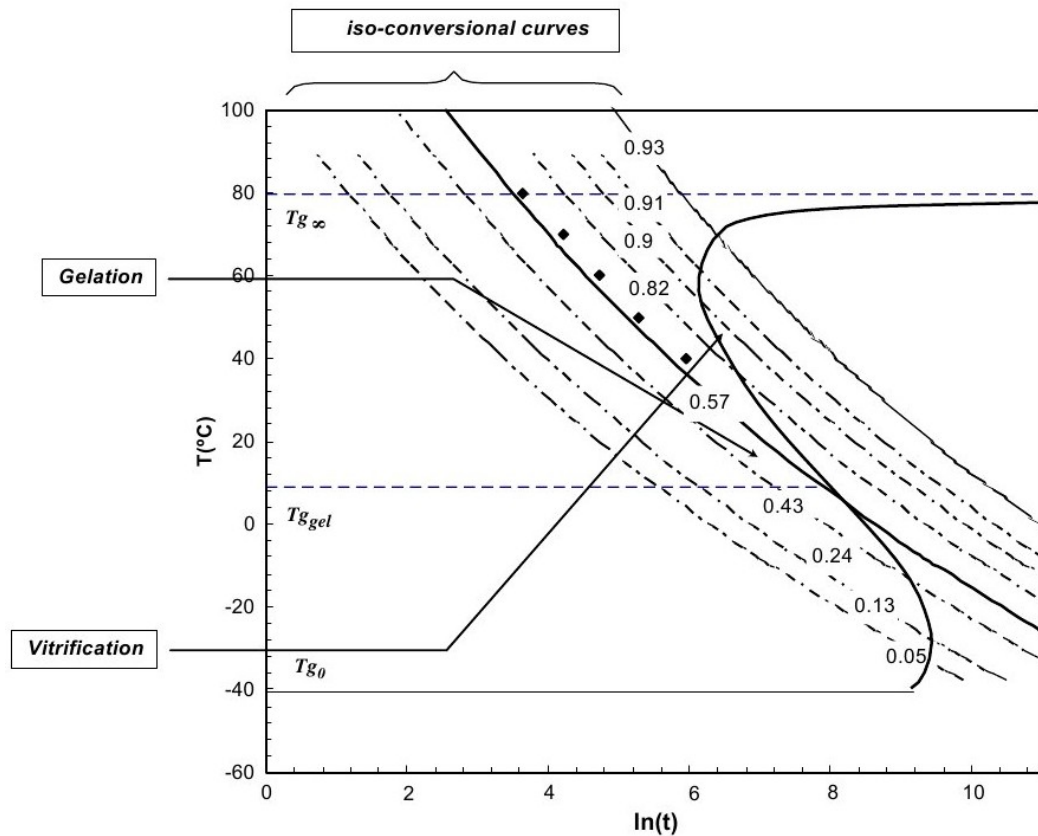


Figure 32: TTT isothermal cure diagram for generic epoxy systems ⁵⁴

This diagram shows experimental time to reach various events depending on the temperature of curing. In particular, it can observe three temperatures relating to crosslinking event:

- ~ T_{g0} : below this temperature there is no reaction between prepolymer and hardener.
- ~ T_{ggel} : for ideal systems gelation and vitrification occur simultaneously and the corresponding temperature is indicated as T_{ggel} . At a temperature comprised between T_{g0} and T_{ggel} , the liquid resin reacts until begins the vitrification. After that, reaction speed will be strictly dependent on diffusion processes of the reactant species.
- ~ $T_{g\infty}$ is the treatment temperature to which the degree of reaction reaches the maximum value; it is theoretically equal to one but experimentally very difficult to obtain.

The presence of amorphous portions in DGEBA:DETA (3:2) and

⁵⁴ <http://thermosets.wordpress.com/category/ttt-diagram/>

DGEBA:ethylenediamine (3:2) resins is, probably, due to reduced segmental mobility of gel system that restricts diffusion of sol phase. Therefore the presence of these amorphous portions makes necessary the use of higher curing temperatures or times to complete crosslinking event.

Structural Analysis

Finally, the resins were characterized by means of FT-IR spectroscopy. Comparative spectra are shown in Figure 33 and the relative signals are indicated in Table 9.

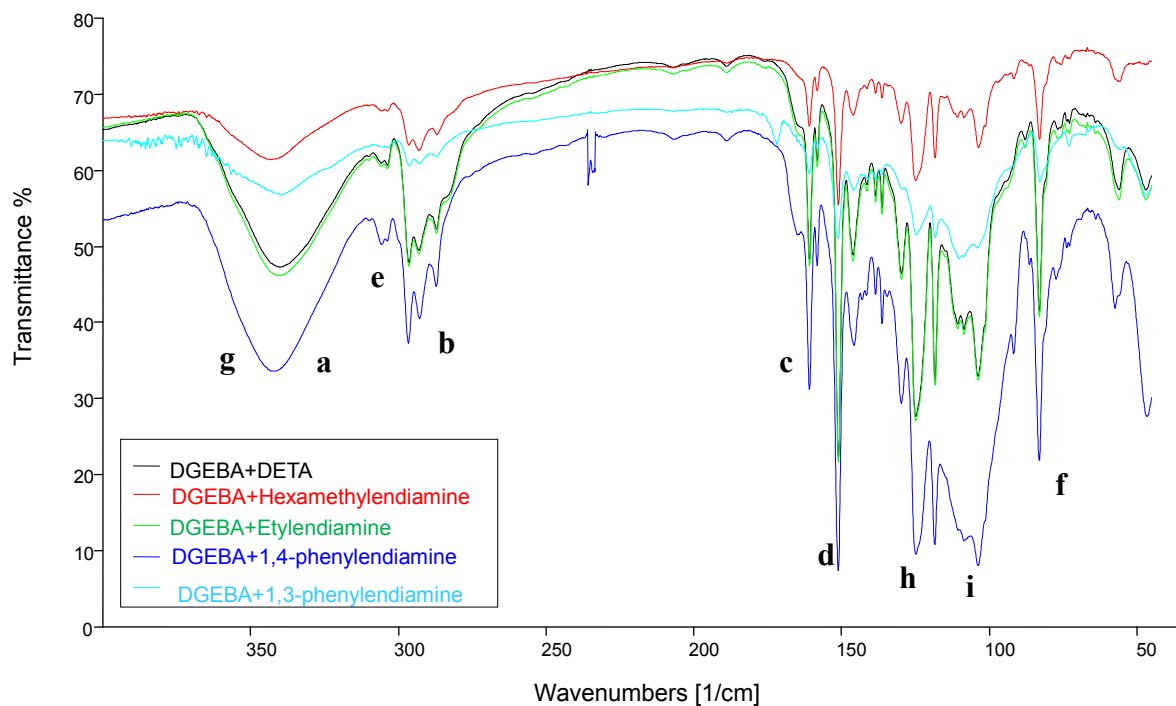


Figure 33: FT-IR spectra of resins DGEBA+DETA, DGEBA+Hexamethylenediamine, DGEBA+Etylendiamine, DGEBA+1,4-phenylenediamine (3:2), DGEBA+1,3-phenylenediamine

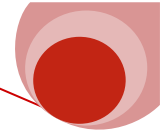


Table 9: resins FT-IR signals
(s = strong signal; m = medium; w = weak; sh = sharp; br = broad)

Bond	Wavenumbers (cm ⁻¹)
O-H (stretching)	3426-3401 m br (a)
C-H (methyl stretching)	2874-2867 w (b)
C-C (aryl stretching)	1608 m sh (c) 1510 s sh (d)
C-H (aryl stretching)	3102-3036 w br (e)
C-H (aryl bending)	824-831 m sh (f)
N-H (amino stretching)	O-H overlying (g)
C-O-C (arylalkyl ether asymmetric stretching)	1247-1238 s sh (h)
C-O-C (arylalkyl ether symmetric stretching)	1037-1026 s br (i)

Spectra show a strong signal relative to hydroxyl due to epoxy rings of DGEBA opening and traces of water (3426-3401 cm⁻¹). Aromatic, aliphatic and ether systems belong to DGEBA. We also observed disappearance of epoxy ring stretching signal, typical of the DGEBA prepolymer.

4. Fillers

Fillers are, generally, additives in solid form, and differ from polymer matrix in both structure and composition. The union between polymer and fillers has a synergistic effect: each material contributes to compensate for defects of other. This effect depends on various factors: polymer and filler nature, their shape, size and distribution in polymer matrix. Fillers can be inorganic or organic compounds and, according to their behavior, can be inert or active fillers (reinforcing)⁵⁵.

Inert fillers, such as talc and CaCO_3 , are currently employed also to increase the mass of product and consequently decrease price. Active fillers produce specific improvements in mechanical, thermal, physical, and are therefore known as reinforcing fillers. The presence of a filler having a high thermal conductivity and/or high thermal resistance, could improve thermal efficiency of polymer matrix⁵⁶, that is the aim of our research. For this purpose, it was used various types of fillers: organic or inorganic, synthetic or commercial.

In particular, as organic fillers were used polyamidic (poly(*meta*-phenylene isophthalamide), poly(*para*-phenylene terephthalamide), Kelin 130⁵⁷), polyimidic (poly(*para*-phenylene-pyromellitimide) and polycyclic (Grafenoxide) compounds. As inorganic fillers were used SiO_2 and MoS_2 .

SiO_2 , MoS_2 , and Kelin 130 are commercial products, while all the others have been specially synthesized.

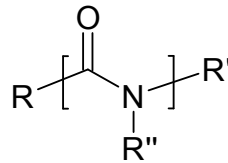
⁵⁵ G. Vittorio Villavecchia “Nuovo dizionario di merceologia e chimica applicata”, Vol. 2, p. 805

⁵⁶ E.R. Egan, C.H. Amon, “A Study on the Thermal Conductivity Enhancement of Several Polymer Composites for Embedded Electronics Applications” - ASME-PUBLICATIONS-HTD, 1997 - ASME

⁵⁷ Courtesy of “Spin Tech International s.r.l.” Via G. Galilei, 16 - 25030 Adro (BS) Italy.

4.1 Polyamidic fillers

Polyamides are macromolecules characterized by amino group (Scheme 5) from which depend their properties.



Scheme 5: amide group

Polyamides can be synthesized by condensation polymerization of a dicarboxylic acid (or their derivatives) and a diamine⁵⁸ or via ring-opening polymerization of a lactam⁵⁹.

Polyamides have a lot of inter-chain hydrogen bonds giving intense forces of molecular cohesion, reinforced by significant percentages of crystallinity due to structural chains regularity.⁶⁰ This generates excellent mechanical properties with a high elastic modulus, hardness and abrasion resistance.

Polyamides can be classified in aliphatic and aromatic; particularly, aromatic polyamide have higher thermal efficiency than aliphatic, in fact they have a maximum rate degradation higher than 700 °C⁶¹, while aliphatic polyamide at 400-500°C.⁶²

In addition, some aromatic polyamides have a high thermal conductivity (10-30 W/mK^{63,64}).

For this reason, as polyamidic filler for package composites, we have chosen aromatic polyamides:

- ✘ poly-(*meta*-phenylene isophthalamide),
- ✘ poly-(*para*-phenylene terephthalamide),
- ✘ Kelin 130.

⁵⁸M. I. Kohan, S. A. Mestemacher, R. U. Pagilagan, K. Redmond, "Polyamides", Ullmann's Encyclopedia of Industrial Chemistry, 2003.

⁵⁹C. Brisi, *Chimica applicata*, 3th ed., Levrotto & Bella, Torino, 1997, p. 448

⁶⁰K. Weissermel, H. J. Arpe, C. R. Lindley, "Industrial organic chemistry", 4th ed., Wiley-VCH, 2003, pp. 239-266

⁶¹Mark J.E., "Polymer Data Handbook", Oxford Univ. Press, 1999, p.140.

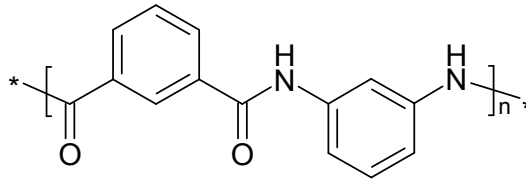
⁶²Mark J.E., "Polymer Data Handbook", Oxford Univ. Press, 1999, pp. 172-229.

⁶³Choy, C. L., et al., *J. Polym. Sci., Part B: Polym. Phys.*, 33(14), 1995.

⁶⁴Poulaert, B., et al. *Polym. Commun.* 26(5), 1985.

4.1.1 Synthesis and characterization of Poly(*meta*-phenylene isophthalamide)

Poly(*meta*-phenylene isophthalamide) is commercially known as “Nomex” (Scheme 6), Du Pont registered trademark⁶⁵, that indicates a meta-aramid⁶⁶ developed in 1967.



Scheme 6: Poly-(*meta*-phenylene isophthalamide)

Nomex is heat-resistant, flame-retardant and electrical insulator. It has high extensibility relative to other aromatic polyamide, high degradation and glass transition temperature, excellent dielectric property, and good spinnability.⁶⁷

To obtain approximately 6 g of Poly(*meta*-phenylene isophthalamide) having a polymerization degree of about 12, were used 2.4 g of 1,3-Phenylenediamine (0.022193 mol) and 4.3 g of isophthaloyl chloride (0.019542 mol), in a molar ratio 13:12.

This molar ratio was chosen on Equation 3:

$$X_n = \frac{1 + r}{1 - r}$$

Equation 3

Where $r = \frac{N_{AA}^0}{N_{BB}^0}$ ($N_{AA}^0 < N_{BB}^0$).

N_{AA}^0 are isophthaloyl chloride moles and N_{BB}^0 are 1,3 phenylene diamine moles. Polymer was obtained in two steps (Scheme 7). At first, 120 ml of a mixture THF/DMF (70:30) were dried and degassed. Subsequently, the mixture was divided into equal portions: one portion was used to solubilize 1,3-phenylene diamine and 6 ml of

⁶⁵ Stamatoff, G. S. U.S. Patent 3,228,910 (to E. I. du Pont), 1966.

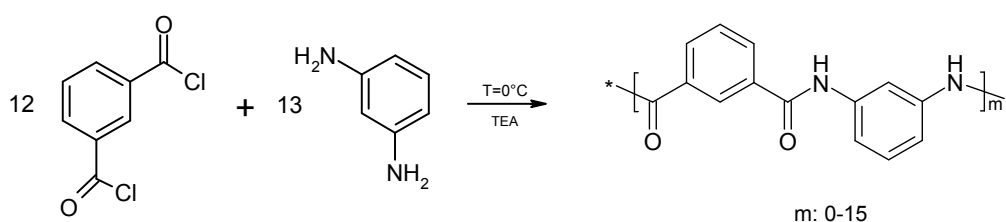
⁶⁶ “Aramid” is contraction of “Aromatic Amides”.

⁶⁷ Lewin, M., and J. Preston, eds. Handbook of Fiber Science and Technology. Marcel Dekker, New York, 1983, vol. 3.

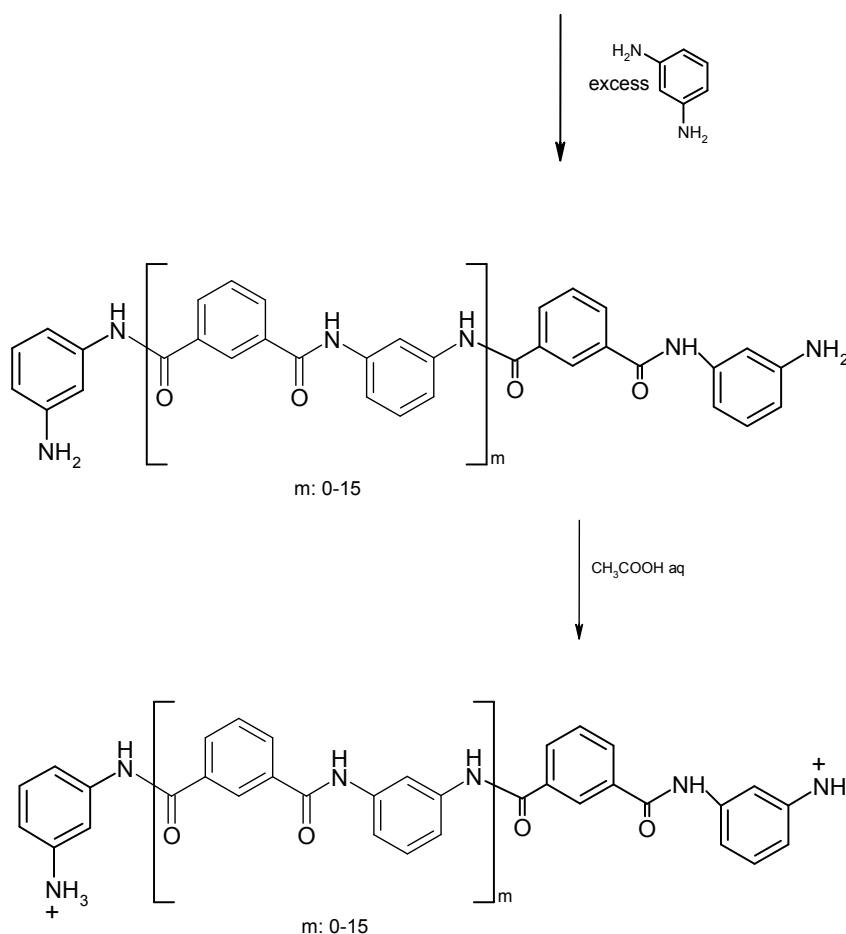
anhydrous Triethylamine (TEA, protons acceptor). Then this solution was placed in ice bath ($T = 0\text{ }^{\circ}\text{C}$).

The second portion of THF/DMF mixture was used to solubilize isophthaloyl-dichloride; this second solution was slowly added to diamine solution placed on ice. N_2 was flushed and the reaction was carried on for one hour.

1st STEP



2nd STEP



Scheme 7: Synthesis of poly(*meta*-phenylene isophthalamide)

Second step concern the addition of 2.4 g (22.19 mmol) of 1,3-Phenylenediamine, to ensure amino as end groups. After 30 minutes, products reaction was precipitate in acidified H_2O (acidification was obtained with acetic acid until a pH of about 2-3) to

remove amine excess and protect terminal amino groups; precipitate was several times washed with deionized water.

Finally, obtained product was placed in oven at 40 °C for one hour, and then under vacuum for 3 days.

Poly(*meta*-phenylen isophthalamide) obtained as above described, was thermally and structurally characterized by means of TGA, DTA, FT-IR, MALDI-TOF and ¹H-NMR.

Thermal Analysis

Figures 34 and 35 shows respectively TGA analysis in air atmosphere (black curves) and nitrogen atmosphere (red curves) of Poly(*meta*-phenylen isophthalamide) and relative derivative curves.

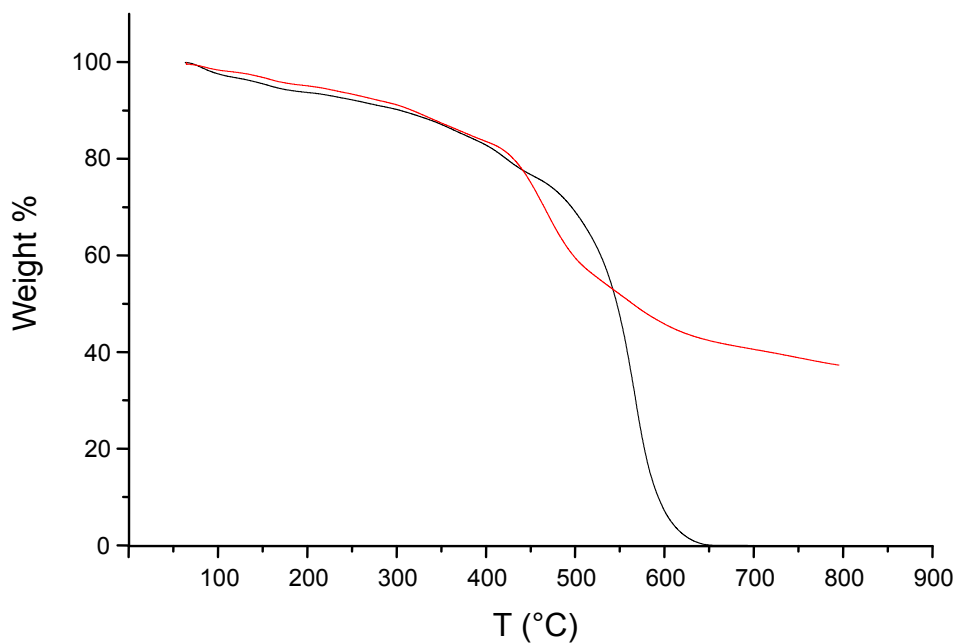


Figure 34: Thermogravimetric curves of Poly(*meta*-phenylene isophthalamide)

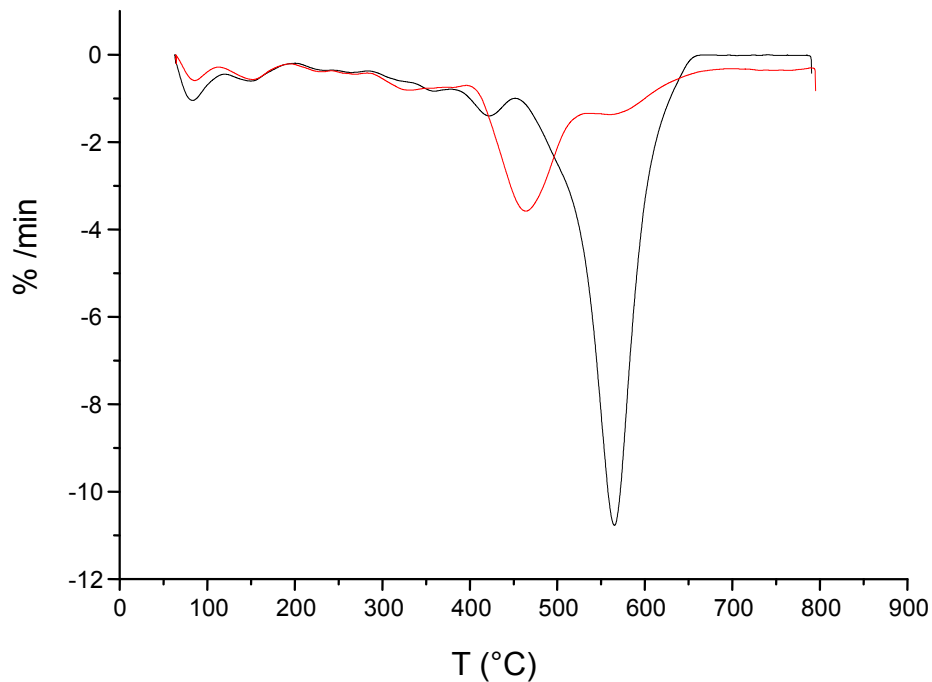


Figure 35: Derivative curves of Poly(*meta*-phenylene isophthalamide)

TGA shows that Nomex, in air flow, starts to degrade at 532 °C, while in nitrogen, at 432 °C. This difference is a consequence of synthesis impurities (free amine, water, and amine salts); in particular TGA analysis under nitrogen flow, avoiding oxidation of free amino groups, favors aminolysis of polyamide chains. Rate of degradation for this system reaches a maximum at about 500 °C.

Residual percentage in air is equal to zero, because everything is oxidized.

Overall, thermal behavior of this synthesized compound, more oligomeric than polymeric, is close to literature.⁶⁸

DTA in nitrogen atmosphere of Poly(*meta*-phenylene isophthalamide) is shown in figure 36.

⁶⁸ Mark J.E., "Polymer Data Handbook", Oxford Univ. Press, 1999, p.709.

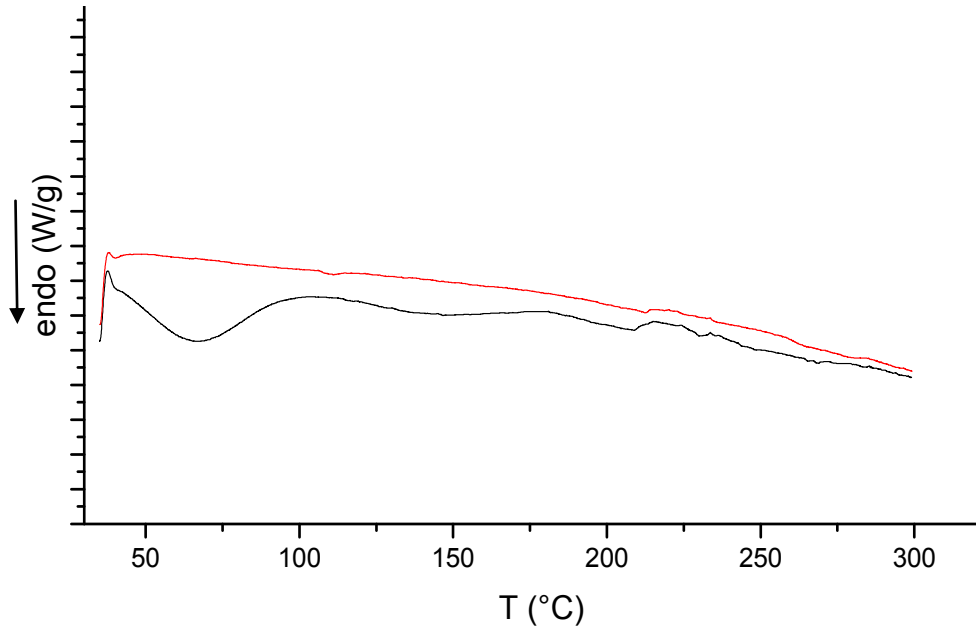


Figure 36: First (black) and second (red) DTA runs of Poly-(meta-phenylene isophthalamide)

In particular, two runs were conducted: the first (black curve) shows presence of an endothermic peak due to water loss (100 °C). This confirms typical hygroscopicity of polyamides; this is further demonstrated by thermogravimetric measurements with a weight loss below 100 °C.



Structural Characterization

Figure 37 shows FT-IR analysis of Poly(*meta*-phenylene isophthalamide) and its precursors (1,3-Phenylenediamine and isophthaloyl dichloride).

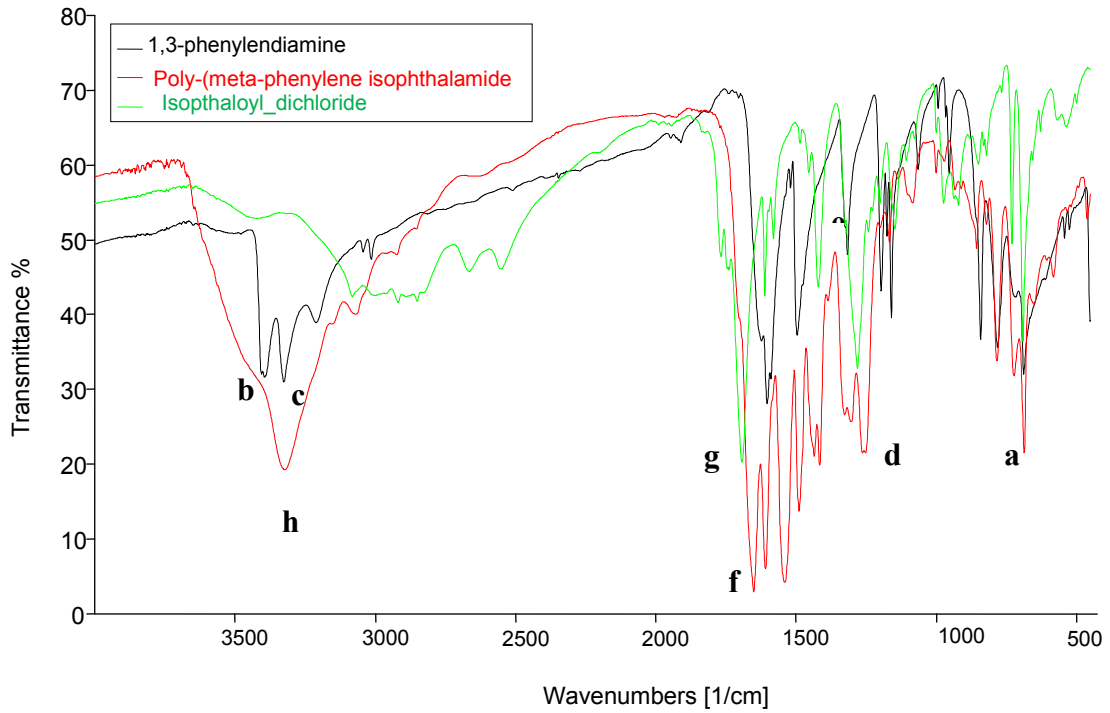


Figure 37: FT-IR analysis of Poly-(*meta*-phenylene isophthalamide) and its precursors (1,3-Phenylenediamine and isophthaloyl dichloride)



Table 10: signals of FT-IR analysis of Poly-(meta-phenylene isophthalamide) and its precursors (1,3-Phenylenediamine and isophthaloyl dichloride) (s = strong signal; m = medium; w = weak; sh = sharp; br = broad)

Bond	Wavenumbers (cm ⁻¹)
Aryl C-H bending	683-686 m sh (a)
Amine and amide N-H asymmetric stretching	3398 w (b)
Amine and amide N-H symmetric stretching	3327 w (c)
Amine aryl N-H bending	1315 (d)
Amide C-N stretching	1416 m sh (e)
Amine C-N stretching	1316 m sh (d)
Amide C=O stretching	1649 s sh (f)
Acyl C=O stretching	1692 s sh (g)
Salts of amine N-H stretching	3327 (h)

Spectrum relative to Nomex shows appearance of amidic characteristic signals, such as the amide C = O and amide N-H bonds. Both in the spectra of reagents and product there are signals related to aromatic C-H bond. C-N aromatic bond is evident both in Nomex and 1,3-phenylenediamine spectra. There are also typical reagents signals such as amine N-H bond of 1,3-Phenylenediamine and C = O bond of isophthaloyl dichloride, which disappear in final product.

Because obtained polymer was treated in acidulated water, we also recognize typical amine salts signals.

Oligomeric species constituting synthesized Poly(*meta*-phenylene isophthalamide) were recognized by means of MALDI-TOF(+) analysis in figure 38, which relatives peaks are then tabulated.

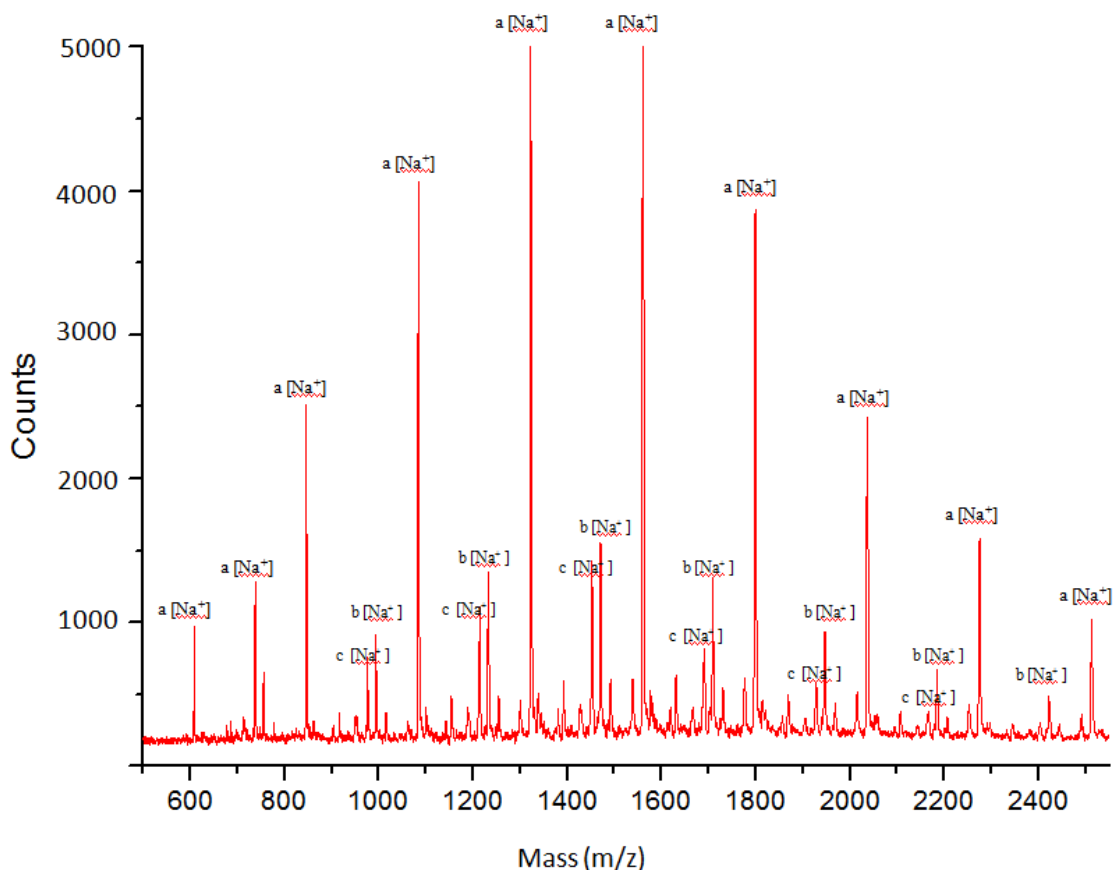
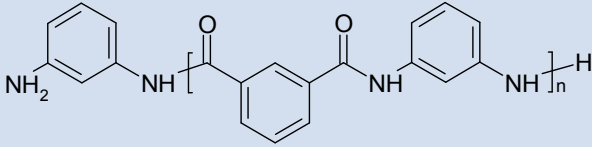
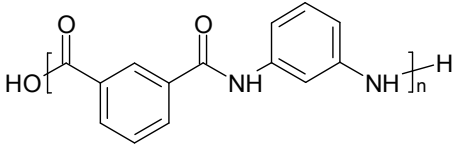
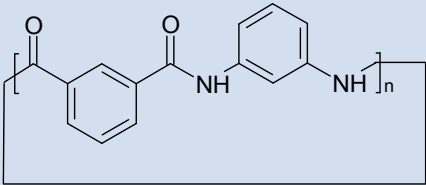


Figure 38: MALDI-TOF (+) spectrum of Poly(*meta*-phenylene isophthalamide), Matrix: IAA

Poly(*meta*-phenylene isophthalamide) is only little soluble and to obtain mass spectra was used REG (Resolving Evaporation Grinding) method⁶⁹, which make possible to have a MALDI spectrum from a solid phase sample. This method consists in the formation of a solid solution between matrix and sample and eventual cationizing agent. In particular, for Poly(*meta*-phenylene isophthalamide) analysis, we proceeded with the homogenization of samples in an agate mortar, using a molar ratio of matrix (IAA)/sample of 25:1 by adding 60 μ L of THF to facilitate homogenization; when the sample was dry, it was put on MALDI plate and pressed down. At the end, 1 μ L of THF was put on sample to enhance its adhesion with MALDI plate.

⁶⁹A. Gies and W. Nonidez: "A Technique for Obtaining Matrix-Assisted Laser Desorption/Ionization Time-of-Flight Mass Spectra of Poorly Soluble and Insoluble Aromatic Polyamides", *Macromolecules*, 2006, 39 (3), pp 941–947

Table 11: Structural peak assignment relative to mass spectrum in figure 38

Peaks	Oligomer Structures	m/z (n) [Na ⁺]
a		608 (2) 846 (3)
		1084 (4) 1322 (5)
		1561 (6) 1799 (7)
		2037 (8) 2275 (9)
		2513 (10)
b		994 (4) 1232 (5)
		1470 (6) 1709 (7)
		1947 (8) 2185 (9)
		2423 (10)
c		976 (4) 1214 (5)
		1452 (6) 1690 (7)
		1928 (8) 2167 (9)

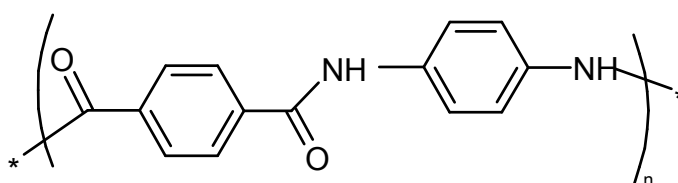
MALDI-TOF(+) spectrum of Poly(*meta*-phenylene isophthalamide) shows:

- ∞ the presence of an oligomeric distribution centered on hexameric unit,
- ∞ the existence both of linear and cyclic oligomers,
- ∞ amine or hydroxyl end groups.

To confirm Poly(*meta*-phenylene isophthalamide) structure were performed both mono-dimensional and bi-dimensional H¹-NMR analysis.

4.1.2 Synthesis and characterization of Poly(*p*-phenylene terephthalamide)

Poly(*para*-phenylene terephthalamide) is commercially known as “Kevlar” (Scheme 8), registered trademark developed by Stephanie Kwolek at DuPont in 1965⁷⁰. Its main characteristic is the large mechanical resistance to traction: five times stronger than steel (at equal weight)⁷¹: when Kevlar is spun, the resulting fiber has a tensile strength of about 3,620 MPa⁷².



Scheme 8: poly(*para*-phenylene terephthalamide)

High tensile strength at low weight, low elongation to break, structural rigidity, low electrical conductivity, high chemical resistance, low thermal shrinkage, high toughness, excellent dimensional stability, high cut resistance, flame resistant, self-extinguishing are all important characteristic making Kevlar a good filler for microelectronic Packaging.⁷³

Furthermore, poly(*para*-phenylene terephthalamide) has a high thermal conductivity: 10-30 W/Km^{74,75}: it was experimentally known that thermal conductivity value increase proportionally to temperature⁷⁶.

The polymer owes its high strength to the many inter-chain bonds between the carbonyl groups and NH centers (Scheme 9).

⁷⁰ Stephanie Kwolek, Hiroshi Mera and Tadahiko Takata “High-Performance Fibers” in Ullmann's Encyclopedia of Industrial Chemistry 2002, Wiley-VCH, Weinheim.

⁷¹ Kevlar Technical Guide, <http://www.dupont.com>

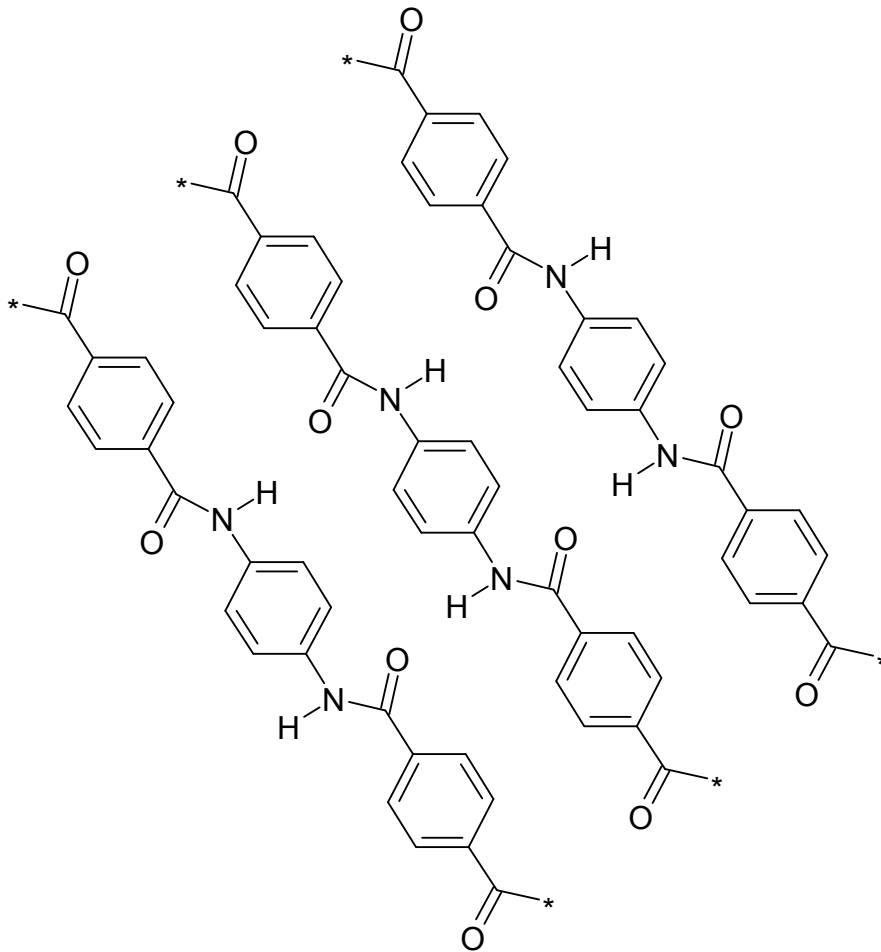
⁷² Quintanilla, J. "Microstructure and properties of random heterogeneous materials: a review of theoretical results". Polymer engineering and science, **39** (1990): pp. 559–585

⁷³ Mark J.E., “Polymer Data Handbook”, Oxford Univ. Press, 1999, pp.140-155.

⁷⁴ Poulaert, B., et al. Polym. Commun. 26(5) (1985).

⁷⁵ Choy, C. L., et al. J. Polym. Sci., Part B: Polym. Phys., 33(14) (1995).

⁷⁶ G. Ventura, V. Martelli: “Thermal conductivity of Kevlar 49 between 7 and 290 K”, Cryogenics Volume 49,2009, Pages 735–737.



Scheme 9: Molecular structure of Kevlar with inter-chain interconnections.

Additional strength is derived from aromatic stacking interactions between adjacent strands. These interactions have a greater influence on Kevlar than the van der Waals interactions. The presence of salts and certain other impurities, especially calcium, could interfere with the strand interactions and care is taken to avoid inclusion in its production. Kevlar's structure consists of relatively rigid molecules which tend to form mostly planar sheet-like (Figure 39) structures.⁷⁷

⁷⁷ Michael C. Petty, *Molecular electronics: from principles to practice*, John Wiley & Sons, 2007, p. 310.

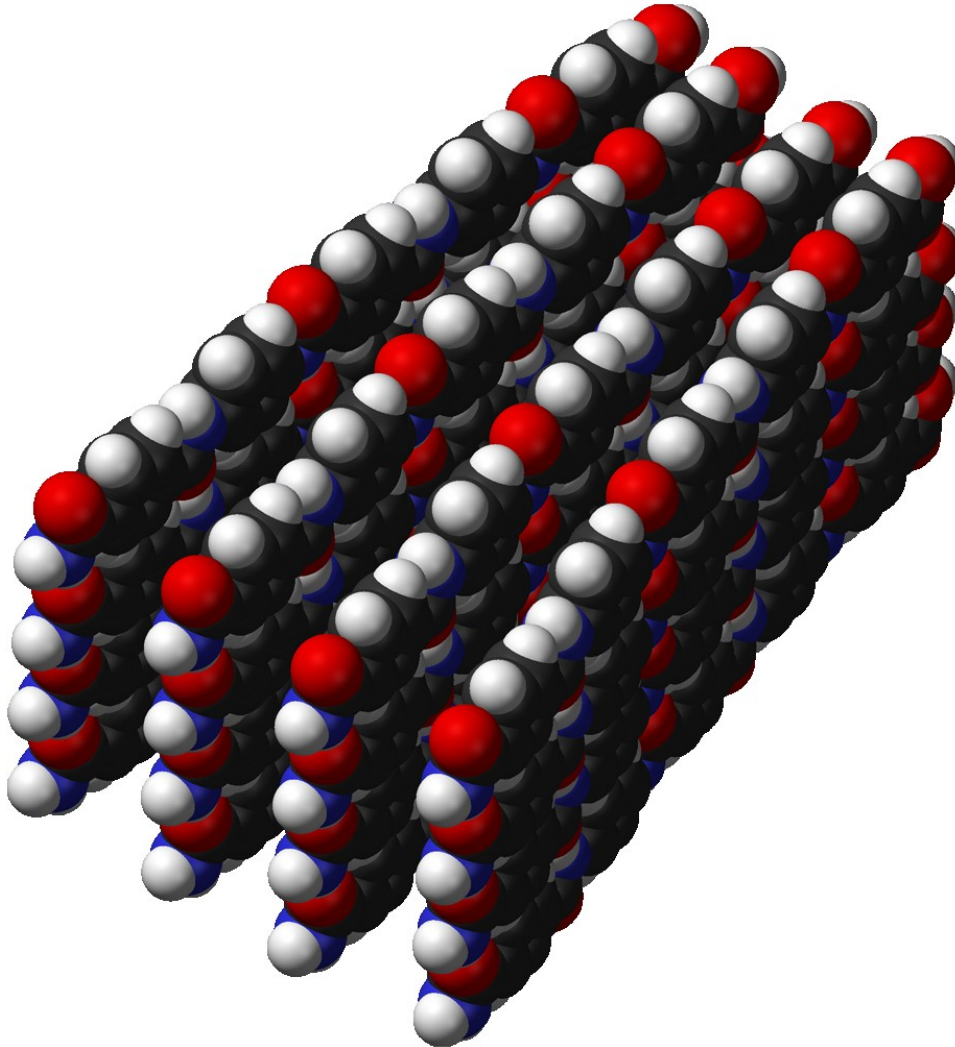
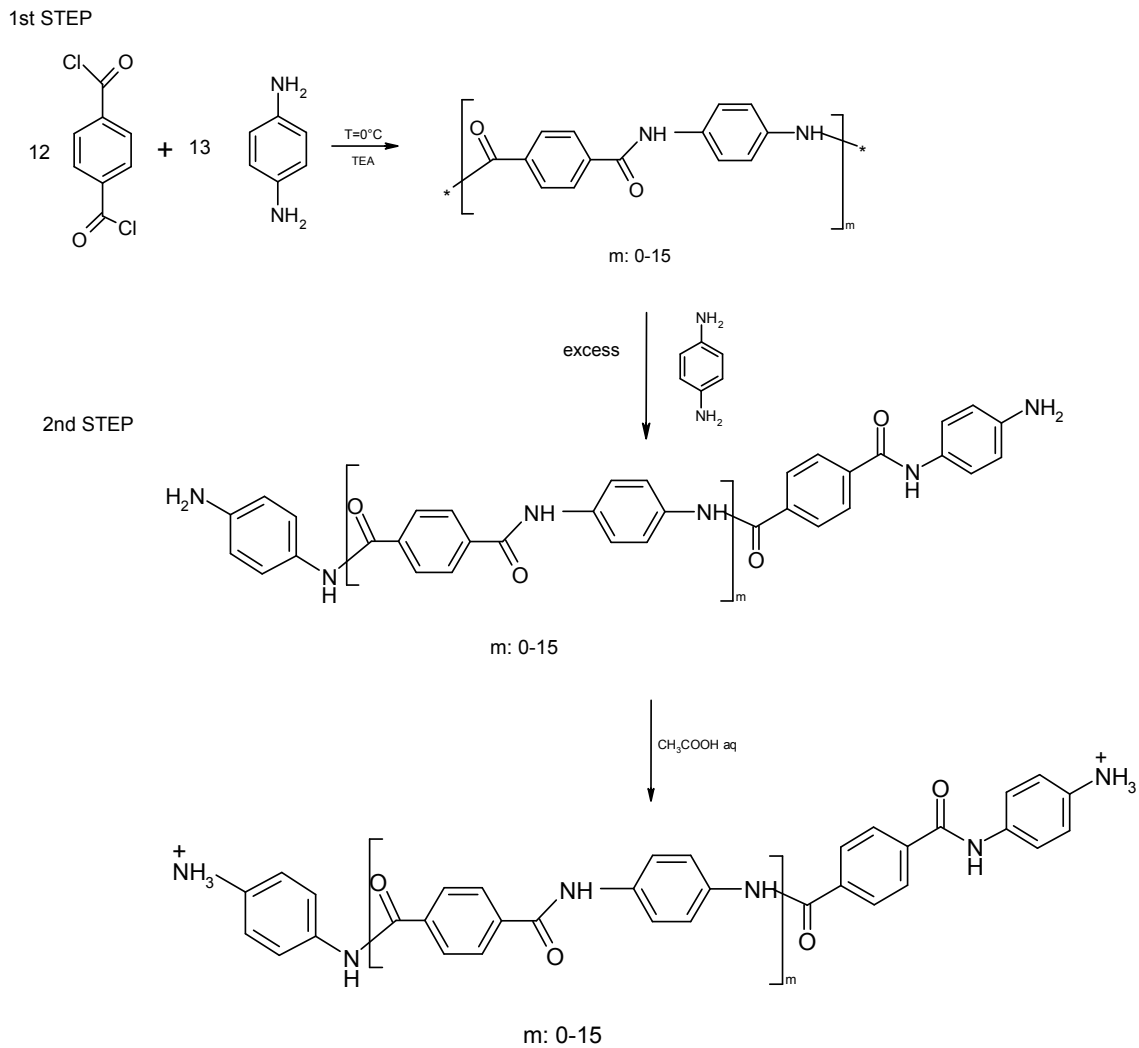


Figure 39: aromatic π -stacking between Kevlar planar-sheets

To obtain approximately 6 g of Poly(*para*-phenylene terephthalamide) having a polymerization degree of about 12, were used 2.4 g of 1,4-Phenylenediamine (0.022193 mol) and 4.3 g of terephthaloyl chloride (0.019542 mol), in a molar ratio 13:12 (Scheme 10), according to *Equation 3* and experimental evidences.

Synthesis proceeds in the same way as already described for the poly(*meta*-phenylen isophthalamide), except for solvent mixture THF/DMF equal to 60:40.



Scheme 10: Synthesis of poly(*p*-phenylene terephthalamide)

Poly(*para*-phenylene terephthalamide) was thermally and structurally characterized by means of TGA, DTA, MALDI-TOF, FT-IR and $^1\text{H-NMR}$.

Thermal Characterization

Figures 40 shows TGA analysis in air or nitrogen atmosphere of Poly(*para*-phenylene terephthalamide) and relative derivative curves.



4. Fillers

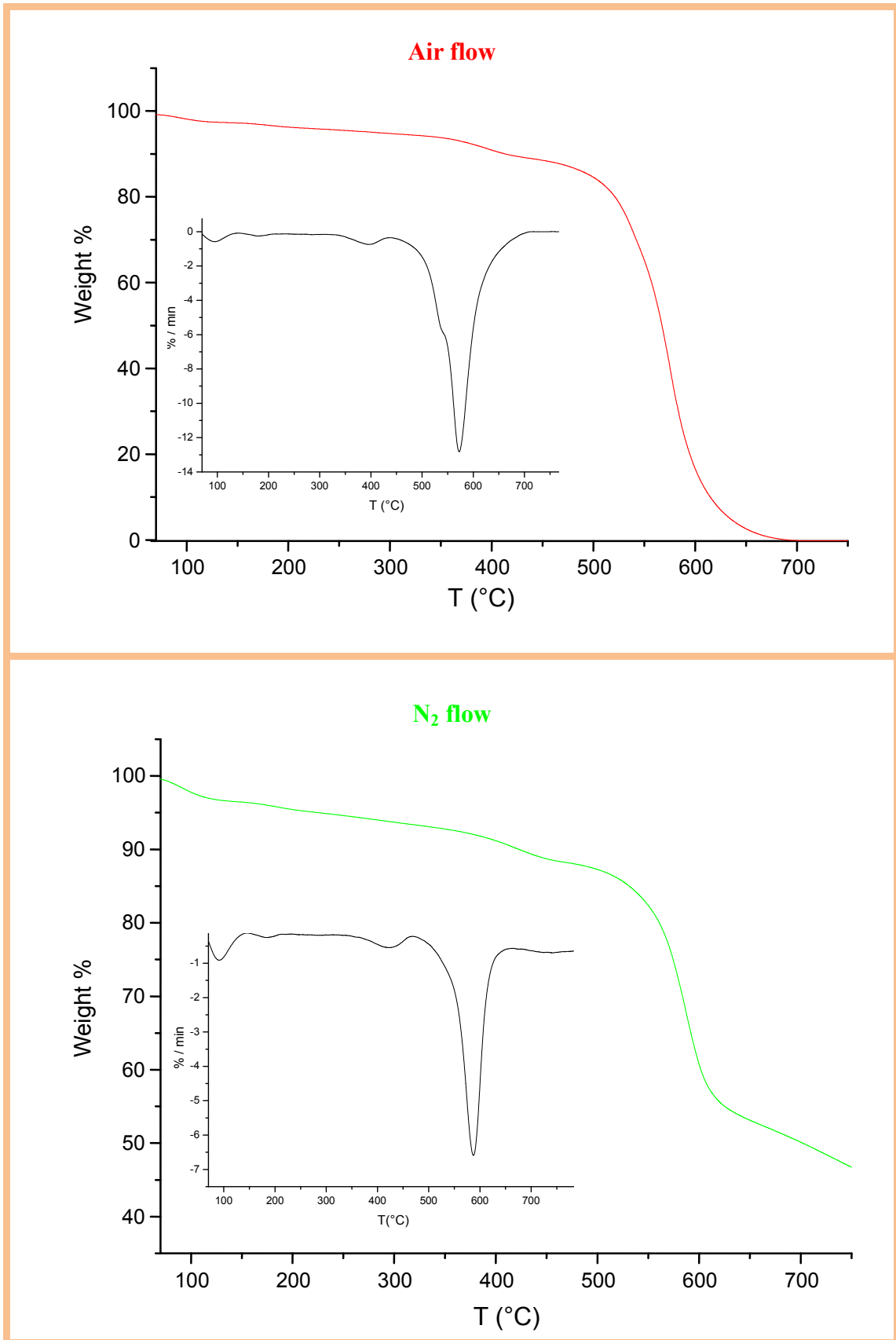


Figure 40: TGA analysis of poly(*para*-phenylene terephthalamide) and relative derivative curves

Thermograms shows that Poly(*para*-phenylen terephthalamide) analyzed in air flow starts to degrade at 514 °C, reaching a maximum rate of degradation at 572 °C. In nitrogen flow, degradation begins at 542 °C and maximum rate at 587 °C. Furthermore, the residual percentage of Poly(*para*-phenylen terephthalamide) in air flow is zero (totally oxidized) while in nitrogen flow is 44%.

DTA analysis (figure 41) don't shows any particular event; two runs were conducted: the first (black curve) shows presence of an endothermic peak due to water loss (100 °C), confirming typical hygroscopicity of polyamides.

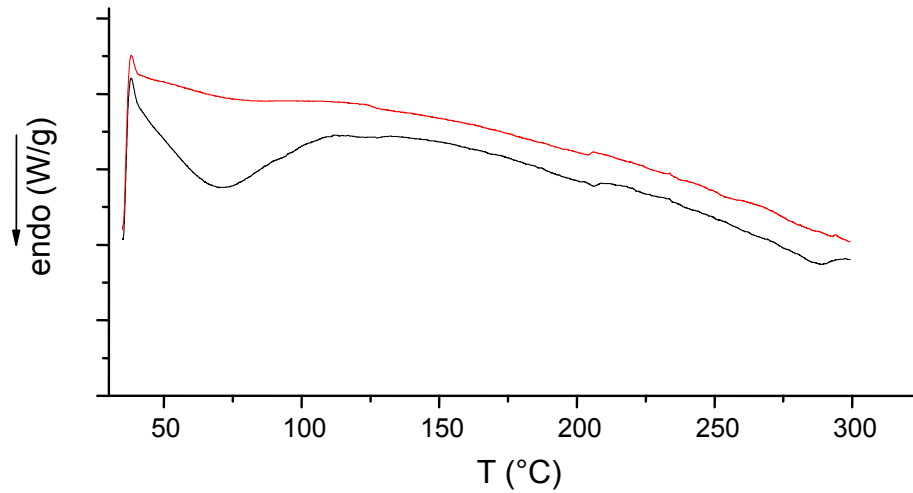


Figure 41: DTA thermogram of Poly(*para*-phenylen terephthalamide)

Structural Characterization

Figure 42 shows FT-IR analysis of Poly(*para*-phenylene terephthalamide) and its precursors (1,4-Phenylenediamine and terephthaloyl dichloride).

Characteristic signals are tabulated following (Table 12).



4. Fillers

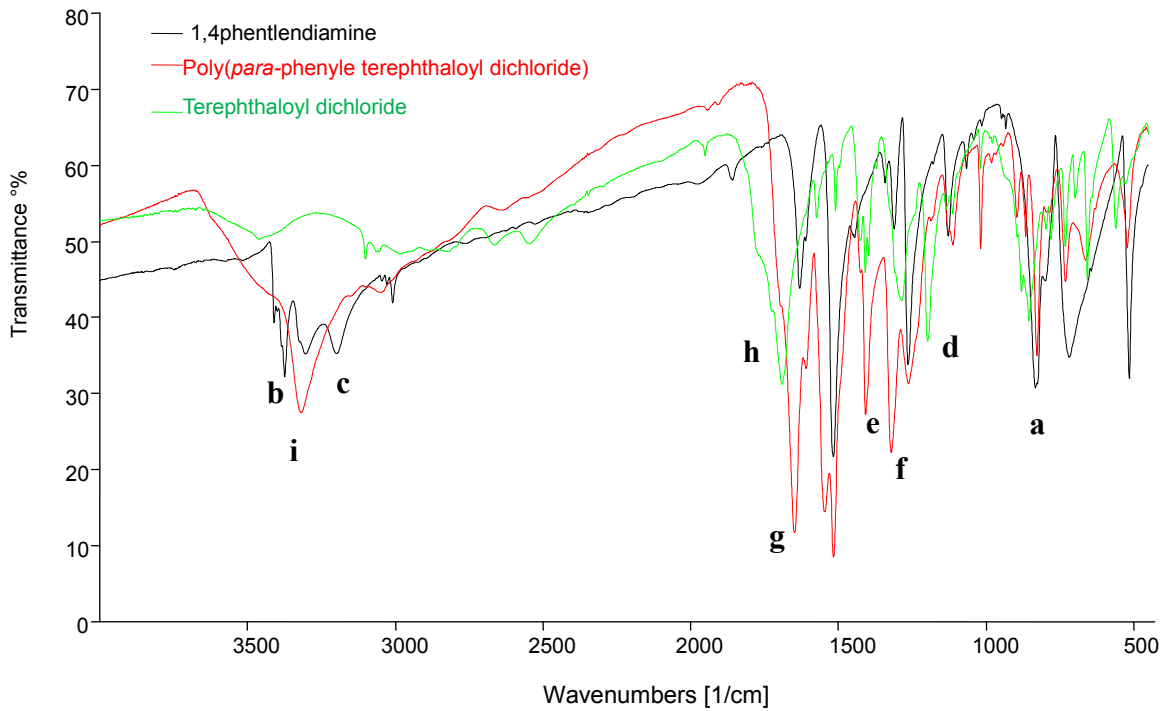


Figure 42: FT-IR analysis of Poly-(*para*-phenylene terephthalamide) and its precursors (1,4-Phenylenediamine and terephthaloyl dichloride).

Table 12: resins FT-IR signals

(s = strong signal; m = medium; w = weak; sh = sharp; br = broad)

Bond	Wavenumbers (cm ⁻¹)
Aromatic C-H bond (bending)	824-860 m sh (a)
Amine and amide N-H bond (stretching asymmetric)	3302 w (b)
Amine e amide N-H bond (stretching symmetric)	3196 w (c)
Amine aryl N-H (bending)	1263 (d)
Amide C-N (stretching)	1407 m sh (e)
Amine aryl C-N (stretching)	1309 m sh (f)
Amide C=O (stretching)	1646 s sh (g)
Acyl C=O (stretching)	1692 m (h)
Amine salt N-H (stretching)	3320 (i)

From spectrum signals can be observe the appearance of characteristic polyamidic signals, such as the amide C=O bond (1646 cm^{-1}) and amide N-H bond ($3302\text{-}3196\text{ cm}^{-1}$). Aromatic C-N bond (1309 cm^{-1}) is found both in the spectrum of polyamide and in 1,4-phenylenediamine. Characteristic reagents signals are the amine N-H (1263 cm^{-1}) of 1,4-Phenylenediamine and the C=O of terephthaloyl dichloride (1692 cm^{-1}), which disappear in the final product. Cause polyamide amine end groups were protected by reaction with acetic acid, FT-IR shows salts of amine absorption.

Poly(*para*-phenylene terephthalamide) is insoluble and to obtain MALDI-TOF mass spectra was used REG⁷⁸ method. In figure 43 is reported MALDI-TOF(+) spectrum and subsequently oligomeric species are tabulated (Table 13).

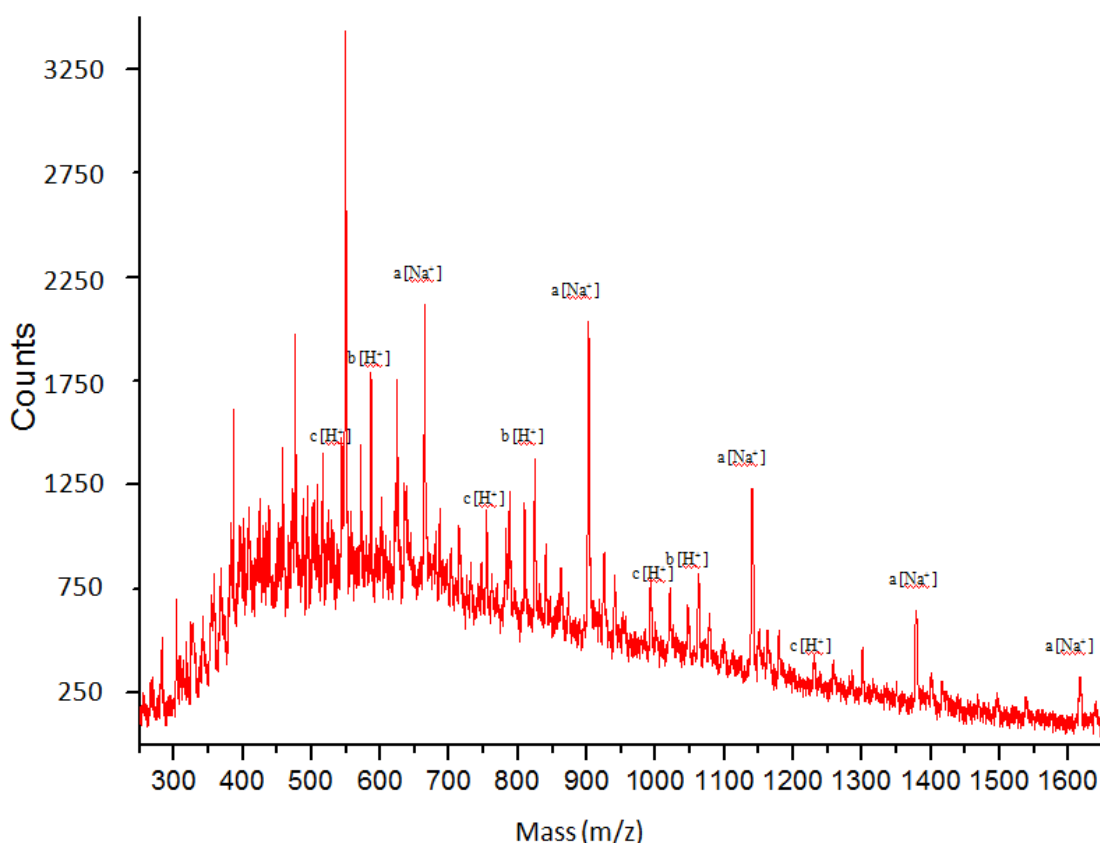


Figure 43: MALDI-TOF (+) spectrum of Poly(*para*-phenylene terephthalamide)

⁷⁸A. Gies and W. Nonidez: "A Technique for Obtaining Matrix-Assisted Laser Desorption/Ionization Time-of-Flight Mass Spectra of Poorly Soluble and Insoluble Aromatic Polyamides", *Macromolecules*, 2006, 39 (3), pp 941–947.

Table 13: Oligomeric structures observed by MALDI-TOF (+) mass spectra of Poly(*para*-phenylene terephthalamide)

Series	Oligomer Structures	H ⁺ (n)	Na ⁺ (n)
a		664 (2)	
		902 (3)	
		1140 (4)	
		1378 (5)	
		1617(6)	
b		586 (2)	
		824 (3)	
		1062 (4)	
c		517 (2)	
		755 (3)	
		993 (4)	
		1231 (5)	

MALDI TOF signals of poly(*para*-phenylene terephthalamide) are not very pronounced, for this reason we get further confirmation by making the acquisition in negative (figure 44): can be observed oligomers having as terephthalic or amine terminal groups (Table 13).

Table 14: Oligomeric structures observed by MALDI-TOF (-) mass spectra of Poly(*para*-phenylene terephthalamide)

Series	Oligomer Structures	M ⁻ (n)
a		403 (1)
		641 (2)
		878 (3)
b		493 (2)
		730 (3)

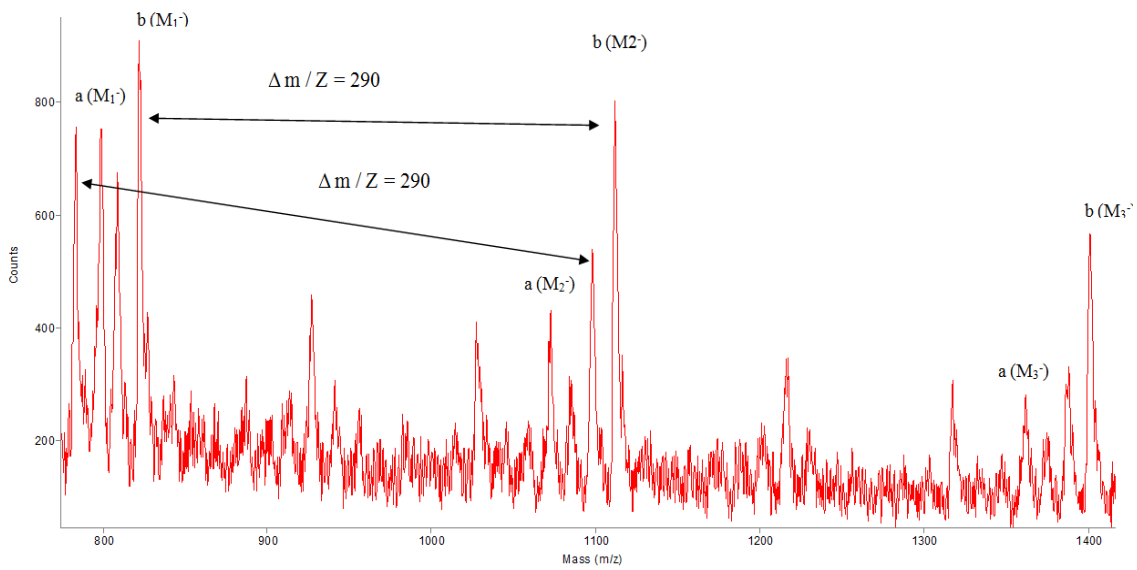


Figure 44: MALDI-TOF (-) spectrum of Poly(*para*-phenylene terephthalamide)

¹H-NMR analysis of Poly(*para*-phenylene terephthalamide), had confirmed structures.

4.1.3 Characterization of Kelin 130⁷⁹

As commercial polyamidic filler was used a woven of poly(*para*-phenylene terephthalamide), Kelin 130. In order to use it as a filler of epoxy resin the woven has been appropriately broken into small fibers (figure 45).



Figure 45: picture Kelin 130

⁷⁹ Courtesy of "Spin Tech International s.r.l." Via G. Galilei, 16 - 25030 Adro (BS) Italy.



4. Fillers

Kelin was thermally characterized by means of TGA: Figure 46 shows obtained thermograms in nitrogen or in air atmosphere with relative derivative curves.

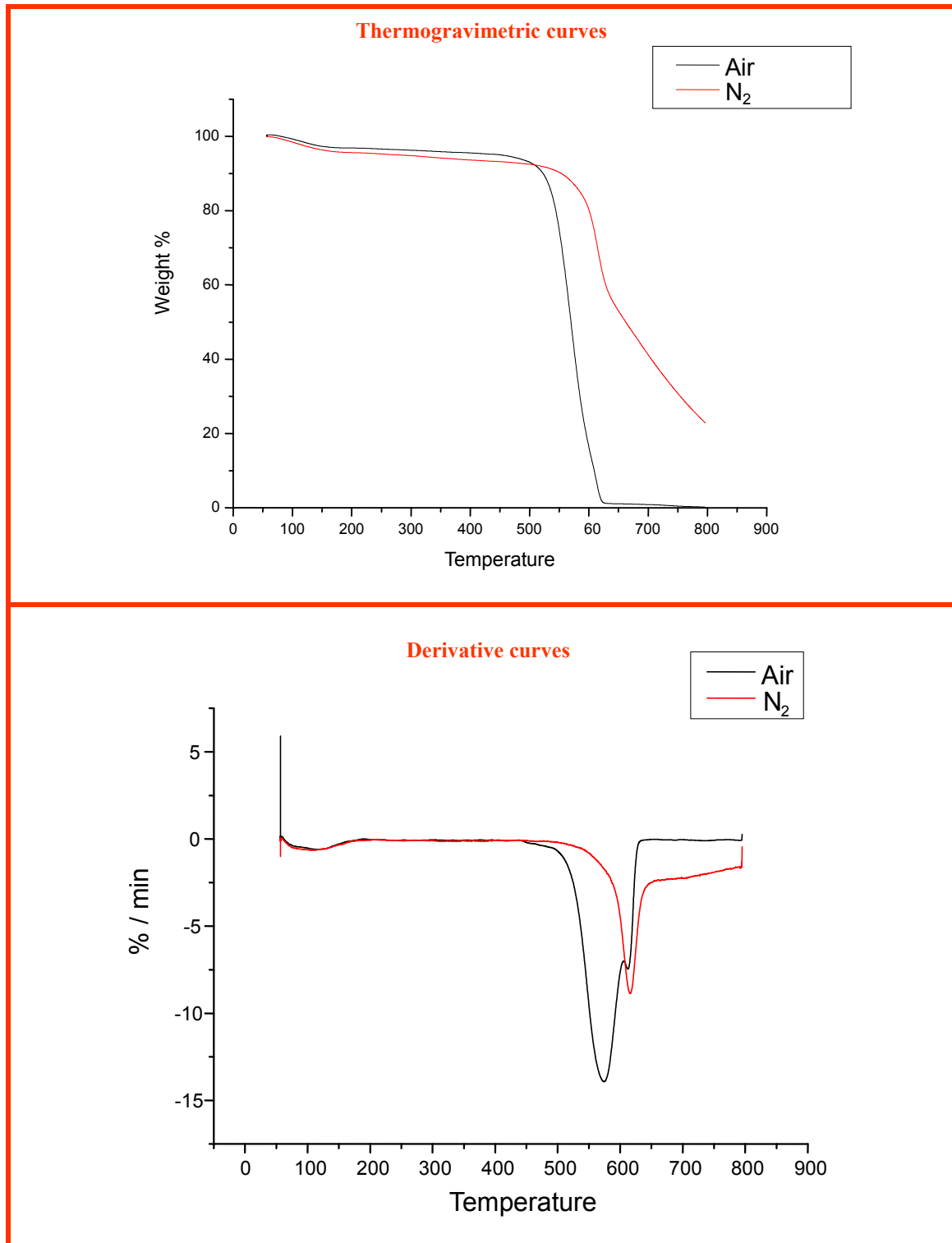


Figure 46: TGA analysis of Kelin 130

The TGA analysis shows that Kelin130 has a beginning degradation temperature in nitrogen atmosphere equal to 495 °C while in air, cause oxidative events, degradation starts already at 447 °C. Furthermore, in air atmosphere, sample is totally oxidized, not presenting any final residue after analysis, while in nitrogen is observed the presence of a char equal to 22.9% of the initial weight.

The highest degradation rate (%/min), as shown by derivative curves, is reached at 625 °C or 572 °C respectively in nitrogen or air atmosphere.

In recent years commercial poly(*para*-phenylen terephthalamide) have been studied using thermal analysis, thermogravimetry and thermomechanical analysis⁸⁰.

The volatile products of poly(*para*-phenylen terephthalamide) at the beginning of decomposition, have been analyzed by mass spectrometry⁸¹ which showed the presence of: CO, CO₂, H₂O, Benzene, Aniline, Benzonitrile, Hydrogen cyanide, Formamide, Cyanhydric acid and Benzoic acid.

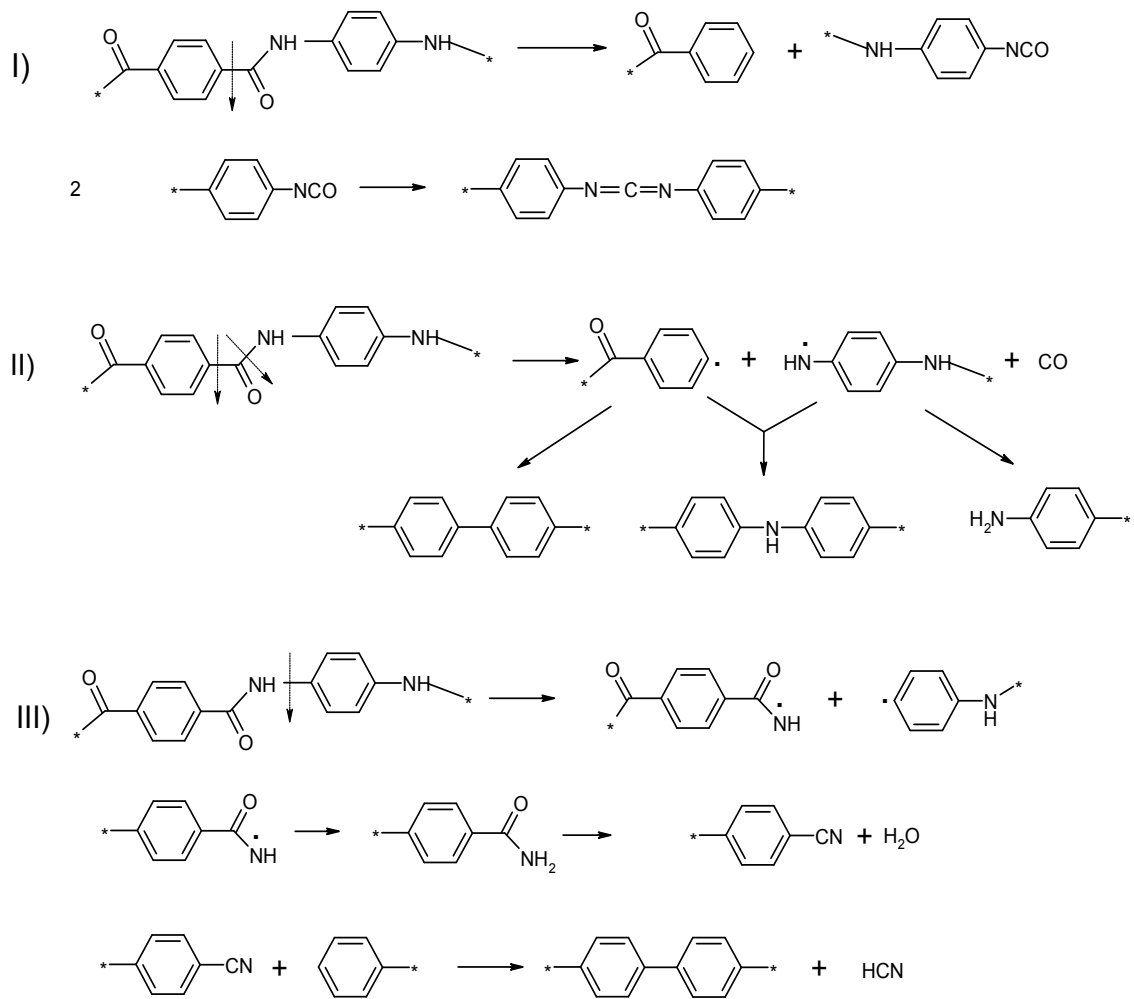
Solid phase degradation products include *para*-phenylenediamine and N-amino phenylbenzamide.

The mechanism that have proposed to account for some of these products⁸² is shown in Scheme 11. They all involve initial scission of the ester linkage.

⁸⁰ J.R. Brown, B.C. Ennis. *Textile Res. J.*, 47 (1977), p. 62

⁸¹ T. Kalashnik, V.Ya. Yefremov, N.V. Mikhailov, G.I. Kudryavtsev, A.M. Shchetinin, N.P. Panikarova, M.A. Dubrovina, Yu.P. Pankratov: "The kinetics and mechanism of the heat and thermal-oxidative stability of aromatic polyamides" *Polymer Science U.S.S.R.*, Vol. 14 (1972) pp. 1567-1574

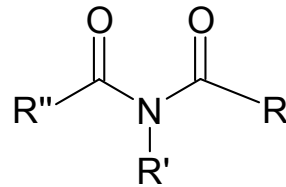
⁸² R.T.Conley, R.A Gaudiana: "Thermal and Oxidative Degradation of Polymers".R.T. Conley, M. Dekker, New York,1970, Vol. 1, p. 347.



Scheme 11: Thermal degradation mechanisms of poly(*para*-phenylene terephthalamide)

4.2 Polyimidic filler

Polyimides are characterized by imide functional group, they can be obtained by condensation of an anhydride with an aminic or a diisocyanate group (Scheme 12).⁸³



Scheme 12: imide group

They are polymers for high temperature uses: may be exposed for a long time at temperatures above 300 °C. Their chemical resistance is good, although they can be degraded by acidic or basic solutions.

They are used in the electricity sector as paints or lacquers insulation in electric motors and other devices.⁸⁴

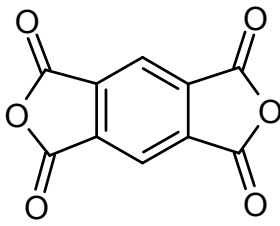
They can be used in as is or as composites filled with graphite, PTFE, glass wool, or metal powders as a reinforcement to parts subject to high stress. Polyimides are chemically classified as homo-polyimides or modified polyimide, ie also containing amide linkages, ester or ether. The purpose of modification is to obtain stable materials such as non-modified, but much more processable.⁸⁵

Unmodified polyimides are prepared by means of polycondensation of aromatic dianhydrides with aromatic diamines. In general, dianhydrides used are shown in Scheme 13.

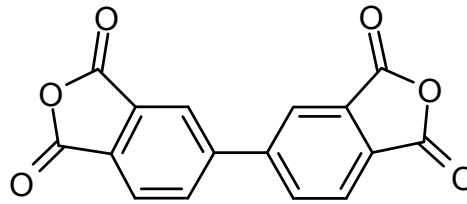
⁸³ N. A. Adrova, et al., "Polyimides, A New Class of Heat-Resistant Polymers", pp. 4-13, Jerusalem, (1969).

⁸⁴ J. D. Hensel: "When, where and how to use polyimides", *Plastics Eng.* 33 (10), 20 (1977).

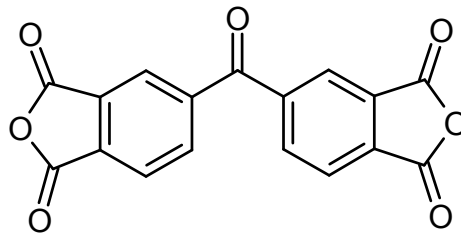
⁸⁵ M.W.Ranney: "Polyimide manufacture", *Chem. Progr. Rev.*, Vol. 54, Noyes Data Corp., New Jersey (1969).



Pyromellithic anhydride



3,3',4,4' diphenyl-tetracarboxylic anhydride



3,3',4,4'- benzophenonic anhydride

Scheme 13: Principal di-anhydrides used for polyimides synthesis

The synthesis is conducted in two steps⁸⁶. In the first the diamine is dissolved in a polar solvent and the dianhydride is added to it while maintaining temperature below 50 °C (the reaction is fast and exothermic). It forms a viscous solution of prepolymer called polyamic acid.

The second phase of this process is the *imidization*: it consists on condensation of polyamic acid to form polyimide. This reaction is carried out by heating at 150-200 °C with a final treatment to 300 °C to stabilize material.

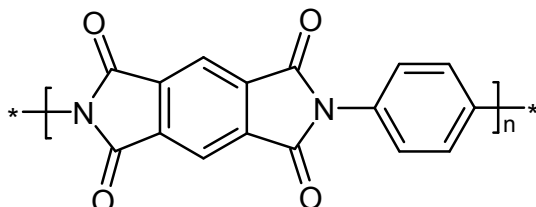
Elimination of water (byproduct) is very important to avoid alteration of final product shape. To facilitate the elimination of water, is added acetic anhydride and pyridine.

As Polyimidic filler for packaging composites has been synthesized the Poly(*para*-phenylen pyromellitimide) as follow described.

⁸⁶ T. Takekoshi : “*Polyimides- Fundamentals and Applications*”, Ed. Ghosh, M.K. and Mittal, K.L., Marcel Dekker, New York (1996)Chapter 2.

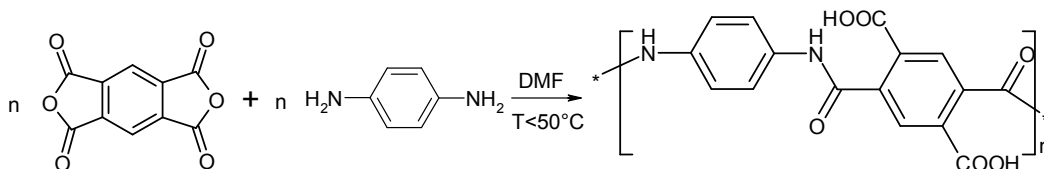
4.2.1 Synthesis and characterization of Poly(*para*-phenylen pyromellitimide)

Poly(*para*-phenylen pyromellitimide) (Scheme 14) was obtained into two-step synthesis.



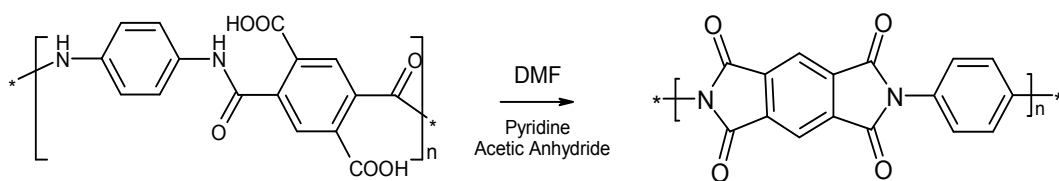
Scheme 14: Poly(*para*-phenylen pyromellitimide)

The first step was carried out in solution starting from 3.4 g (15.5963 mmol) of pyromellitic anhydride and 1.68 g (15.5963 mmol) of *para*-phenylenediamine in 1:1 ratio. Reagents dissolved in DMF (anhydrous) were kept under stirring at room temperature for a time of three days, then polyamic acid is formed (Scheme 15), colorful yellow.



Scheme 15: Polyamic acid synthesis

In the second step, in order to favorite polyamic acid condensation, to solution were added 2.52 ml (31.1927 mmol) of pyridine and 1.89 ml (31.193 mmol) of acetic anhydride (Scheme 16). Then the mixture was heated at 150°C and then at 300°C for 2 h. Finally, obtained product is in solid state.



Scheme 16: Polyamic acid condensation



Structural Characterization

To follow this reaction, were performed MALDI-TOF characterizations of a sample extracted during reaction and a sample of end product. Obtained spectra are shown in Figures 47 and 48 and the corresponding signals are indicated in Tables 15 and 16 respectively.

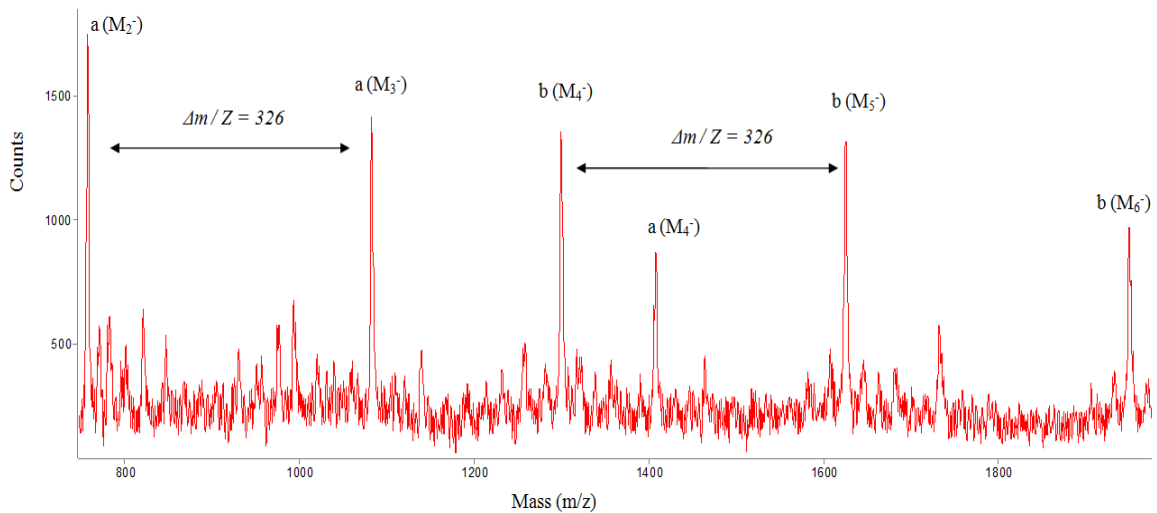


Figure 47: MALDI-TOF spectrum of polyamic acid

Table 15: Oligomeric species observed in MALDI-TOF (-) spectrum of polyamic acid

Series	Struttura oligomeri	M ⁻ (n)
a		759 (2)
		1085 (3)
		1411 (4)
b (cyclic)		1303 (4)
		1629 (5)
		1955 (6)

Table 15 shows that the first sample extracted is a mixture of low oligomers of polyamic acid having amino end groups (a), due the excess of *para*-phenylenediamine used, or cyclic species (b).

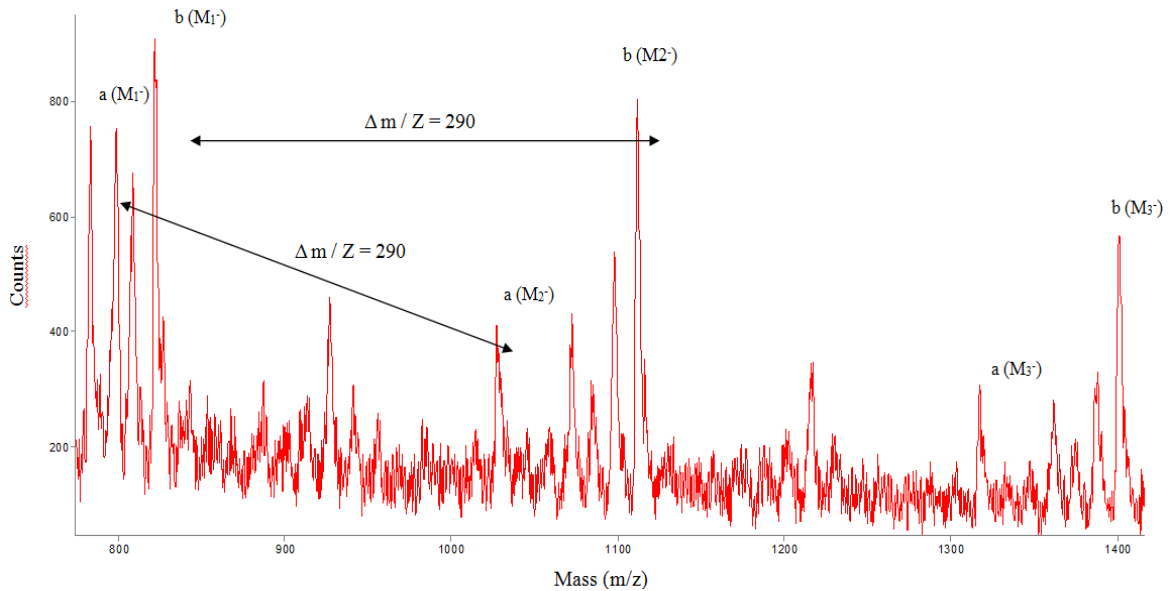


Figure 48: Spettro di massa MALDI-TOF (+) della Poli-(paraphenylene pyromellitimide)

Table 16: Oligomeric species observed in MALDI-TOF (-) spectrum of poly(*para*-phenylene pyromellitimide)

Series	Oligomeric Structures	M ⁽ⁿ⁾
a		784 (1) 1074 (2) 1364 (3)
b		826 (1) 1116 (2) 1406 (3)



4. Fillers

It is evident as final product of reaction is aromatic polyimide acid, whose terminal groups are pyridinium salt: the presence of pyridinium salt is due use of pyridine during the second stage of reaction in order to favor the condensation of polyamic acid.

Reaction mechanism is confirmed by FT-IR analysis of reagents (*para*-phenylenediamine and pyromellitic anhydride), polyamic acid and poly(*para*-phenylen pyromellitimide).

Comparative spectra are presented in Figure 49 and related signals are shown in Table 17.

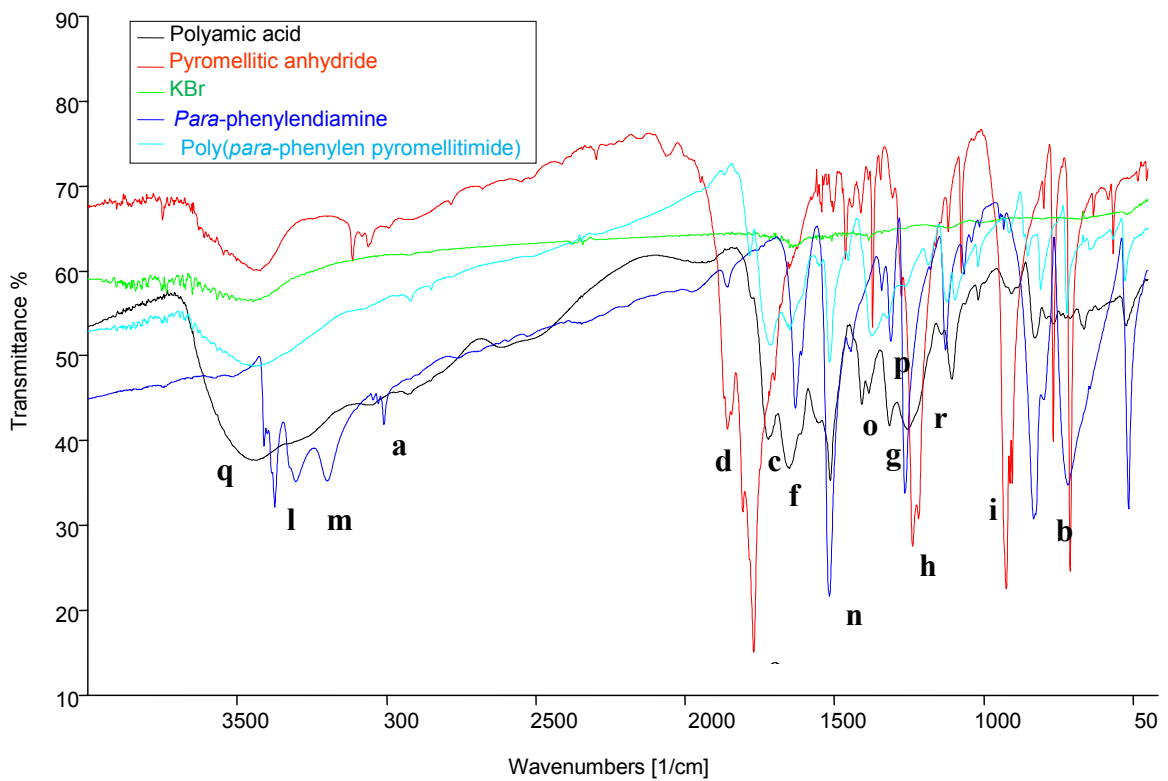


Figure 49: FT-IR spectra of Polyamic Acid, Pyromellitic Anhydride, KBr, *para*-phenylenediamine, poly(*para*-phenylen pyromellitimide).



Table 17: signals of FT-IR analysis of Poly(*para*-phenylene pyromellitimide) and its precursors (*para*-Phenylenediamine, pyromellitic anhydride and polyamic acid) (s = strong signal; m = medium; w = weak; sh = sharp; br = broad)

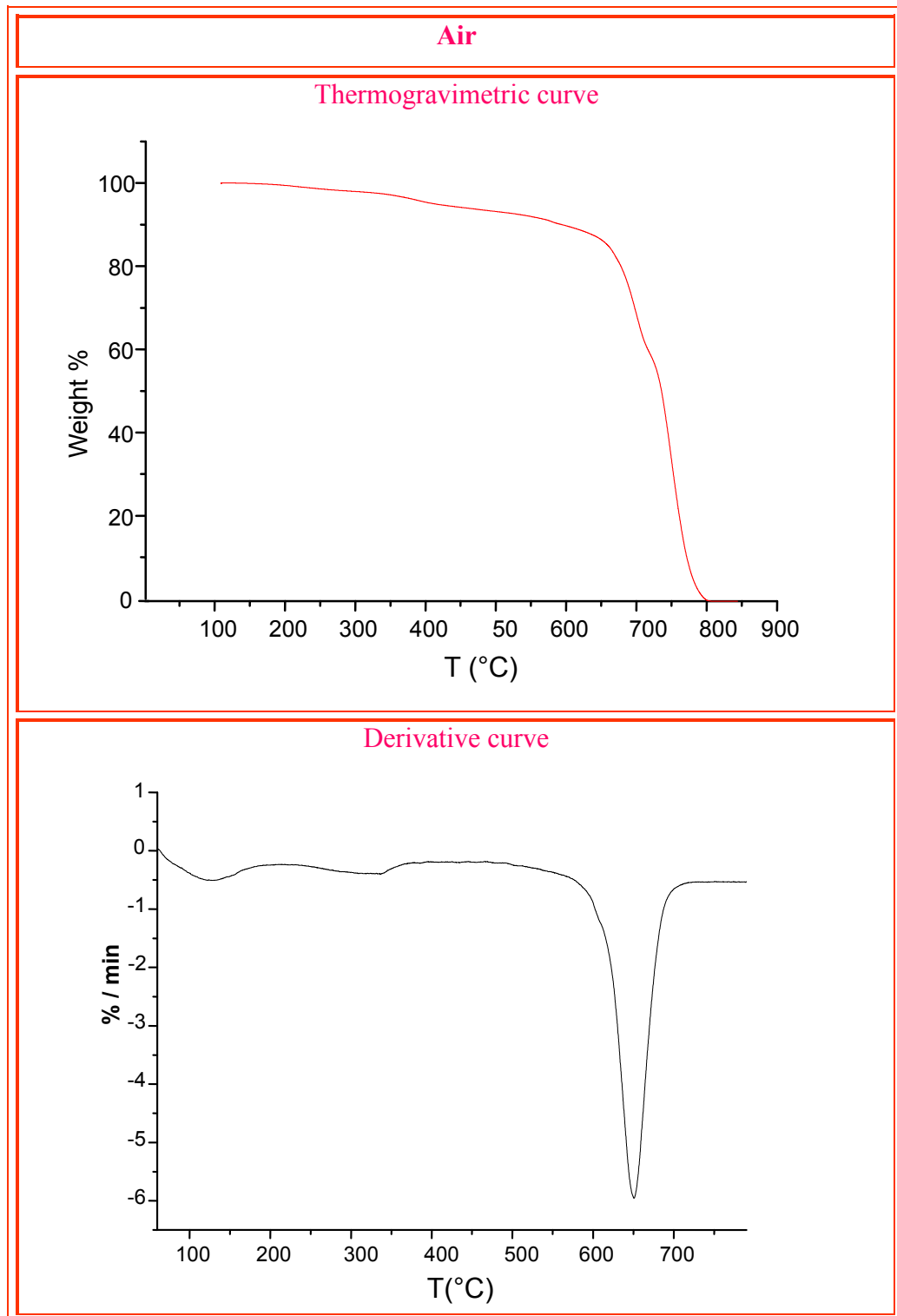
Bond	Wavenumber (cm ⁻¹)
Aryl C-H bond (asymmetric stretching)	3118-3008 w sh (a)
Aryl C-H bond (bending)	831-796 m sh (b)
Aryl carboxyl C=O bond	1723 m sh (c)
Aryl anhydride C=O bond (symmetric stretching)	1862 m sh (d)
Aryl anhydride C=O bond (asymmetric stretching)	1766 s sh (e)
Aryl amidic C=O bond (stretching)	1653 m b (f)
Carboxylic C-O bond (stretching)	1317 w sh (g)
Anhydridic C-O bond (stretching)	1235 s sh (h) 924 s sh (i)
Aminic N-H bond (asymmetric stretching)	3302 m br (l)
Aminic N-H bond (asymmetric stretching)	3196 m br (m)
Aminic N-H bond (bending)	1518 s sh (n)
Aminic C-N bond (stretching)	1407 m sh (o)
Aryl aminic C-N bond	1309 w sh (p)
Carboxylic O-H bond (stretching)	3451 m br (q)
Carboxylic O-H bond (bending)	1316 m sh (r)

FT-IR analysis shows the obtaining of the poly(*para*-phenylene pyromellitimide). It's possible to observe characteristic signals relative to stretching vibrations of aminic N-H bond (l, m, n). These signals are totally absent in both polyamic acid and polyimide, confirming that amino group becomes amide and imide respectively. Also it is possible to notice that in FT-IR spectrum of pyromellitic anhydride (one of reactants) there is a strong signal relative to asymmetrical stretching of aryl anhydridic C = O bond (e); this signal decreases until disappear in polyimide. Even O-H (q) bond stretching is a proof of the reaction mechanism because it is can found only in polyamic acid.



Thermal Characterizations

Thermal analysis (TGA) of the poly(*para*-phenylen pyromellitimide) were carried in air or N₂ atmosphere. Thermograms obtained are shown in Figure 50.



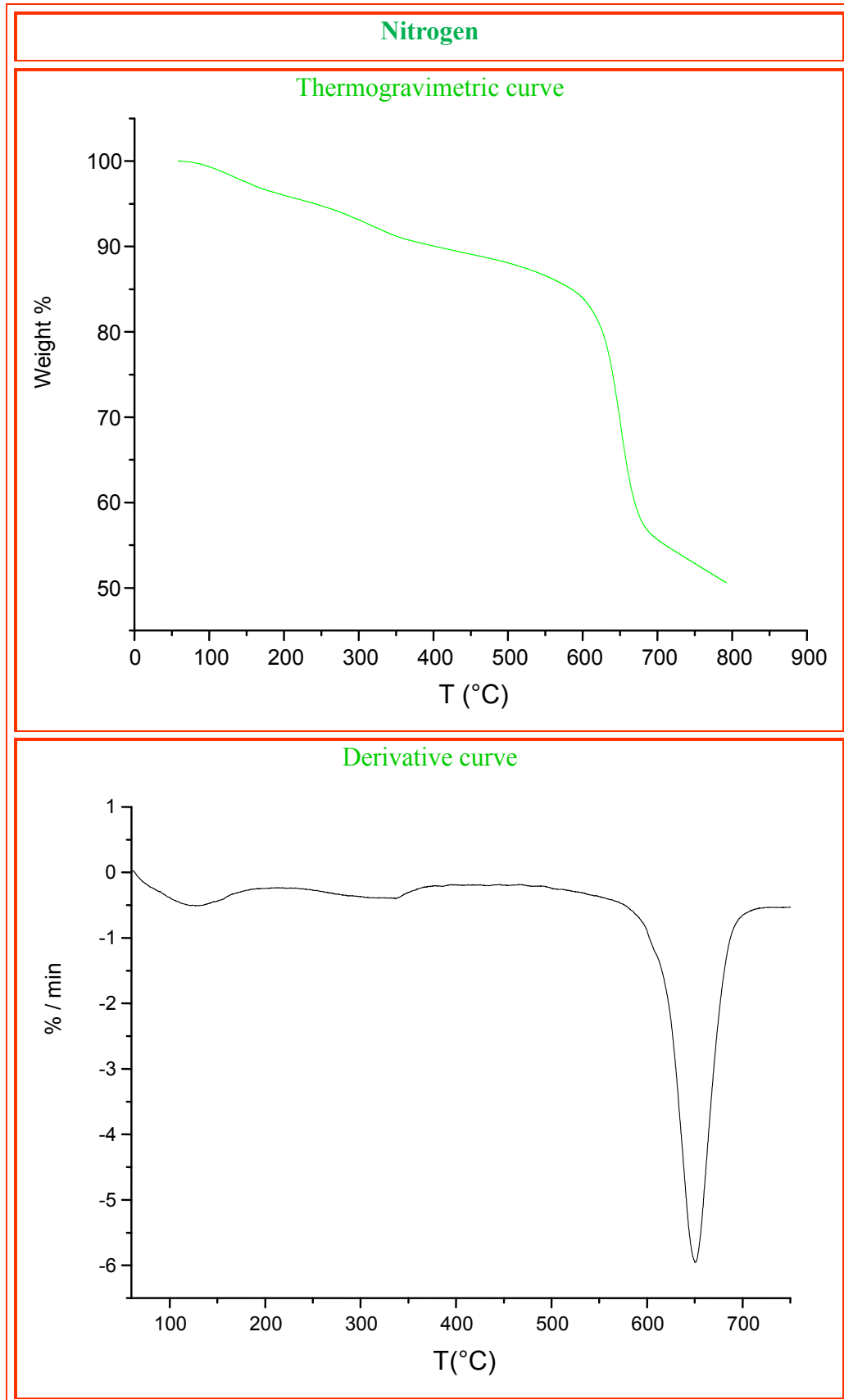


Figure 50: Thermogravimetric and derivative curves of poly(para-phenylene pyromellitimide) analyzed in air or nitrogen atmosphere



4. Fillers

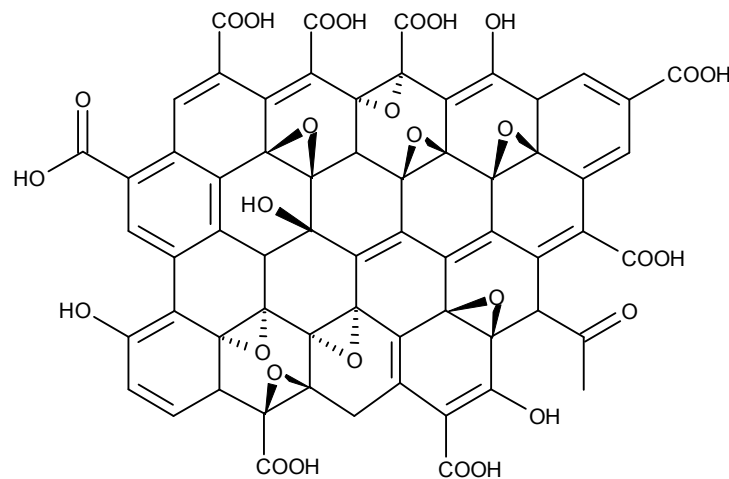
TGA analysis show that poly(para-phenylen pyromellitimide), both in air and nitrogen, starts to degrade at 613 °C and reaches maximum degradation rate in air at 695 °C and in nitrogen at 650 °C. Residual char in air flow is zero because polyimide is completely oxidized. Instead, when it is analyzed under nitrogen atmosphere residual char is about 50%.

4.3 Graphenoxidic filler

Graphene is pure carbon in the form of a very thin sheet and it conducts heat and electricity with great efficiency. Thermal conductivity at RT (room temperature) of graphene is $4.84\text{-}5.30 \times 10^3 \text{ W}\cdot\text{m}^{-1}\cdot\text{K}^{-1}$.⁸⁷

Graphene oxide (GO) is a layered material produced by graphite oxidation. In contrast to graphite, the graphene oxide is highly oxygenated, with C:O ratio between 2.1 and 2.9.⁸⁸

GO has hydroxyl and epoxy functional groups on the basal planes, in addition to carbonyl and carboxylic groups located at the edges of the planes (Scheme 17).



Scheme 17: Graphene oxide structure

The synthesis of graphene oxide was performed by the modified method of Hummers and Offeman⁸⁹.

This synthetic method⁹⁰ has the aim of π bonds breakage and involves:

- * the dispersion of graphite powder in a solvent (H_2SO_4),

⁸⁷ A. A Balandin, S. Ghosh, W. Bao, I. Calizo, D. Teweldebrhan, F. Miao: "Superior Thermal Conductivity of Single-Layer Graphene", Nano Letters ASAP 8 (3): 902–907 (2008).

⁸⁸ H. He, J. Klinowski, M. Forster; A. Lerf: "A new structural model for graphite oxide", Chemical Physics Letters, (1998): 287: 53.

⁸⁹ W. S. Hummers, R. E. Offeman: "Preparation of Graphitic Oxide". Journal of the American Chemical Society 80 (6), (1958).

⁹⁰ Thanks for cooperation in GO synthesis and characterization, Prof. G. Compagnini and Dr. G. Isgrò of Thin Films and Nanostructures Laboratory of the University of Catania - Department of Chemical Sciences.

- * the intercalation in the graphitic structure of an oxidant agent, consisting of a mixture of KMnO_4 and NaNO_3 .

In particular, a becker with 1 g of graphite powder with 1 g of NaNO_3 and 46 ml of H_2SO_4 were put in ice bath, under stirring. Then 6 g of KMnO_4 were added and the reaction was carried on for 1 hour at 35-40 °C.

Deionized water and 3 ml of hydrogen peroxide were added to the solution and the temperature was raised to 90°C and then lightly centrifuged.

After this, the supernatant solution, dark yellow colorful, was centrifuged several times in order to remove small GO pieces and water-soluble product.

GO, typically, preserves the layer structure of graphite, but the layers are buckled and the interlayer spacing is about two times larger (~0.7 nm) than that of graphite.

GO is a poor conductor, but its partial reduction restores some of the properties of graphite starting approaching it to graphene properties.

Characterization

In Figure 51 are reported thermogravimetric analysis, in nitrogen flow, of Graphenoxide obtained as previously described.

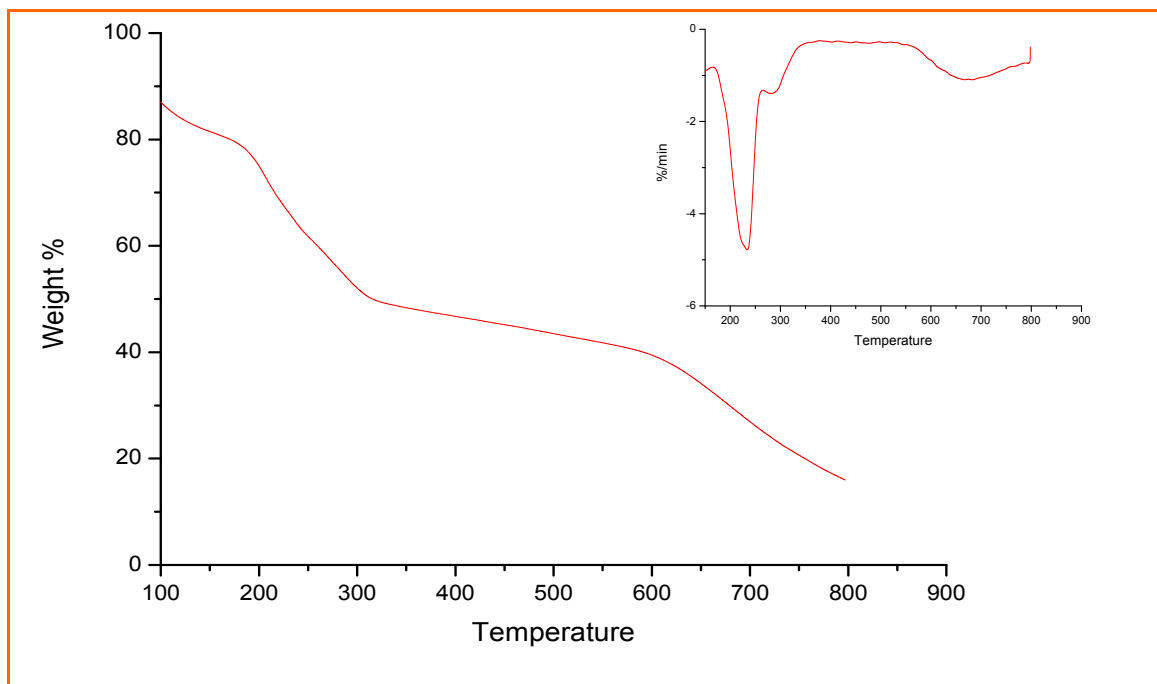


Figure 51: GO thermogravimetric analysis, in air flow, and relative derivative curve (insert)



Thermogravimetric analysis shows that, particular GO oxydate structure, makes it degrades easily, probably starting with decarboxylation and epoxy ring opening, that catalyze other structural degradations.

FT-IR spectrum (figure 52) allows to confirm GO structure, showing characteristic signals for O-H bond(3420 cm^{-1}), C=O bond (1735 cm^{-1}), aromatic C=C bond (1622 cm^{-1}), epoxy bond ($1220, 1050, 890\text{ cm}^{-1}$) and C–O bond (1110 cm^{-1})⁹¹ vibrational transitions.

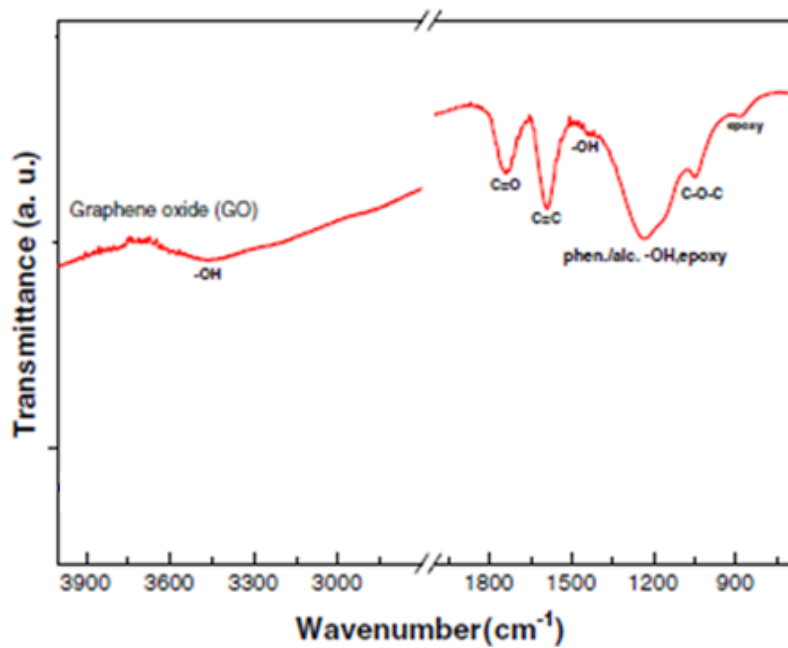


Figure 52: FT-IR spectrum of Graphene oxide

⁹¹ C. Gonget al. *J. Phys.Chem. C* 116, 9969 (2012)

5. Composites

As previously described, packages of commercial electronic device were analyzed to study its composition and chemical-physical properties: it was found they are based on polymers (epoxy resins, polyesters, polyamides).

Also their filler content was evaluated, by means of thermogravimetry; these analysis show that filler range amount is from about 30% to 90% by weight. Besides, FT-IR analysis revealed that Silica is the main used filler.

In Chapter 3 various epoxy resins have been described as possible polymeric matrix for composites; all these resins were obtained using the same prepolymer (DGEBA) and varying the type of curing agent. After thermal properties determination of obtained resins, DGEBA/DETA was that chosen, but for analytical purpose were used even other curing agents.

Therefore, it was designed a series of composites having DGEBA/DETA epoxy resin as polymer matrix and suitable fillers capable to improving thermal efficiency of the final product compared to commercial materials.

To check how they change resin properties, different organic or inorganic fillers were used. Particularly, were employed, in addition to silica as comparative filler to commercial package, aramides, polyimides, graphene oxide and MoS₂ (see Chapter 4).

Weight percentage of filler in composites was 33%, although for analytical purposes were also prepared some composites containing 10%.

5.1 Synthesis of composites

Composites were obtained by heating DGEBA, then adding filler and homogenized thoroughly. Curing agent (DETA or Examethylendiamine or Ethylendiamine) was added and crosslinking reaction begin placing reactants mixture in a thermoblock at 155 °C for 2 hours under Nitrogen atmosphere.

All composites have a molar ratio DGEBA/Curing agent equal to 3:2 and percentage of filler is equal to 10% or 33% by weight. Obtained composites are tabulated in Table 18.

Table 18: Obtained composites with relative employed fillers

Composites	Filler (%)
1) NOM.10D (Curing agent: DETA)	Poly(<i>m</i> -phenylen isophthalamide) (10 %)
2) NOM.10H (Curing agent: Hexamethylenediamine)	Poly(<i>m</i> -phenylen isophthalamide) (10 %)
3) NOM.10E (Curing agent: Ethylenediamine)	Poly(<i>m</i> -phenylen isophthalamide) (10 %)
4) NOM.33 (Curing agent: DETA)	Poly(<i>m</i> -phenylen isophthalamide) (33 %)
5) KEV.33 (Curing agent: DETA)	Poly(<i>p</i> -phenylen terephthalamide) (33%)
6) SIL.33 (Curing agent: DETA)	High Pressure Silica, diameter:0.04- 0.63 μm (33%)
7) KAP.33 (Curing agent: DETA)	Poly(<i>p</i> -phenylen pyromellitimide) (33%)
8) GO.33 (Curing agent: DETA)	Graphenoxide (33%)
9) MO.33 (Curing agent: DETA)	Molybdenum disulphure (33%)
10) KEL.33 (Curing agent: DETA)	Kelin 130 ⁹² (33%)

⁹² Courtesy of “Spin Tech International s.r.l.” Via G. Galilei, 16 - 25030 Adro (BS) Italy.



5.2 Composites Characterization

In order to determine their thermal efficiency, all composites, previously described, were thermally characterized by means of TGA and DTA. In particular, TGA analysis allowed to obtain information about composites start degradation temperature and, therefore, the range of usability of each composite. DTA analysis, however, allowed to verify chemical stability of various composites, underlining the presence of any not degradative thermal events.

For some composite was also made an evaluation of the thermal conductivity by means of direct or indirect methods.

5.2.1 TGA and DTA analysis of "NOM.10" type composites

"NOM.10" composites were obtained, as seen in Table 18, using three different curing agents, and a meta-aramid filler, poly(*m*-phenylen isophthalamide), with a percentage of 10% by weight.

Thermogravimetric analyzes of these composites were conducted in air and in nitrogen flow. Corresponding thermograms are shown in Figure 53 and relative data are shown in Table 19.

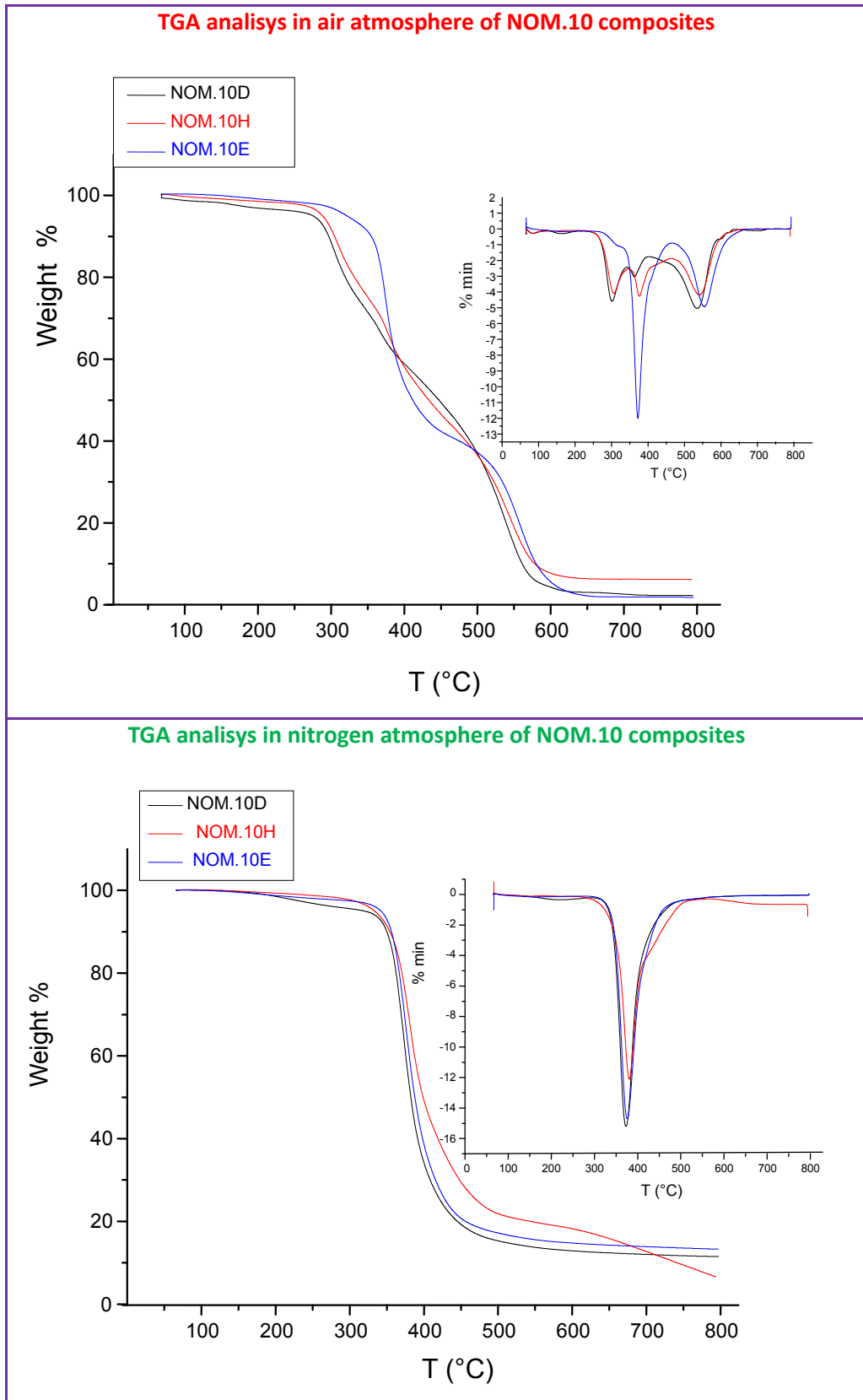


Figure 53: Thermograms, in air and nitrogen flow, of NOM.10 composites; the insert shows the derivatives curve



Table 19: Thermogravimetric data

Composites	Gas flow	T _{onset} (°C)	PDT (°C)	% residue
NOM.10D	air	280,6	301,3	3
	N ₂	348,5	372,9	11
NOM.10H	air	281,8	306,2	6
	N ₂	350,1	380,6	7
NOM.10E	air	350,4	372,3	2
	N ₂	349,9	375,8	7

Tabulated data shows that composites, heated both in air or in nitrogen atmosphere, begin to degrade at a temperature between 300 °C and 350 °C. Furthermore, these systems reach a maximum speed of degradation between 300 °C and 380 °C. Char percentage, 7-11% under nitrogen atmosphere, is higher than in air flow (2-6 %), as expected with an organic filler.

Comparing thermogravimetric data, relative to resins, it can be observed that the composite begin to degrade at just lower temperature (Table 20). Anyway these temperatures allow the use of these composites for packaging applications.⁹³

⁹³www.st.com/st-web-ui/static/active/en/resource/technical/document/datasheet/DM00099968.pdf



Table 20: Thermogravimetric data relatives to NOM.10 composites and relative non filled resins.

Sample	Gas flow	T _{onset} (°C)
DGEBA/DETA	air	349,6
	N ₂	353
NOM.10D	air	280,6
	N ₂	348,5
DGEBA/Etylendiamine	air	348,9
	N ₂	350,6
NOM.10E	air	350,4
	N ₂	349,9
DGEBA/Hexamethylendiamine	air	346,2
	N ₂	360,5
NOM.10H	air	281,8
	N ₂	350,1
poly(<i>m</i> -phenylen isophthalamide)	air	532
	N ₂	432

NOM.10 composites also were analyzed by DTA , showing no thermal events; relative curves are shown in Figure 54.

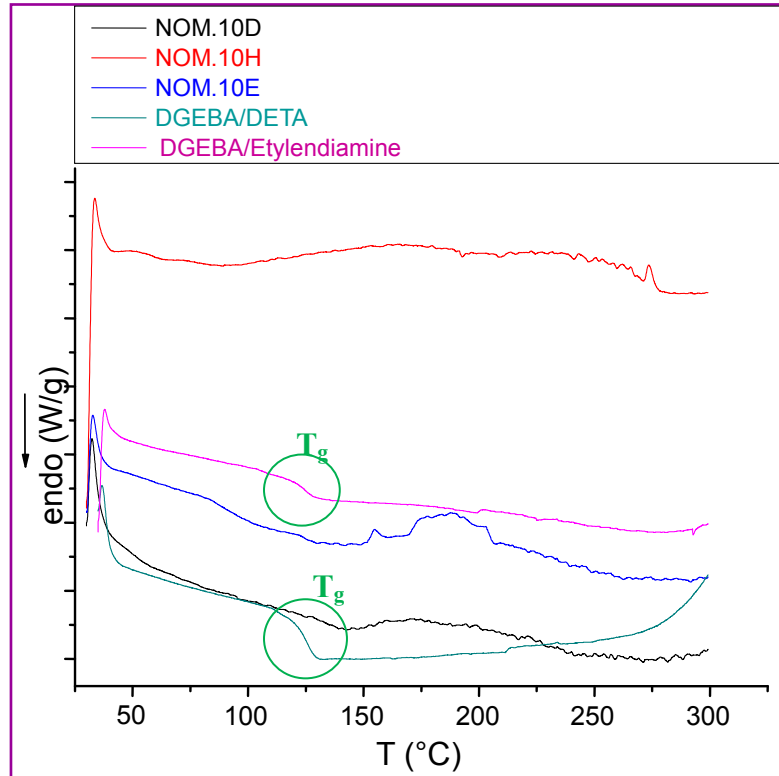


Figure 54: DTA curves of NOM.10 composites and two resins for which it was previously observed a glass transition

Making a comparison between DTA curves of composites and those of two resins, for which it was previously observed a glass transition, it can be observed that filler determines, under the same polymerization conditions, the disappearance of glass transition. Therefore, filler addition gives a structural improvement to final systems.

5.2.2 FT-IR analysis of NOM.10 composites

Structural characterization of obtained composites were carried on by means of FT-IR spectroscopy. Derivative spectra are shown in Figure 55 and relative signals are shown in Table 21.

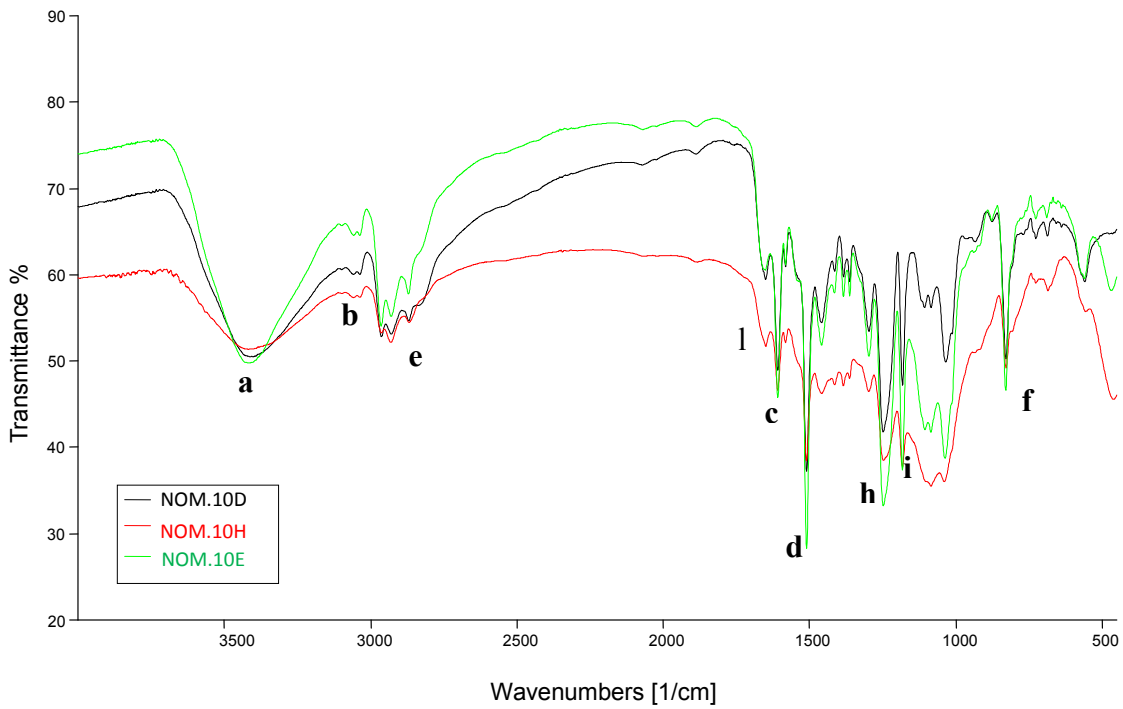


Figure 55: FT-IR spectra of NOM.10 composites

Table 21: NOM.10 composites FT-IR signals
(s = strong signal; m = medium; w = weak; sh = sharp; br = broad)

Bond	Wavenumbers (cm ⁻¹)
O-H (stretching)	3420 m br (a)
Methylic C-H (stretching)	2829-2962 w (b)
Aryl C-C (stretching)	1603 m sh (c) 1510 w sh (d)
Aryl C-H (stretching)	3047 w (e)
Aryl C-H (bending)	828 m sh (f)
Aryl-alkil ether C-O-C (asymmetric stretching)	1247 m sh (h)
Aryl-alkil ether C-O-C (symmetric stretching)	1182 m sh (i)
Amide C=O (stretching)	1649 s sh (l)

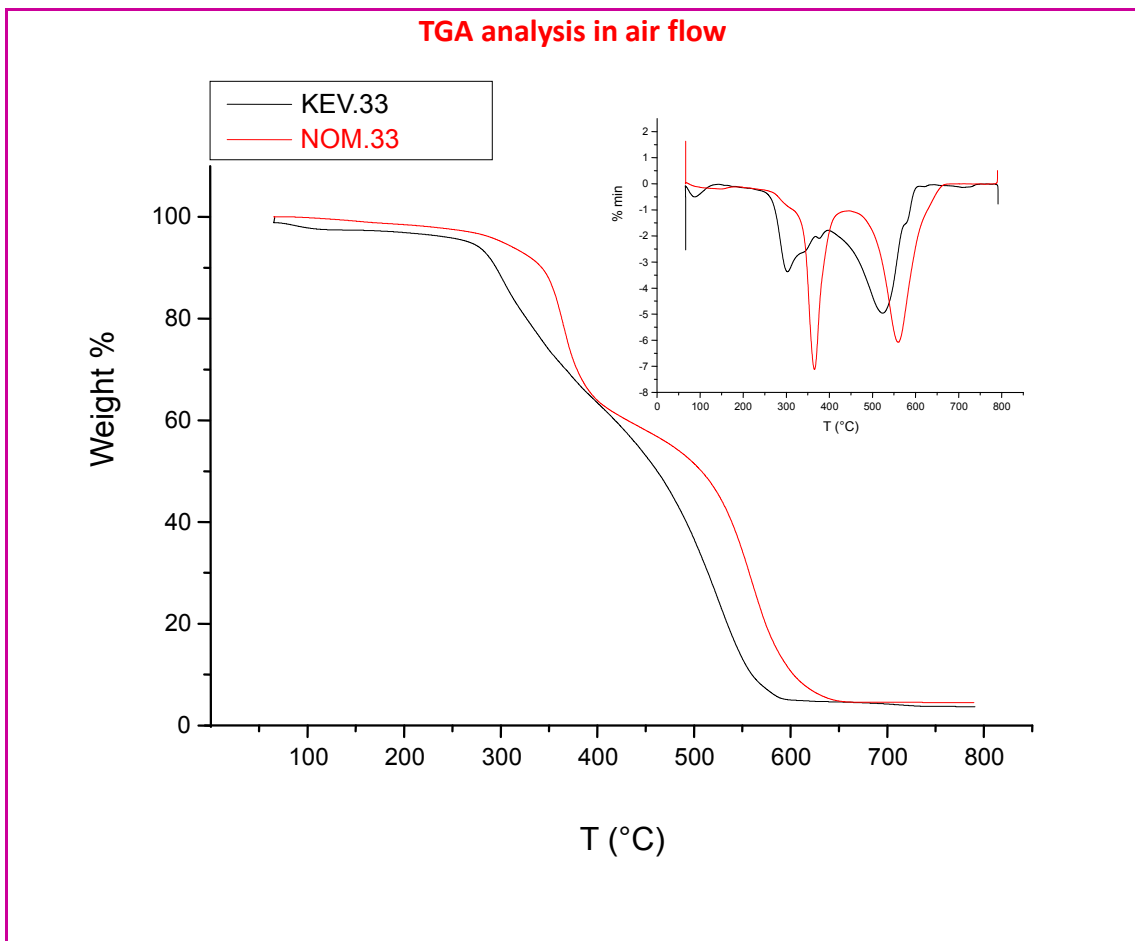


FT-IR spectra show a strong hydroxyl bond absorption (3420 cm^{-1}), due both to water traces and epoxy rings opening of DGEBA. There are also signals of aromatic, aliphatic and ether systems, all relative to DGEBA, while amide stretching $\text{C}=\text{O}$ (1649 cm^{-1}) is relative to filler.

5.2.3 TGA and DTA analysis of NOM.33 and KEV.33 composites

NOM.33 and KEV.33 are composites obtained, as seen in Table 18, using DGEBA and DETA (as curing agents), and a synthetic oligoaramid as filler (see Chap.4); particularly NOM.33 has poly(*m*-phenylen isophthalamide) as filler, with a percentage of 33% by weight, while KEV.33 has 33% by weight of poly(*p*-phenylen terephthalamide).

Thermogravimetric analysis of these composites were conducted in air or nitrogen flow, obtaining thermograms shown in figure 56; relative data are tabulated in Table 22.



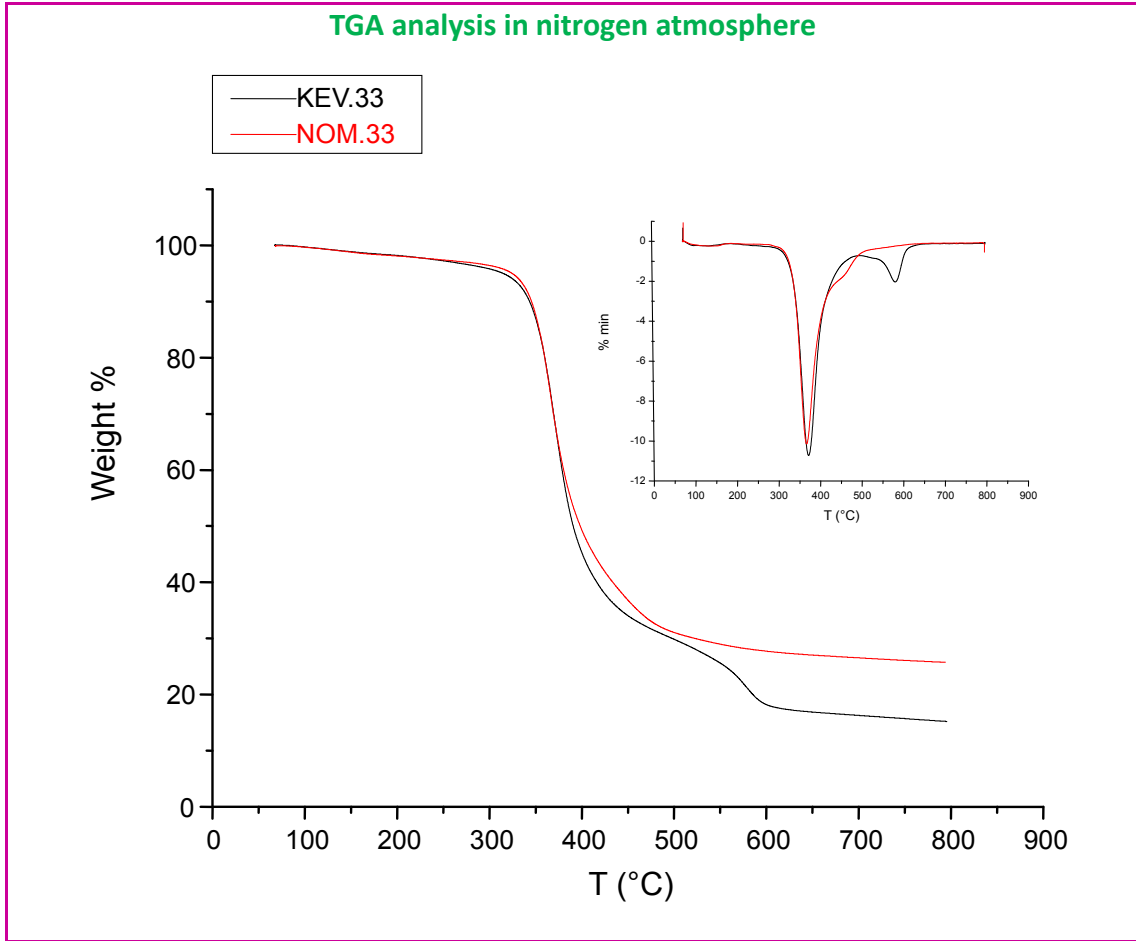


Figure 56: Thermograms, in air and nitrogen flow, of NOM.33 and KEV.33 composites; the insert shows the derivatives curve.

Table 22: Thermogravimetric data relatives to KEV.33 and NOM.33 composites

Samples	Atmosphere	T _{onset} (°C)	PDT (°C)	% Char
KEV.33	aria	276,2	302,7	3,6
	azoto	331,1	370,9	15,3
NOM.33	aria	339,7	365,4	4,5
	azoto	336	366,2	25,7

Tabulated data show that these composites have a similar thermal behavior: beginning to degrade at 270 °C-340 °C with a maximum degradation at about 365 °C. To underline thermal behavior variation with different percentage of filler, in Table 23 are shown thermogravimetric data of: DGEBA/DETA, NOM.10D, NOM.33, and poly(*m*-phenylen isophthalamide as is.



Table 23: Thermogravimetric data relative to composites with different percentage of meta-aramidic filler, poly(m-phenylen isophthalamide) and resin

Samples	Atmosphere	T _{onset} (°C)	% residue
DGEBA/DETA	air	349,6	7,2
	N ₂	353	7,2
NOM.10D	air	280,6	3
	N ₂	348,5	11
NOM.33	air	339,7	4,5
	N ₂	336	25,7
poly(m-phenylen isophthalamide)	air	530	0
	N ₂	434	31

The presence of filler polymer, in air flow, lowers start degradation temperature if compared to unfilled resin; but with quantity of filler polymer increase from 10% to 33% by weight this temperature rises again. In general, all these systems start to degrade between 280 °C and 350 °C.

Char percentage, in air, is below 10%; instead in nitrogen atmosphere, percentage of residue increases with the amount of polymeric filler.

NOM.33 and KEV.33 were also analyzed by means of DTA. Obtained thermograms are represented in Figure 57, showing no event.

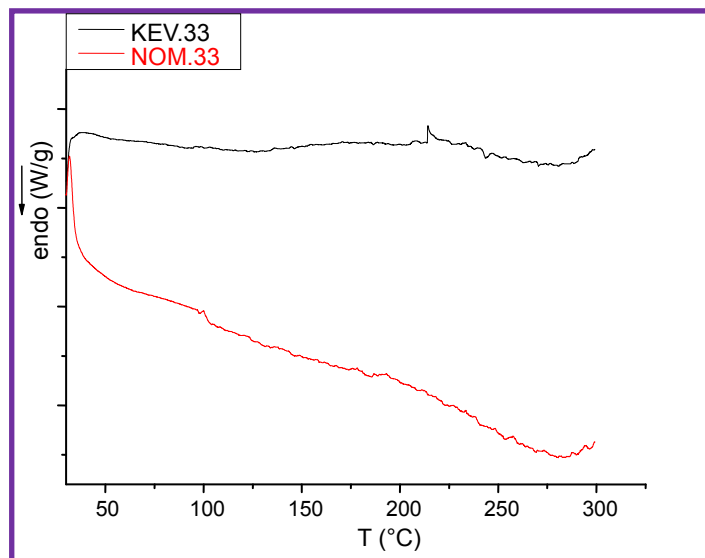


Figure 57: DTA analysis of NOM.33 and KEV.33 composites



5.2.4 FT-IR analysis of NOM.33 and KEV.33 composites

FT-IR spectra of these composites, are shown follow (figure 58) with relative signals in table 24.

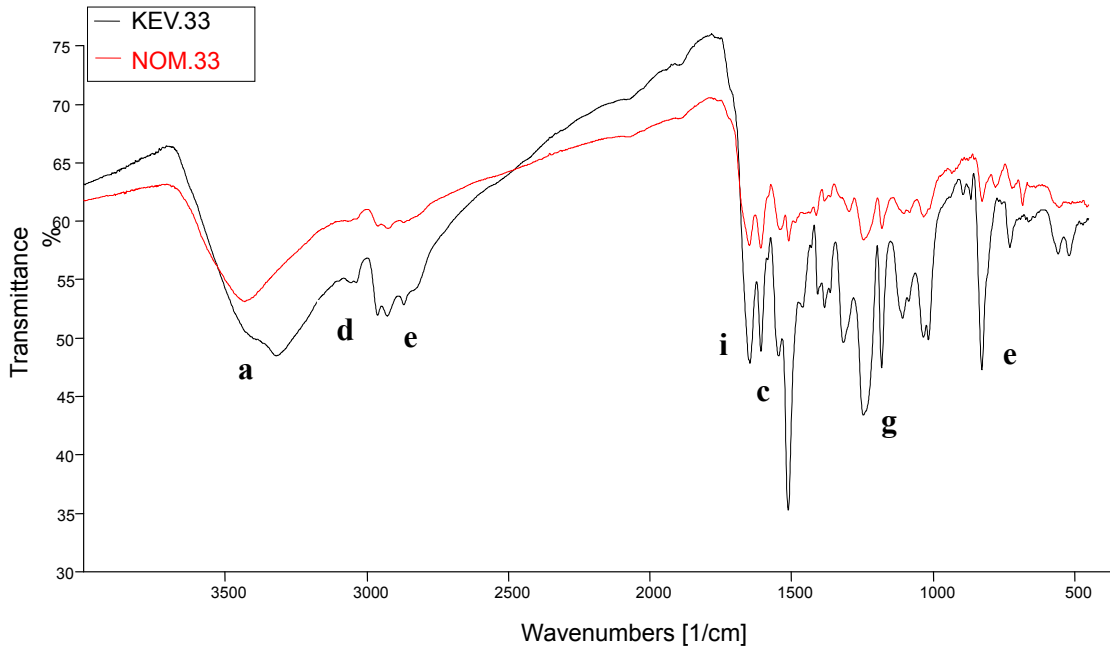


Figure 58: FT-IR spectra of NOM.33 and KEV.33 composites

Table 24: NOM.33 and KEV.33 composites FT-IR signals
(s = strong signal; m = medium; w = weak; sh = sharp; br = broad)

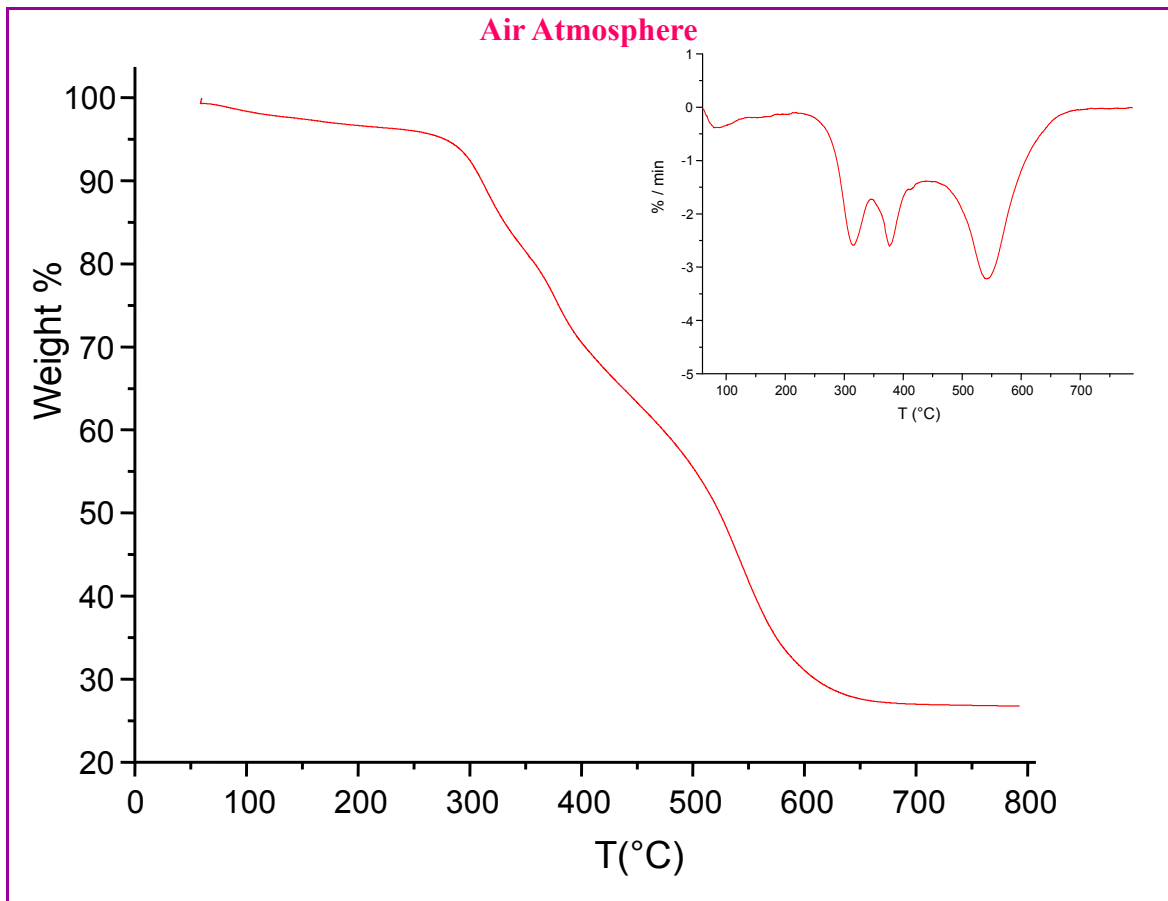
Bond	Wavenumbers (cm ⁻¹)
O-H (stretching) Amine N-H (stretching)	3316-3437 m br (a)
Metyl C-H (stretching)	2828-2962 w (b)
Aryl C-C (stretching)	1607 m sh (c)
Aryl C-H (stretching)	3044 w (d)
Aryl C-H (bending)	828 m sh (e)
Aryl-alkyl ether C-O-C (asymmetric stretching)	1246-1249 s sh (g)
Amide C=O (stretching)	1650 s br (i)

There are signals exclusively attributable to polymeric matrix, such as methylene C-H ($2828-2962\text{ cm}^{-1}$), Aryl-alkyl ether C-O-C ($1246-1249\text{ cm}^{-1}$), as well as signals due to filler, such as amide C=O (1650 cm^{-1}).

5.2.5 TGA and DTA analysis of SIL.33 composite

SIL.33 is a composites obtained, as seen in Table 18, using DGEBA (epoxy prepolymer), DETA (as curing agents), and High Pressure Silica (diameter: $0.04-0.63\text{ }\mu\text{m}$) as filler. Synthesis and characterization of this composite has allowed to have a synthetic term of comparison to commercial package, because, as seen in chapter 2, they have got silica as filler.

Thermal behavior of this composite was studied by thermogravimetric analysis (TGA) and DTA. Thermograms are shown in Figure 59.



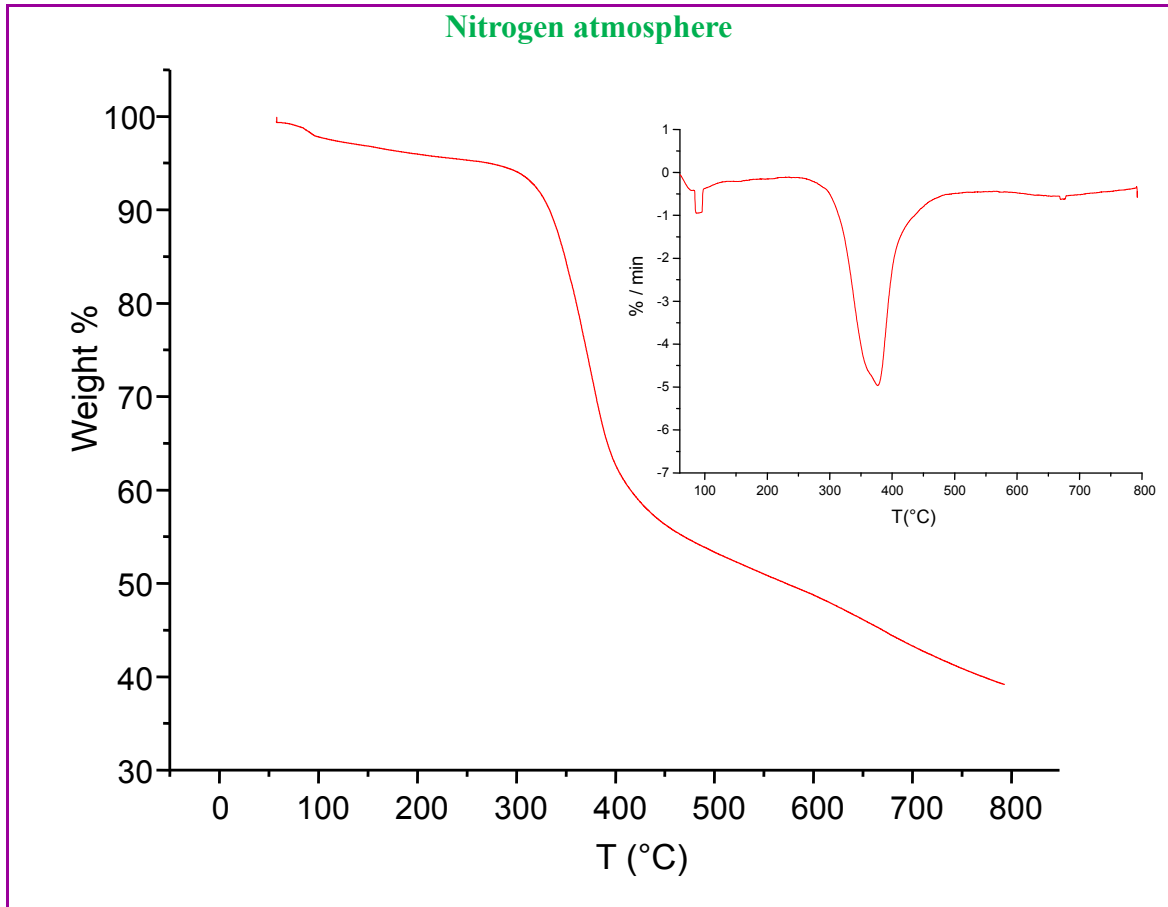


Figure 59: Thermograms, in air and nitrogen flow, of SIL.33 composites; the insert shows the derivatives curve.

Data above shows that composite, in air atmosphere, has a start degradation temperature as 298 °C, while in nitrogen atmosphere, as 333 °C. Furthermore, composites, analyzed in nitrogen atmosphere, has only a maximum degradation temperature (376-379 °C), while in air flow there are multiple steps of degradation.

Char residue in air is attributable to inorganic filler (27%), while in N₂, char includes both organic and inorganic species (39%).

DTA analysis don't show any event (figure 60).

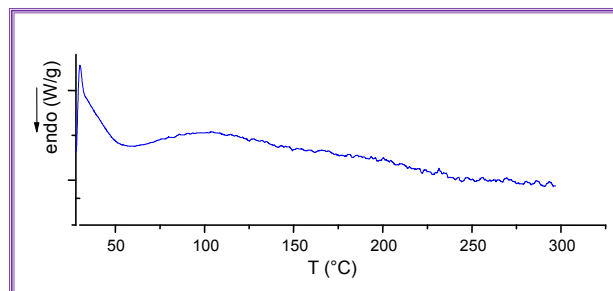


Figure 60: DTA analysis of SIL.33 composite



5.2.6 FT-IR analysis of SIL.33 composite

SIL.33 was structurally characterized by means of FT-IR. Obtained spectrum is reported in figure 61, while in Table 25 there are relative signals.

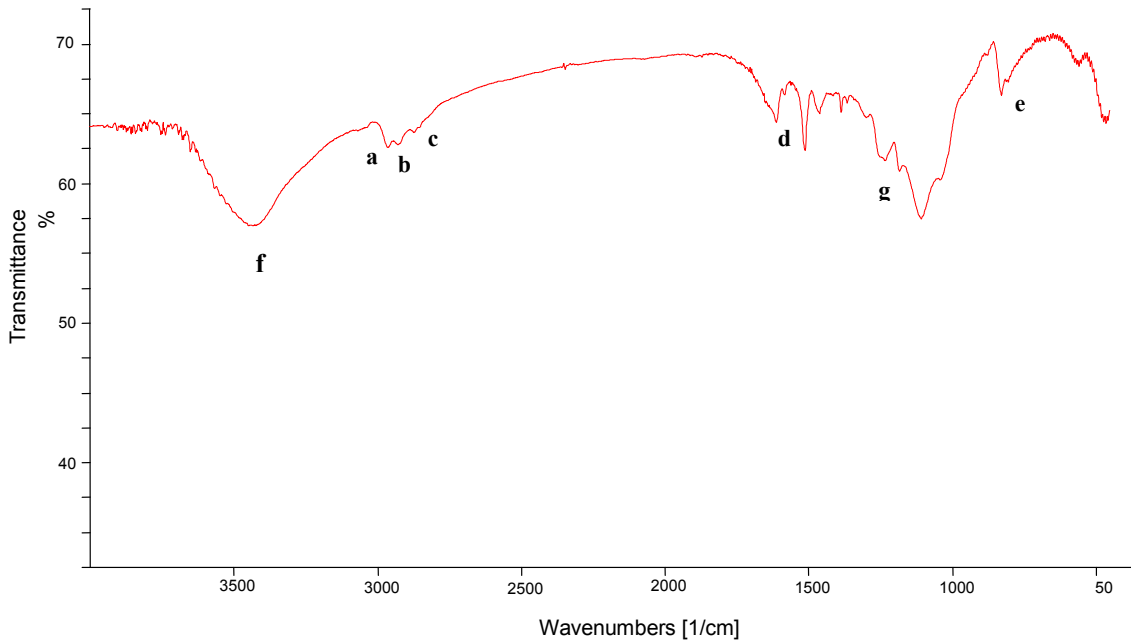


Figure 61: FT-IR spectrum of SIL.33 composite

Table 25: FT-IR signals relative to analysis of SIL.33 composite (s = strong signal; m = medium; w = weak; sh = sharp; br = broad)

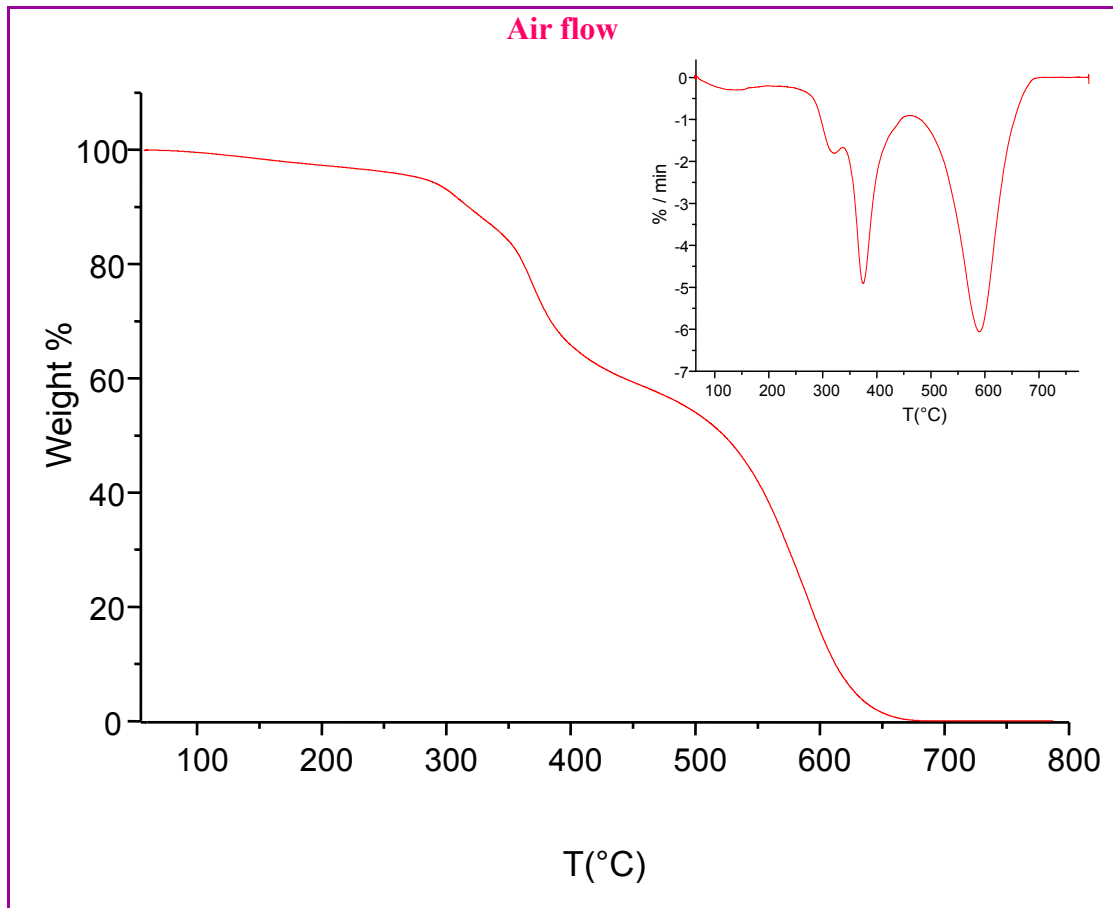
Bond	Wavenumber (cm ⁻¹)
Methyl C-H (asymmetric stretching)	2966-2959 m sh (a)
Methyl C-H (symmetric stretching)	2870-2867 m sh (b)
Methylenic C-H (asymmetric stretching)	2927-2923 w sh (c)
Aryl C-C (stretching)	1511-1508 s sh (d)
Aryl C-H (bending)	828-821 m sh (e)
O-H (stretching)	3430-3419 s br (f)
Si-O (stretching)	1104-1097 s br (g)



FT-IR spectrum of SIL.33 shows a strong absorption of hydroxyl bond ($3430-3419\text{ cm}^{-1}$), due to both water traces and DGEBA epoxy rings opening. Furthermore, there are aromatic (d, e), and aliphatic (a; b; c) signals. Finally, this is the typical Si-O bond stretching signal ($1104-1097\text{ cm}^{-1}$) due to inorganic filler.

5.2.7 TGA analysis of "KAP.33" composite

"KAP.33" composite was obtained, as seen in Table 18 using DGEBA (epoxy prepolymer), DETA (as curing agents), and poly(*p*-phenylen pyromellityimide) as filler. Thermogravimetric analyzes of this composite was conducted in air or nitrogen flow, giving follow thermograms (figure 62).



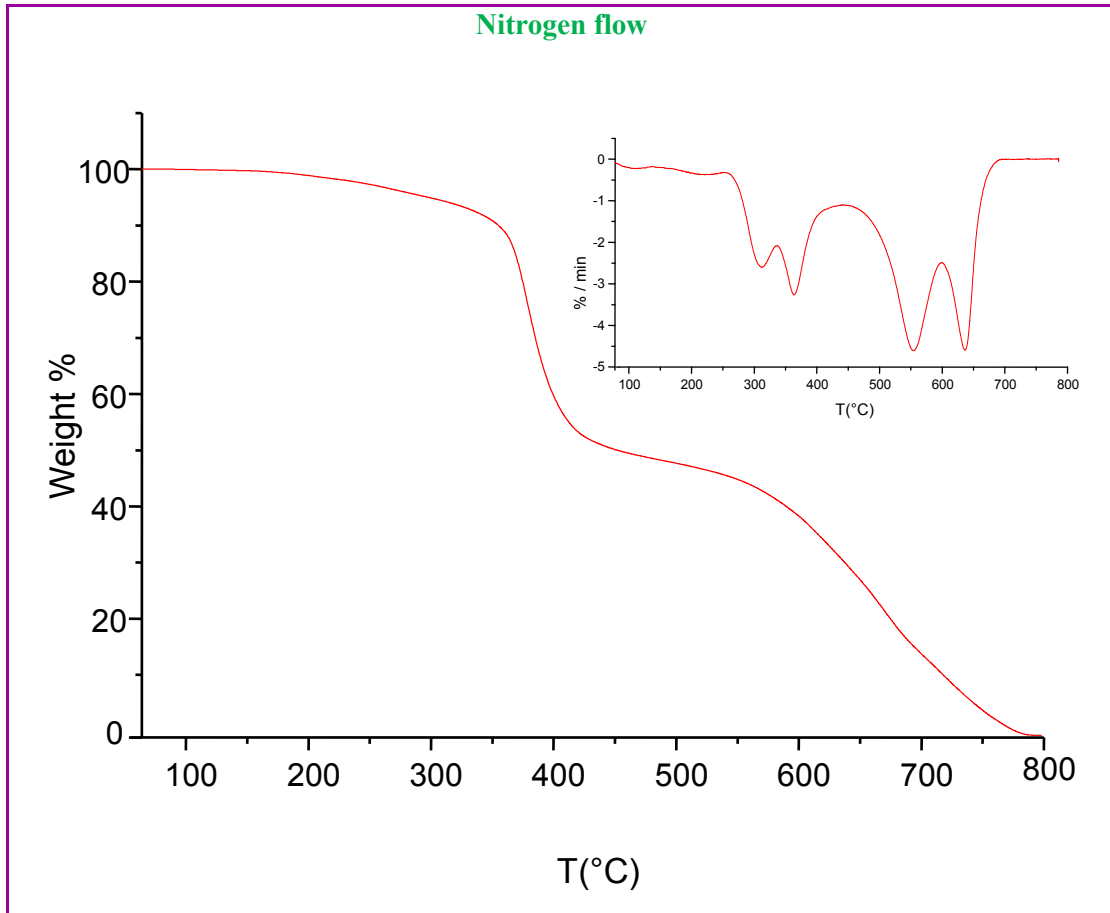
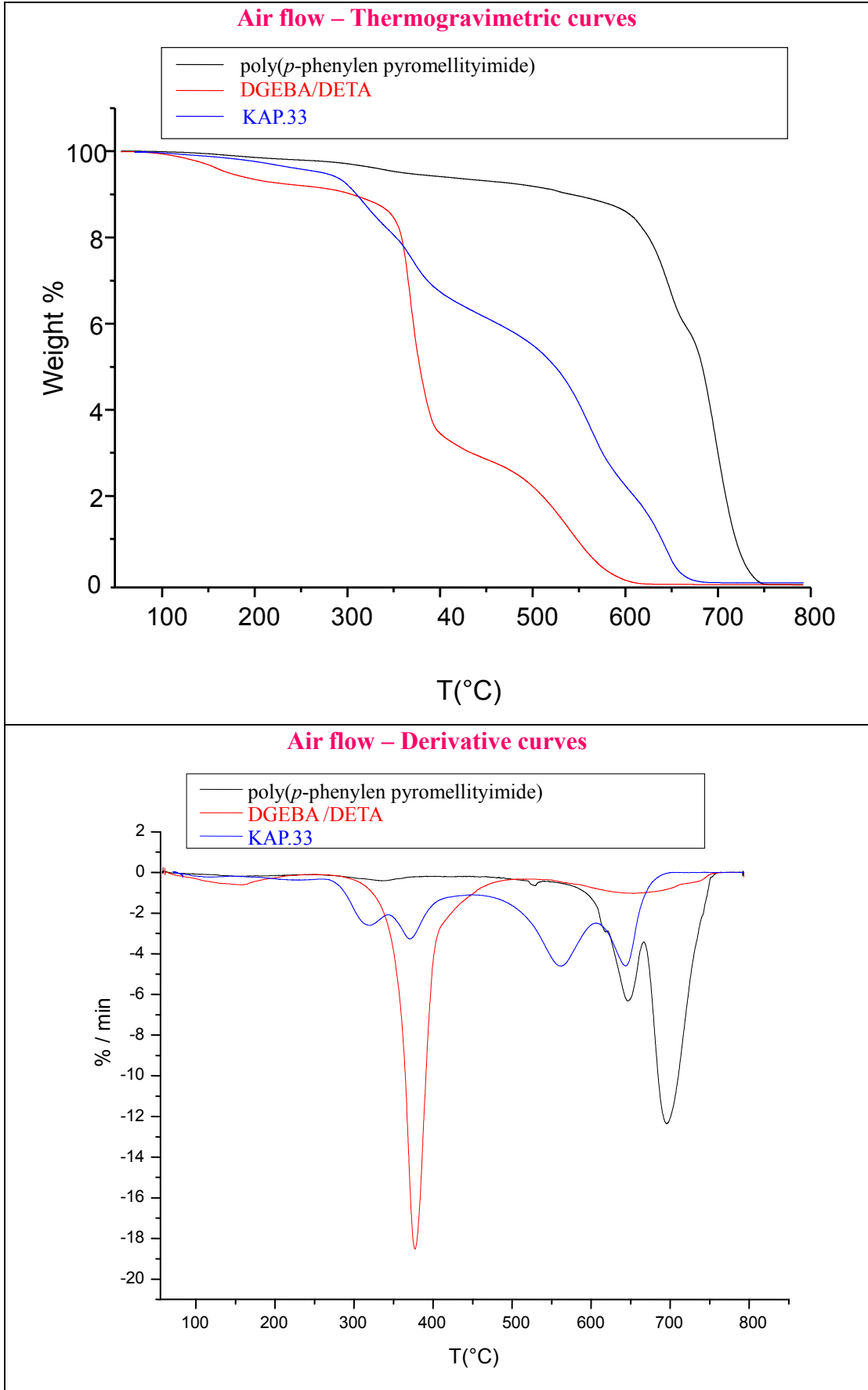


Figure 62: Thermograms, in air and nitrogen flow, of KAP.33 composite; the insert shows the derivatives curve.

Thermograms show, for examined composite in air, a start degradation temperature as 339 °C and 358 °C in nitrogen; while the maximum degradation rates are achieved at 370 °C in air and at 375 °C in nitrogen; moreover char percentage is zero, both in air and in nitrogen atmosphere, although this value is reached at higher temperatures in the latter case.

In order to understand the influence on thermal behavior of polyimidic filler, in figure 63 they were compared thermograms relative to composite, resin and poly(p-phenylen pyromellityimide) as is; table 26 shows relevant thermogravimetric data.



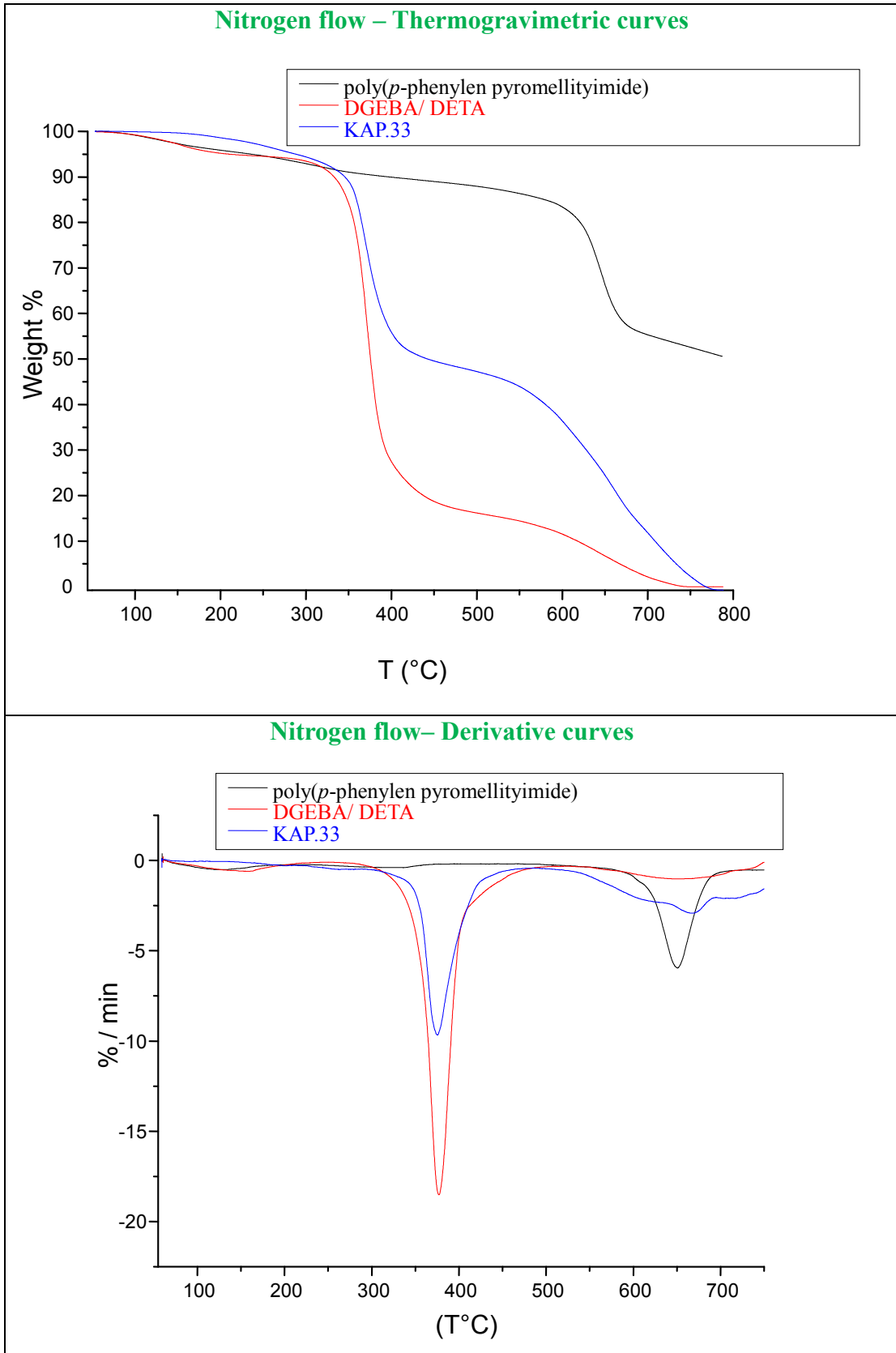


Figure 63: Thermograms, in air and nitrogen flow, of poly(*p*-phenylene pyromellitimide), DGEBA/DETA and KAP:33 composite; the insert shows the derivatives curve.

Table 26: data relative to thermograms of figure 63

Sample	Atmosphere	T _{onset} (°C)	PDT (°C)	% Char
poly(p-phenylen pyromellityimide)	Air	612	695	0
	N ₂	614	650	50
DGEBA/DETA	Air	355	375	0
	N ₂	354	380	0
DGEBA/DETA/33% poly(p-phenylen pyromellityimide)	Air	339	370	0
	N ₂	358	375	0

Thermograms shows that, in air atmosphere, KAP.33 starts to degrade at 339 °C, while in nitrogen at 358 °C; it has two degradation steps, both in air and N₂: the first related to degradation of crosslinked DGEBA/DETA (370-375 °C), the second due to decomposition of organic filler (556-590 °C).

Furthermore, composites both in air and N₂ is totally degraded (char = 0%), while filler as is has a char = 60%; probably the resin degradation gives products that also promote polyimide degradation.

Anyway KAP.33 begin to degrade, both in air and in nitrogen flow, at temperatures greater than 300 °C, temperatures higher than maximum operating temperature of chip inside power modules (250 °C)⁹⁴ and could be used as packages of these devices.

5.2.8 FT-IR analysis of KAP.33

For KAP.33 were carried on structural characterizations through FT-IR spectroscopy (to get information on cross-linked systems); obtained spectrum is presented in Figure 64 and relative signals are shown in Table 27.

⁹⁴ www.st.com/st-web-ui/static/active/en/resource/technical/document/datasheet/DM00099968.pdf

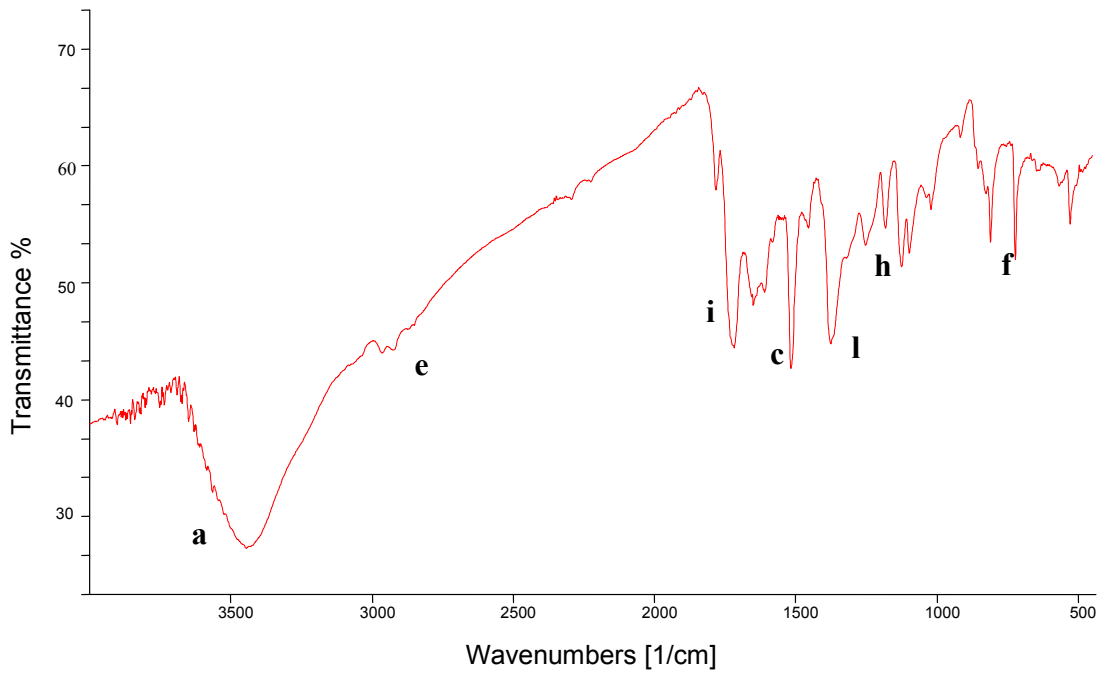


Figure 64: FT-IR spectrum of KAP.33

Table 27: FT-IR signals relative to analysis of KAP.33 composite (s = strong signal; m = medium; w = weak; sh = sharp; br = broad)

Bond	Wavenumber (cm ⁻¹)
O-H (stretching)	3454-3419 m br (a)
Aryl C-C (stretching)	1518 s sh (c)
Aryl C-H (stretching)	3047 w br (e)
Aryl C-H (bending)	821-807 m sh (f)
Aryl-alkyl ether C-O-C (asymmetric stretching)	1249-1246 m sh (h)
Imide C=O (stretching)	1726 s br (i)
Imide C-N (stretching)	1407 m sh (l)

FT-IR spectrum has a strong absorption of the hydroxyl bond (3454-3419 cm⁻¹), relative to water and DGEBA epoxy rings opening. There are aromatic signals (821-807cm⁻¹, 3047 cm⁻¹) relative either DGEBA and polyimide, ether signals (1249-1246



cm^{-1}) due exclusively to DGEBA and signals relative to polyimide ($\text{C}=\text{O}$ 1726 cm^{-1} and $\text{C}-\text{N}$ 1407 cm^{-1}).

5.2.9 Thermal Characterization of GO.33 composite

"GO.33" composite was obtained, as seen in Table 18, using DGEBA (as epoxy prepolymer), DETA (as curing agents), and graphene oxide (synthesized as described in Chap.4) as filler.

Thermogravimetric analyzes of this composite was conducted in air, giving follow thermogram (figure 65).

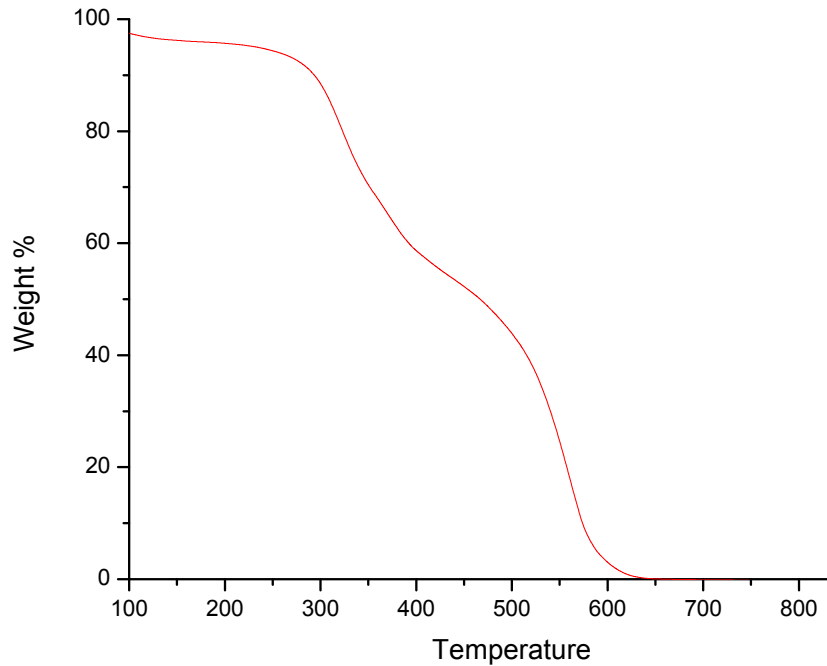


Figure 65: TGA analysis of GO.33 composite in air atmosphere

It is possible to observe how composite, containing graphene oxide, has more step of degradation: the first of which starts at $255 \text{ }^{\circ}\text{C}$ and the second at about 450°C . Furthermore, derivative curve in Figure 72 shows that maximum degradation speed in the is at $323 \text{ }^{\circ}\text{C}$ while the second step at $562 \text{ }^{\circ}\text{C}$.

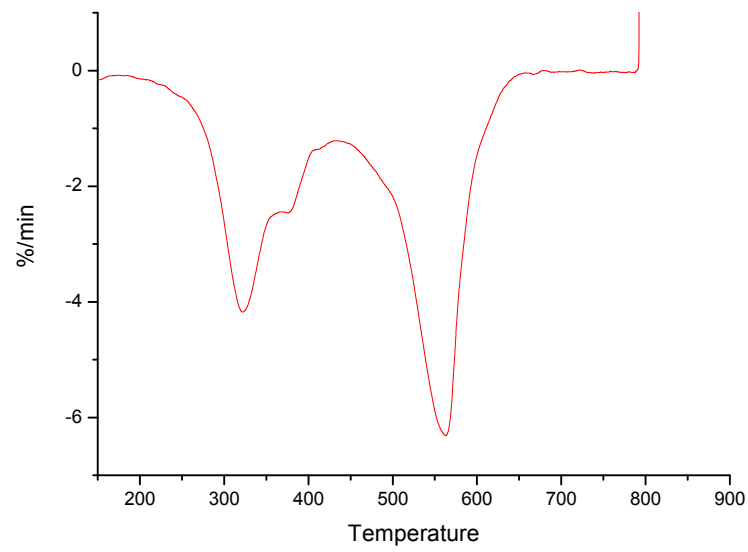


Figure 66: Derivative curve of thermogravimetric analysis of GO.33 composite

DTA analysis (figure 73), conducted at temperatures below that of the start degradation, don't shows any significant event.

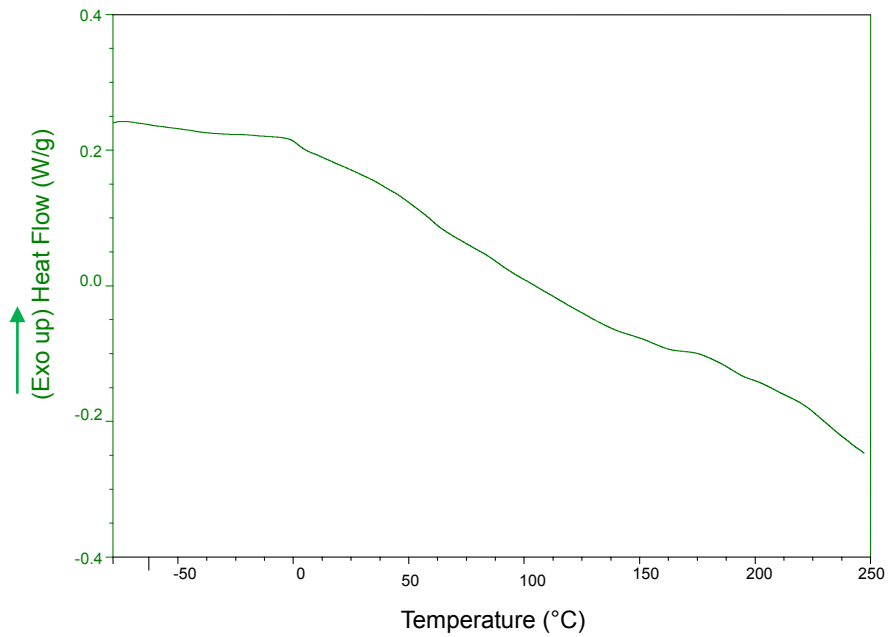
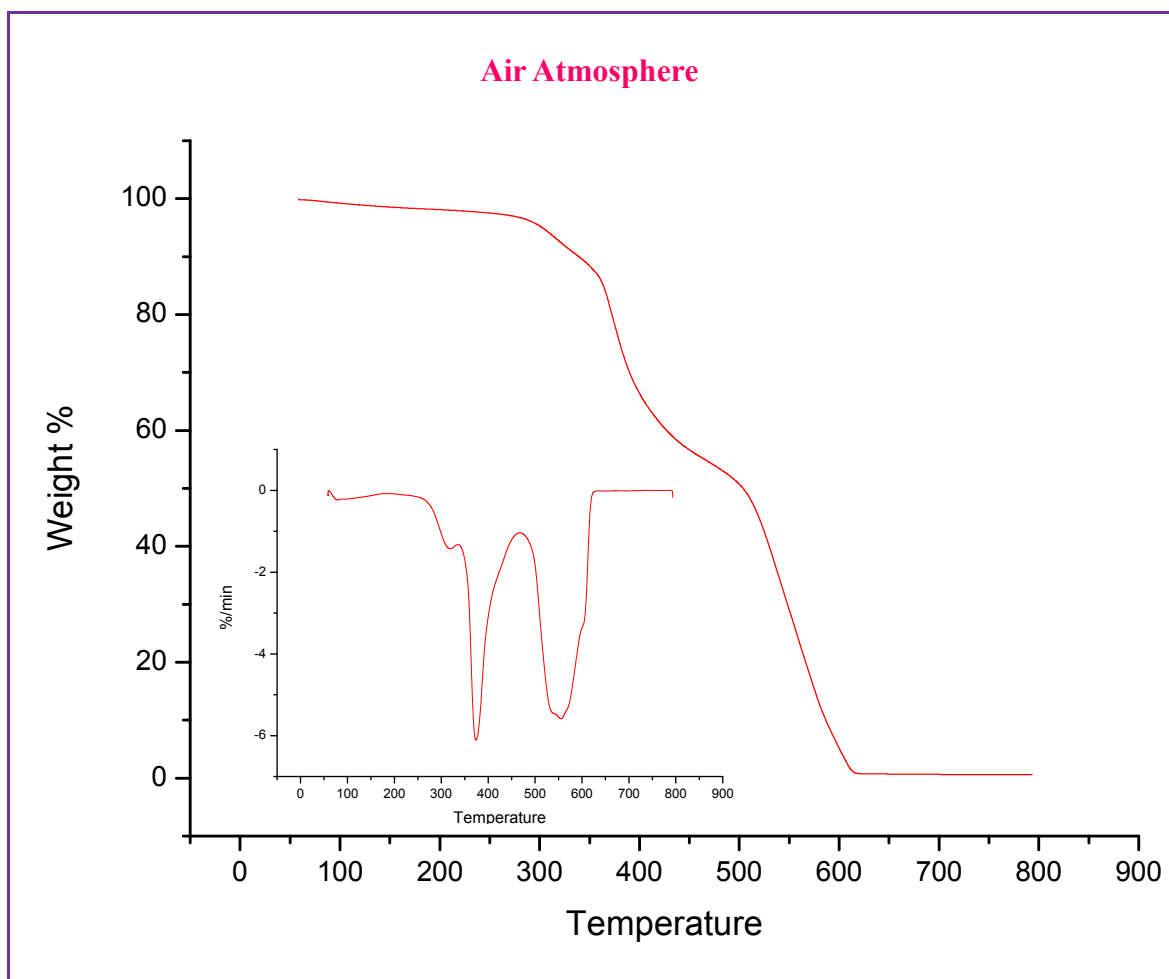


Figure 67: DTA analysis of GO.33 composite

5.2.10 Thermal Characterization of KEL.33 composite

KEL.33 is an epoxy composite obtained, as seen in paragraph 5.2, using DGEBA (as epoxy prepolymer), DETA (as curing agents), and Kelin 130⁹⁵ fiber (a commercial poly(*p*-phenylen terephtalamide) as filler.

In order to obtain indications on possible temperatures use of final product, this composite was thermally characterized by means of TGA; thermograms are reported in figure 68, with relative derivative curve.



⁹⁵ Courtesy of “Spin Tech International s.r.l.” Via G. Galilei, 16 - 25030 Adro (BS) Italy.

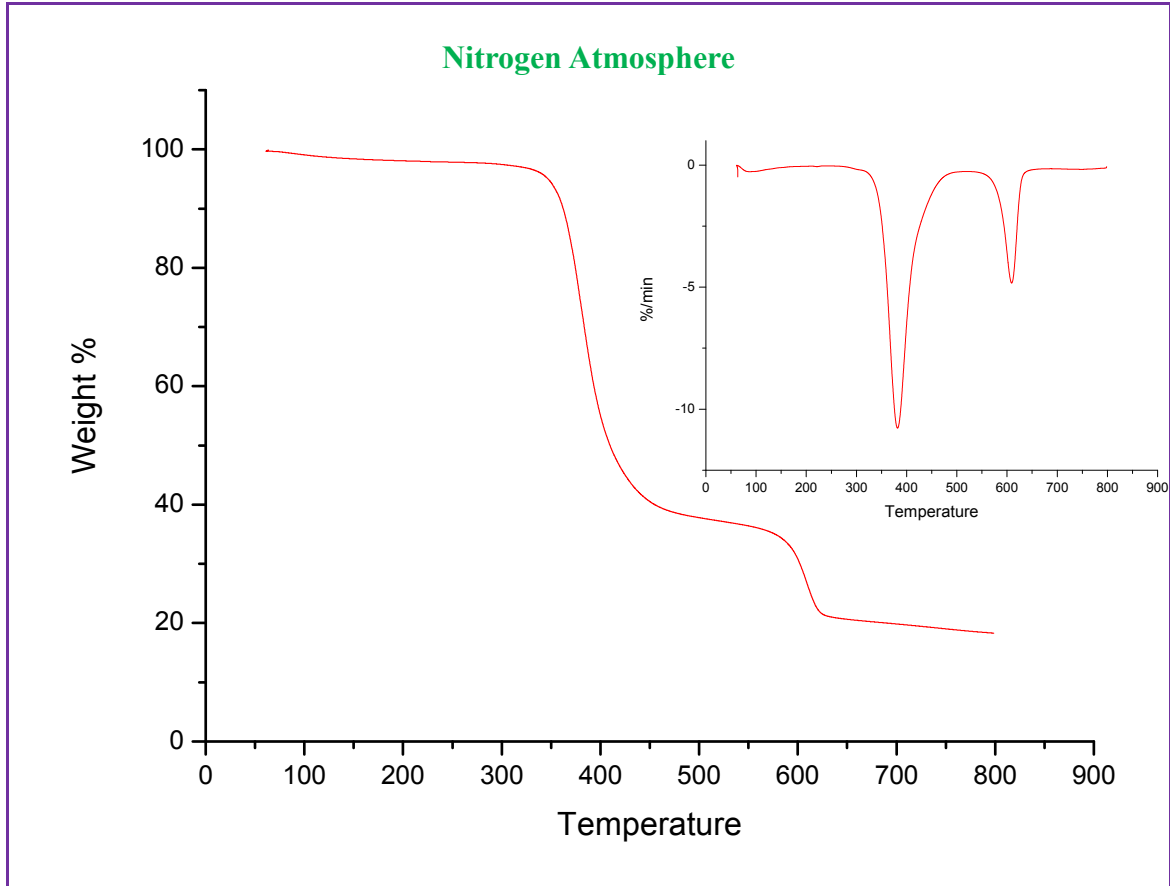


Figure 68: Thermograms, in air and nitrogen flow, of KEL.33 composite; the insert shows the derivative curve.

Thermograms shown in figure 68 underline how the composite KEL.33 has got a start degradation temperature, in air atmosphere, as 310 °C, while in nitrogen, as 329 °C. As already observed for other composites previously analyzed, it is possible to distinguish two steps degradation. In particular, for the analysis in nitrogen atmosphere, two steps reach temperature of maximum rate of degradation at 381°C and 612°C respectively; instead, in air, at 373 °C and 555 °C.

The two degradation steps concern two composite components: Kelin 130 and epoxy resin DGEBA/DETA; in particular to latter is to correlate the first step, to filler, the second step.

DTA analysis (figure 69) shows no significant thermal phenomena.

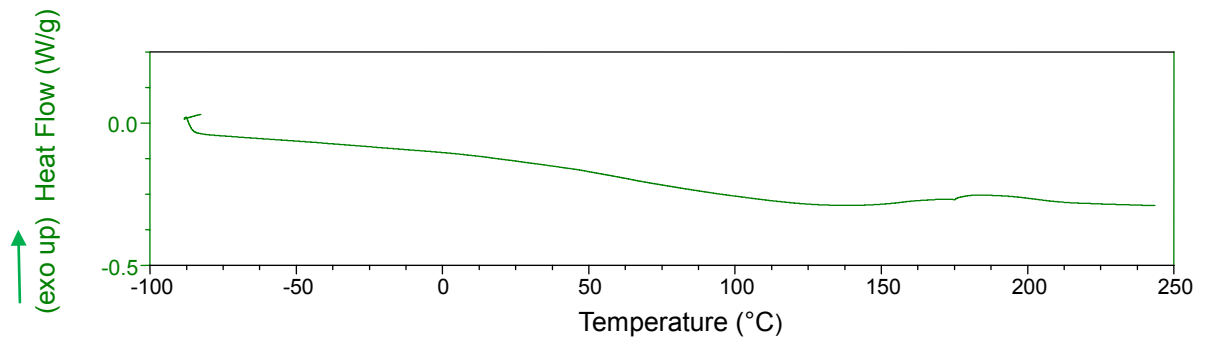


Figure 69: DTA analysis of KEL.33 composite

5.3 Indirect Thermal Conductivity determination

Indirect thermal conductivity determination of composites was performed at 25°C. These determinations were obtained measuring heat capacity by means of M-DSC (Differential Modulated Scanner Calorimeter) Q20 TA-Instrument.

Particularly, ASTM Method E1952⁹⁶ describes the measurement of thermal conductivity by means of Modulated DSC. It is applicable to materials with a thermal conductivity in the limited range of 0.10 to 1.0 W/(K m) and a temperature range from 0 to 90 °C; but several studies extends the working range of MDSC for the thermal conductivity measurement by a factor of 4 to 4.0 W/(K m)⁹⁷.

Heat capacities of composites are measured with Modulated DSC according to Marcus and Blaine method⁹⁸, that allowed to obtain thermal conductivity value by means of analysis on a thick and a thin sample made of same material.

When the thin sample is subjected to a temperature modulation with long period, the sample has a uniform temperature distribution, and the measured specific heat capacity is the thermodynamic heat capacity of the sample. When the thick sample is exposed to a temperature modulation, the measured apparent heat

⁹⁶ E1952, "Method for Thermal Conductivity and Thermal Diffusivity by Modulated Temperature Differential Scanning Calorimetry", ASTM International, West Conshohocken, PA.

⁹⁷ Els Verdonck, Gunther Dreezen: "Thermal Conductivity Measurements of Conductive Epoxy Adhesives by MDSC ®" TA Instruments, Raketstraat 60, 1130 Brussels, Belgium.

⁹⁸ S.M. Marcus, R.L. Blaine "Thermal conductivity of polymers, glasses and ceramics by modulated DSC", Thermochimica Acta, 1994 - Elsevier

capacity is lower in comparison with the thin sample, because of the non-uniform temperature distribution across the height of the sample.⁹⁹

The apparent heat capacity is proportional to the square root of the thermal conductivity of the sample, as shown by equation 4

$$K = \frac{8LC^2}{C_p M d^2 P} \quad \text{Equation 4}$$

where K is the observed thermal conductivity in W/(K m), C is the apparent heat capacity in mJ/K for the thick sample, C_p is the specific heat capacity in J/(g K) for the thin sample, L is the sample height in mm for the thick sample, M is the thick sample mass in mg, d is the thick sample diameter in mm, and P is the modulation period in seconds.

The necessary heat capacity measurements, as seen above, was performed on a TA Instruments Q20 M-DSC, Nitrogen was used as a purge gas. The temperature and enthalpy calibration was performed using indium. The heat capacity calibration was performed with sapphire. The measurements were done at 25 °C, with modulation amplitude of 0.5 °C and a period of 80 seconds (recommended since it provides sufficient time for dynamic equilibrium).

Samples preparation was made according to TA Instrument guidelines¹⁰⁰ as follow.

For each composite were prepared two tablets having a diameter of 6.3 mm and different thickness: thin (0.3-0.5 mm) and thick (3-5 mm); this preparation took place in two steps: at the beginning composite material was pulverized, obtained powder was placed in an evacuable pellet dies and pressed with 5 tons pressure by means of a press. In this way were obtained tablets (or dies) having a diameter of 6.3 mm and a thickness depending on amount of sample used.

Heat capacity measurements was carried on placing samples on a aluminum foil, previously coating both sides of the aluminum foil with a thin coating of silicon oil to ensure the minimum thermal resistance between the DSC cell and aluminum foil and between the foil and test specimen.

A silicone oil coated aluminum foil was used as the reference during this measurement.

From plots obtained for various samples, we get values of heat capacity, so as to apply

⁹⁹ Els Verdonck, Gunther Dreezen: “Thermal Conductivity Measurements of Conductive Epoxy Adhesives by MDSC ®” TA Instruments, Raketstraat 60, 1130 Brussels, Belgium.

¹⁰⁰ Thermal Application Note: http://www.tainstruments.com/library_download.aspx?file=TN17.pdf.



the equation 4. For example, it shows the plot obtained for the composite KEV.33, in particular in the figure 70 there is measurement on the thin sample (0.35 mm), while figure 71 there is one for the thick (3.2 mm) sample.

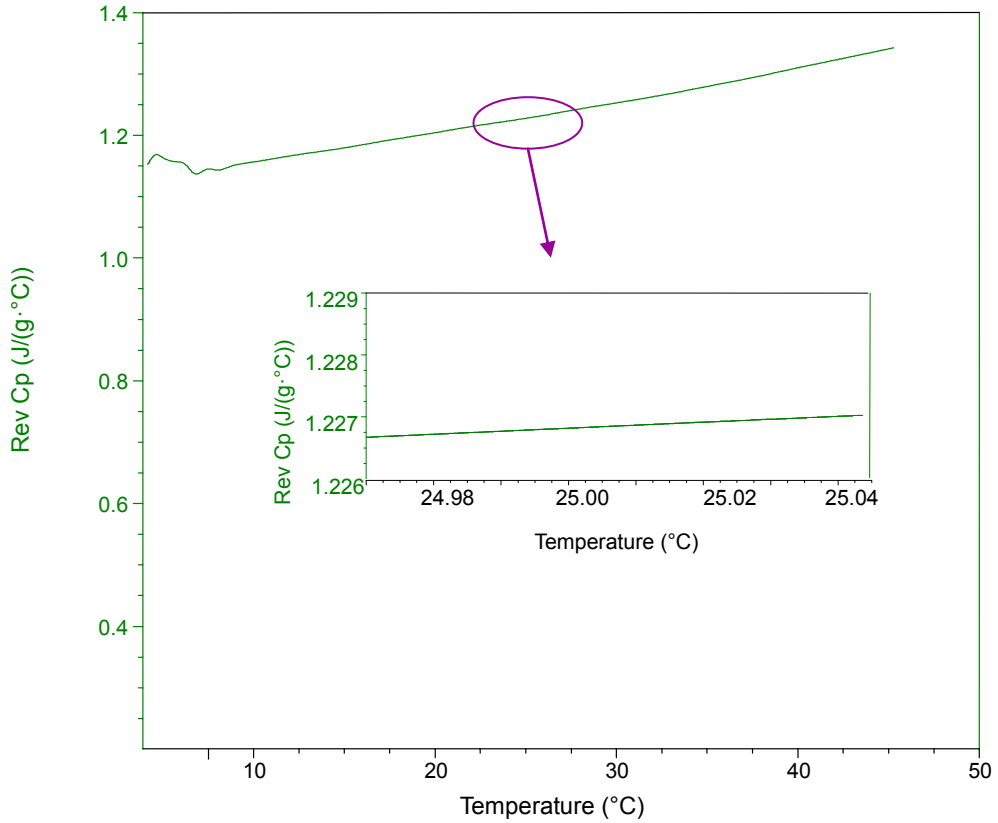


Figure 70: Heat Capacity measurement of KEV.33 composite as thin sample (0.35 mm)

Heat capacity measurement has as a temperature that fall at the mean value of the scan window: in other words, because chosen temperature was 25°C, heat capacity was determined in the range 0°C - 50°C. For thin sample of KEV.33 composite, obtained heat capacity value was 1.227 J/(g °C).

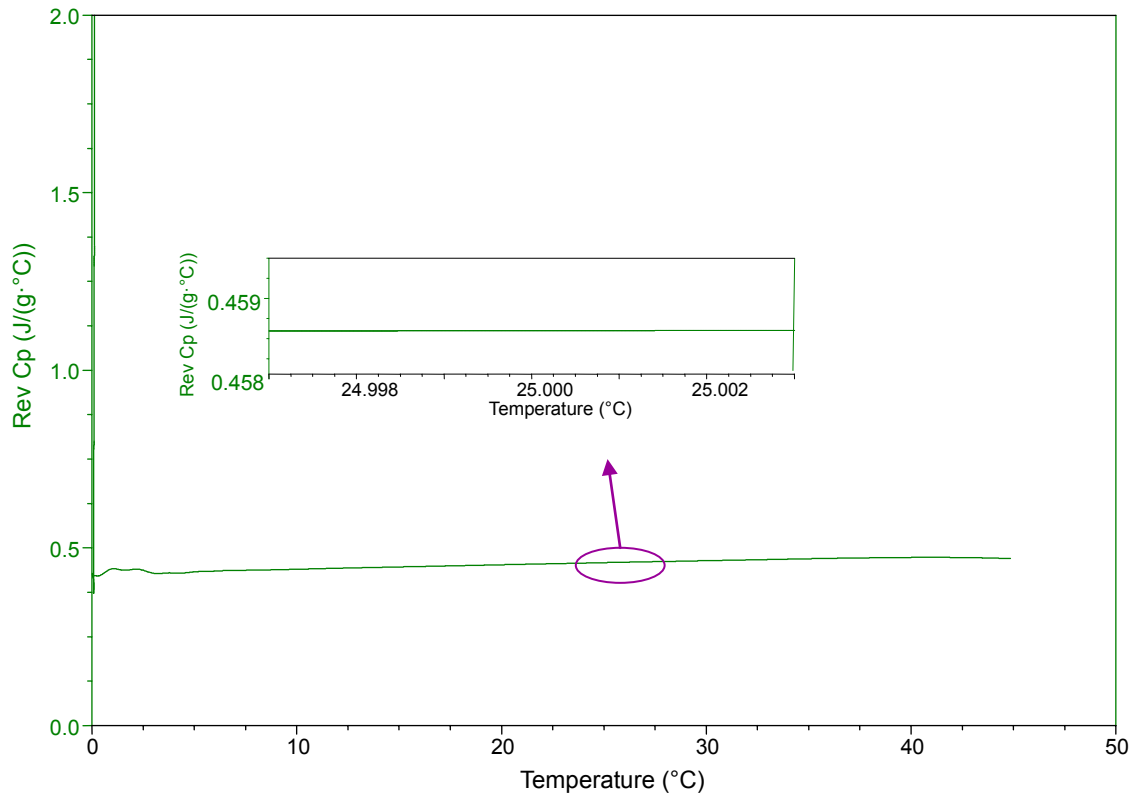


Figure 71: Heat Capacity measurement of KEV.33 composite as thick sample (3.2 mm)

For thick sample of KEV.33 composite, as underline by plot in figure 71, obtained heat capacity value was 0.458 J/(g °C).

To obtain thermal conductivity value according to equation 4, was inserted heat capacity values thus obtained (C for thick sample and C_p for thin sample) and other specifications sample:

$$K = \frac{8LC^2}{C_p M d^2 P} = 12.19 \text{ W/Km}$$

- * L : thick sample height (3.2 mm);
- * C : apparent heat capacity (458 mJ/(g°C));
- * C_p : specific heat capacity (1.227 J/(g °C));
- * M : thick sample mass (112,79 mg);
- * d : thick and thin samples diameter (6,3 mm);
- * P : modulation period (80 s).



The same procedure was followed for all composite materials analyzed, obtaining values reported in the table 28.

Table 28: Thermal conductivity determination of some composites and their geometric specifications

<i>Composites</i>	<i>Thickness (mm)</i>	<i>Mass (mg)</i>	<i>C_p at 25°C (J/g °C)</i>	<i>C at 25°C (mJ/ °C)</i>	<i>K (W/mK)</i>	<i>Diameter (mm)</i>
DGEBA/DETA	0,45	14,2	1,365		8,93	6,3
	3,1	98,9		393		
KEV.33	0,35	11,3	1,227		12,19	6,3
	3,2	112,8		458,6		
KAP.33	0,40	9,6	1,132		8,86	6,3
	4,3	140,0		360		
SIL.33	0,30	6,8	1,426		6,90	6,3
	3,4	127,7		383		
Commercial Package (BD 791)	0,35	12,2	0,7247		7,74	6,3
	3	124,0		303,4		
KEL.33	0,40	11,2	0,8178		7,53	6,3
	4	190,0		338,5		

As can be seen from table above, almost all composites obtained (with the exception of KEL.33), show a thermal conductivity higher than that of analyzed commercial package. In particular, KEV.33 showed the best behavior for purposes of this research, in which the filler is oligo-aramidic type and synthesized as described in Chapter 4.



5.4 Finite Element Method

The Finite Element Method (FEM) is a numerical technique used to seek approximate solutions to problems described by partial differential equations, reducing them to a system of algebraic equations; it is based on some fundamental steps such as the division of the entire studying object (*domain*) into smaller parts (*mesh*), the description of relationships between variables and the assembling of the elements to obtain the relationship between the variables on all domain.

F.E.M. method is applied to physical bodies which may be divided into a number, also very large, of elements having defined shape and dimensions. This continuous domain discretization occurs through the use of simple shape elements such as triangles and quadrilaterals for 2D domains, or hexahedral and tetrahedral for 3D domains (Figure 72).

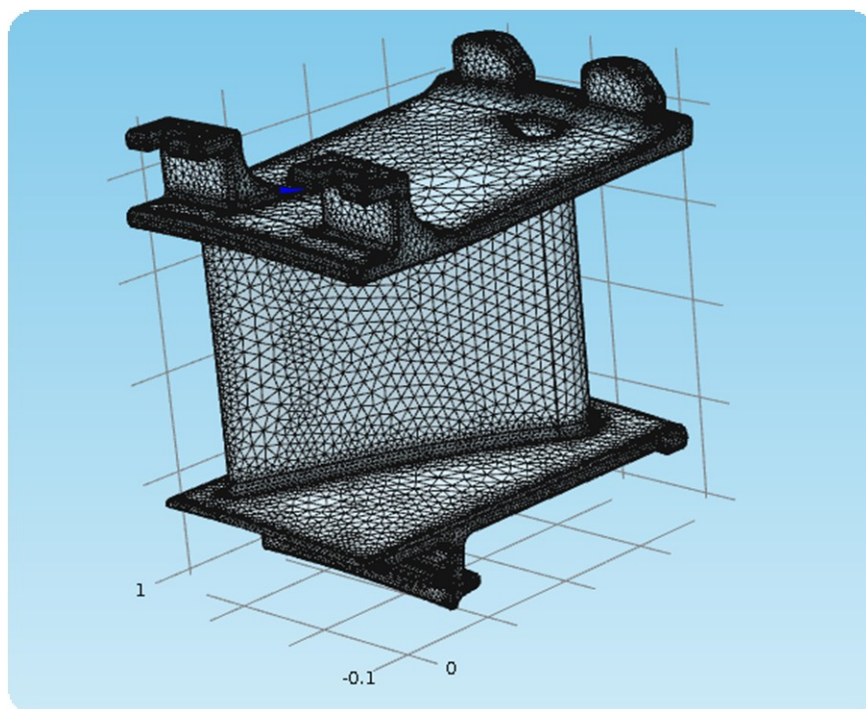


Figure 72: Discretization of the three-dimensional continuous domain of a turbine stator

These elements are connected by nodes, placed at the top of the elements and which possess one or more grade of freedom.¹⁰¹

¹⁰¹ Ray W. Clough, Edward L. Wilson, *Early Finite Element Research at Berkeley*, 1999

It consider, for example, a differential operator L , and a function $\varphi(x, y, z)$ defined on a V domain. It suppose that

$$L[\varphi(x, y, z)] = g(x, y, z) \quad \text{Equation 5}$$

where $g(x, y, z)$ is an assigned function: the solution φ is subject to the V domain boundary conditions.

FEM method allow to pass from differential formulation (Equation 5) into a matrix form, by approximating the true trend of the unknown function φ with that of some known trend functions (polynomial, trigonometric or exponential) said *shape functions*¹⁰².

Therefore the approximate solution of Equation 5 is:

$$\varphi_n(x, y, z) = \varphi_0(x, y, z) + \sum_{i=1}^n a_i \xi_i(x, y, z) \quad \text{Equation 6}$$

where:

- ∞ $\varphi_0(x, y, z)$ is an unknown function introduced in order to satisfy boundary conditions;
- ∞ a_i are unknown coefficients;
- ∞ $\xi_i(x, y, z)$ are the *shape functions*;

For resolution of the finite element simulations is necessary, due to high computational complexity, use computing power of a software. This software has the task of facilitating models compilation and implementation, through the use of graphical interfaces.

5.4.1 Virtual Prototyping

Software used for Virtual Prototyping is composed of several modules corresponding to various physical phenomena that can be combined each other. The software has a graphical interface inside, CAD-style, for creating geometries 1D, 2D and 3D; also can import geometries created by external design tools. 3D geometry may be derivative

¹⁰² D. Lombardo, “Analisi termofluidodinamica agli elementi finiti dei processi di assorbimento e desorbimento di idrogeno in idruri metallici” Tesi di Laurea Magistrale in Chimica Industriale (2008), Università degli Studi di Torino.



from those 2D by extrusion or rotation around a symmetry axis. Within the software it is possible specify parameters and properties of materials constituting analyzed object and put conditions on inner and outer edges. 1D geometry object software divides the subdomains in smaller intervals; in 2D geometry subdomains are divided into elements like triangles or quadrangles; 3D geometry elements, are tetrahedrons or hexagonal prisms, the contours are divided into triangles or quadrilaterals.

On thus divided object, according to the type of physical studio, the solver will act, giving final results of finite element analysis.¹⁰³

Below there is a simulation of thermal transfer to a silicon chip placed on a circuit plate by means of pins. The chip also is subject to a punctual internal heat source of 2×10^8 W/m³ and is placed in the center of package by dissipating heat to the surrounding environment.

Heat transfer from chip to surrounding environment takes place by *conduction*:

$$\nabla \cdot (-k\nabla T) = Q \quad \text{Equation 7}$$

Heat dissipation of surfaces exposed to static air takes place by convection:

$$-n \cdot q = h(T_{inf} - T) \quad \text{Equation 8}$$

Where *h* is convection heat transfer coefficient.

Below, two different models are shown: in the first case, chip is enclosed within a package made of those commercially used (figure 73), for which it was obtained a value of thermal conductivity equal to 7.74 W/mK (see Table 28), while in the second example is used the composite KEV.33, obtained with 33% of poly(*p*-phenylen terephthalamide) as filler, having a thermal conductivity equal to 12.19 W/mK.

Materials chosen for other components are:

- ❖ Silicon, for chip;
- ❖ Aluminum for pins;
- ❖ FR4 (a fiberglass) for pc board;
- ❖ Copper, as chip support base and for interconnections

¹⁰³ Software User Guide.

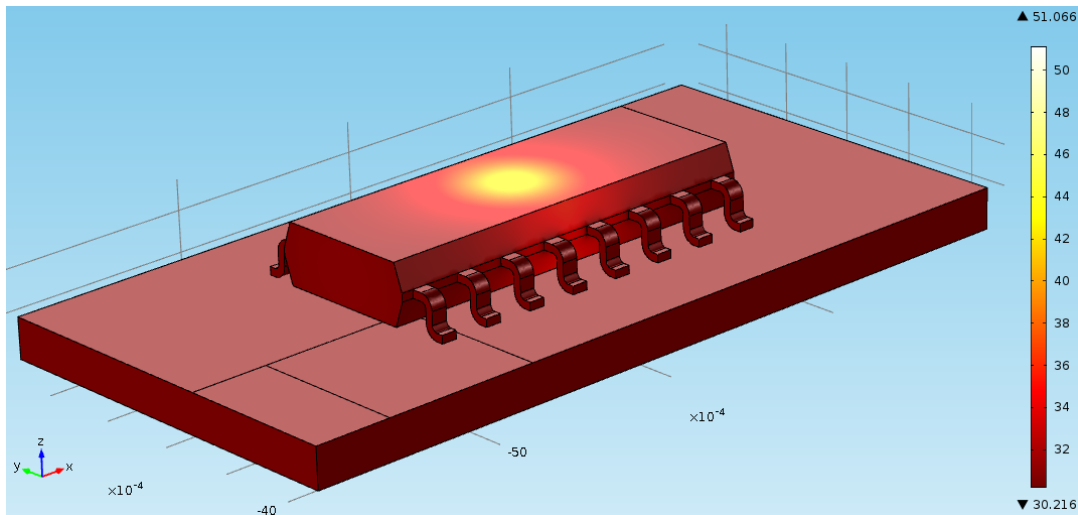


Figure 73: Simulation of thermal transfer of a device with commercial package having an internal heat source equal to $2 \times 10^8 \text{ W/m}^3$

The simulation above shows that, when chip releases $2 \times 10^8 \text{ W/m}^3$ power, it reaches a maximum temperature of $50 \text{ }^\circ\text{C}$ if its package is made by common epoxy resin filled with about 70% of silica. Vice versa, Figure 74 shows simulation with a system where package material is KEV.33; it possible to observe that chip does not exceed temperatures of $35 \text{ }^\circ\text{C}$.

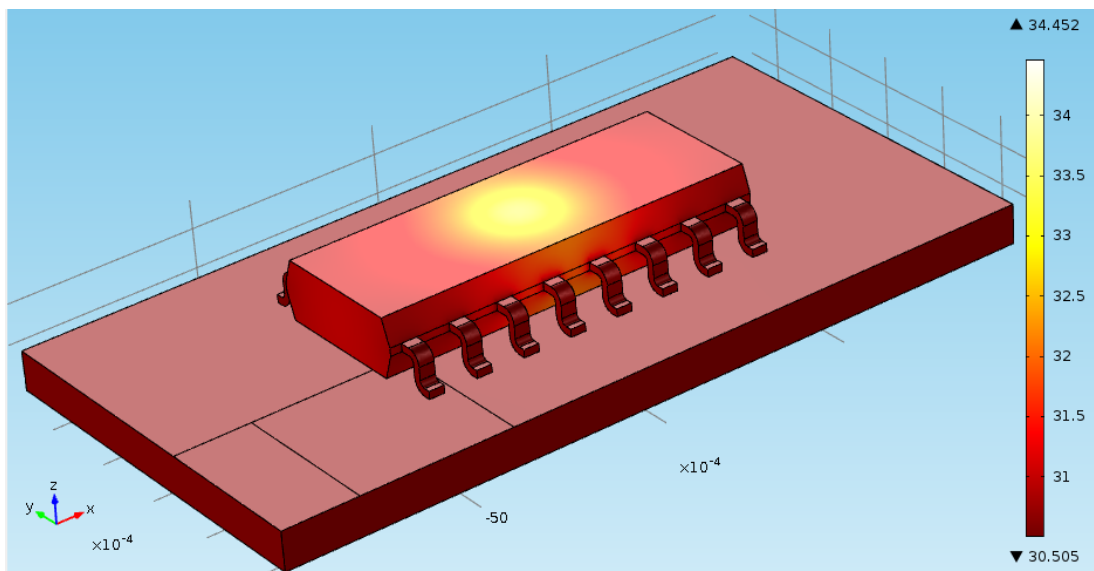


Figure 74: Simulation of thermal transfer of a device with package made of KEV.33 composite and having an internal heat source equal to $2 \times 10^8 \text{ W/m}^3$

Whereas operation efficiency of a chip increases with decreasing temperature reached by it, the use of a package based on KEV.33 would also allow a considerable energy saving. Observing temperature slice plots (Figure 75) along the device, it becomes more visible heat flows trend and how it varies between the two different models.

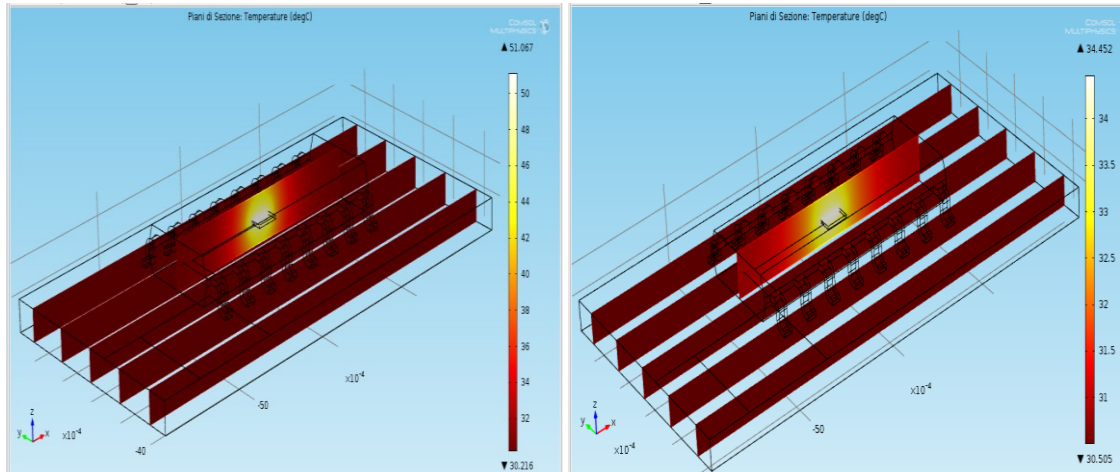


Figure 75: Temperature slice plots for simulation of device with commercial package (on the left) and KEV.33 composite package (on the right)

5.5 Direct Thermal Conductivity measurements

Measurements of thermal conductivity by direct method were carried on in collaboration with Prof. G. Compagnini and Dr. G. Isgrò (Thin Films and Nanostructures Laboratory of the University of Catania - Department of Chemical Sciences) and Prof. Patané and Dr. S. Panarello (University of Messina – Department of Physical Science and Advanced Physical Technology).

The instrumentation used has a system capable of maintaining at a fixed temperature the lower surface of the sample under analysis, and read temperature at upper surface. In this way, knowing geometrical specifications of analyzed sample, it is possible to obtain a direct evaluation of material thermal conductivity.

These analysis can be summarized as follows:

- ✘ Preparation of samples.
- ✘ Realization of static maps of temperature distribution when tablets are subjected to a controlled thermal gradient.
- ✘ FEM analysis.
- ✘ Experimental data fitting.
- ✘ Thermal conductivity numerical calculation.

For each composite were prepared cylindrical tablets following two steps preparation method: at the beginning composite material was powdered and then placed in an evacuable pellet dies and pressed with 5-7 tons pressure by means of a press. In this way were obtained tablets (or dies) having a diameter of about 13 mm (Figure 76) and a thickness depending on amount of sample used.

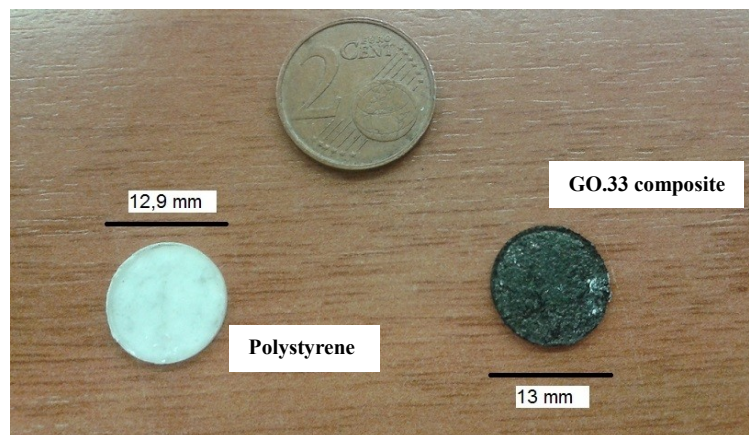


Figure 76: tablets of Polystyrene and GO.33 composite



In order to evaluate composites thermal conductivity, has been realized a measurement system composed of a temperature controller (Peltier cell) and an infrared microscope. The temperature is monitored by means of a solid state control sensor, and a feedback regulates the current flowing inside the Peltier to maintain the temperature constant with a precision of the order of 0.1 °C. The sample is mechanically connected to the Peltier that is able to maintain temperature of a small portion of tested sample, at a fixed value (figure 77). The result is a thermal gradient in the points of the sample, essentially due to the exchange of heat generated by convection with the surrounding atmosphere.

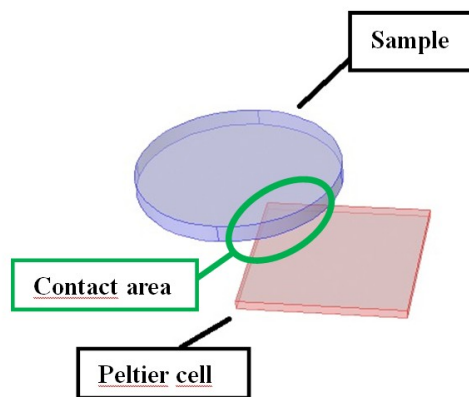


Figure 77: Scheme of contact between peltier cell and sample

In Figure 78 is shown a system measurement picture: Peltier cell is in contact with an area approximately a quarter of sample lower surface (which in figure is made of a steel copper coated). System controls contact area temperature maintaining it at 75 °C. Due to copper high thermal conductivity, microscope detects the same temperature on all sample surface (red is associated with the temperature of 75 °C and is uniform on sample surface).

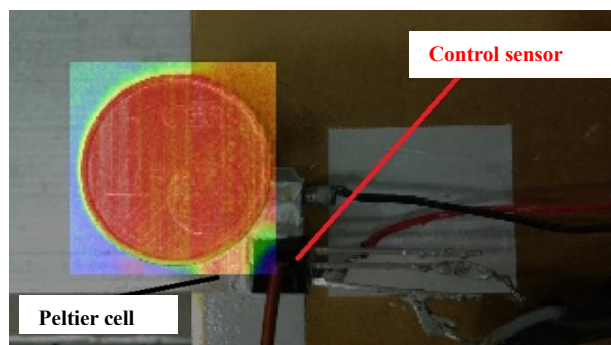


Figure 78: Test carried out on a coin of steel and copper. The coin is at a uniform temperature of 75 °C



Figure 79, shows temperature distribution on GO.33 composite. It is evident a thermal gradient on sample surface. System reveals a hike of about 30 °C between the area in which the sample is in contact with Peltier cell and the most distant areas. In static conditions, heat flow and distribution temperature are, essentially, related to thermal conductivity and to convection coefficient (h) with environment. H depends on sample geometry, heat exchange surface orientation and nature of cooler fluid, but it doesn't depend on chemical nature of heat exchange surface.

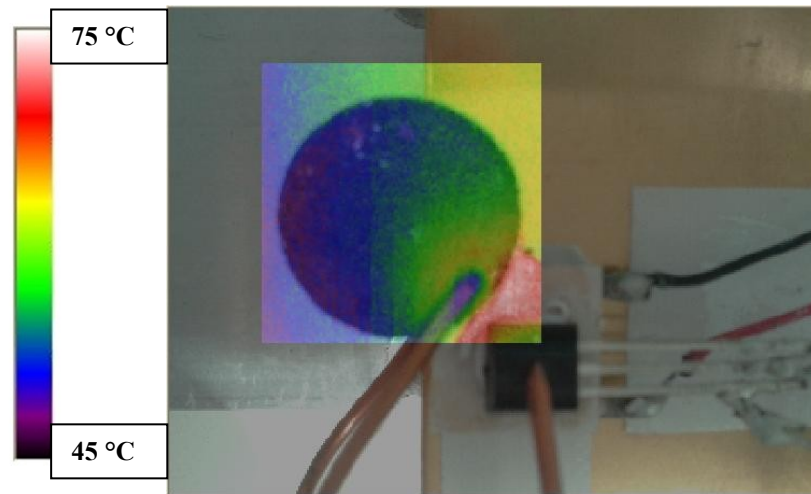


Figure 79: Thermal Analysis on GO.33 composite and obtained thermal gradient

In Figure 80 the same experiment was conducted on a sample of polystyrene.

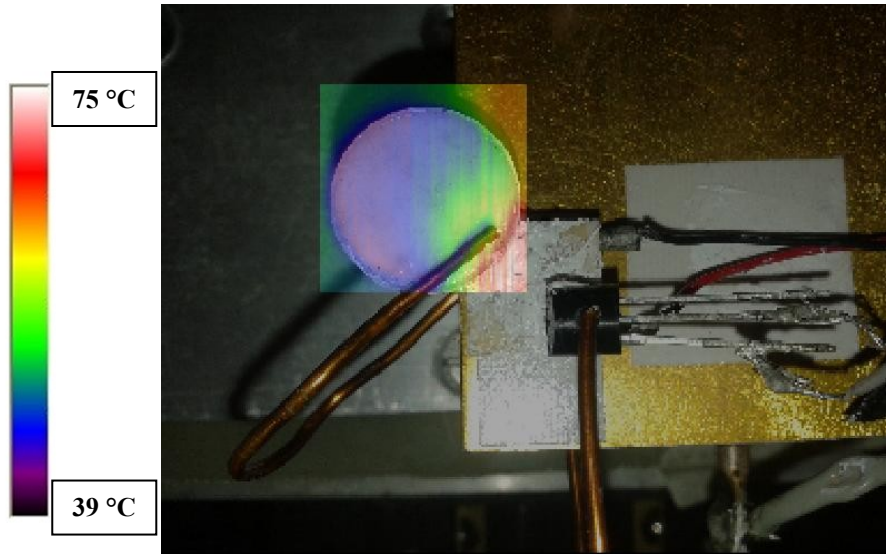


Figure 80: Thermal Analysis on Polystyrene sample and obtained thermal gradient

Polystyrene sample thermal gradient is greater than GO.33 composite: therefore polystyrene thermal conductivity is lower than that of composite. Through FEM analysis is possible, however, to calculate conductivity of the samples tested. FEM model faithfully reproduces tested samples geometry and its thermal study is based on stationary heat transfer by conduction and natural convection.

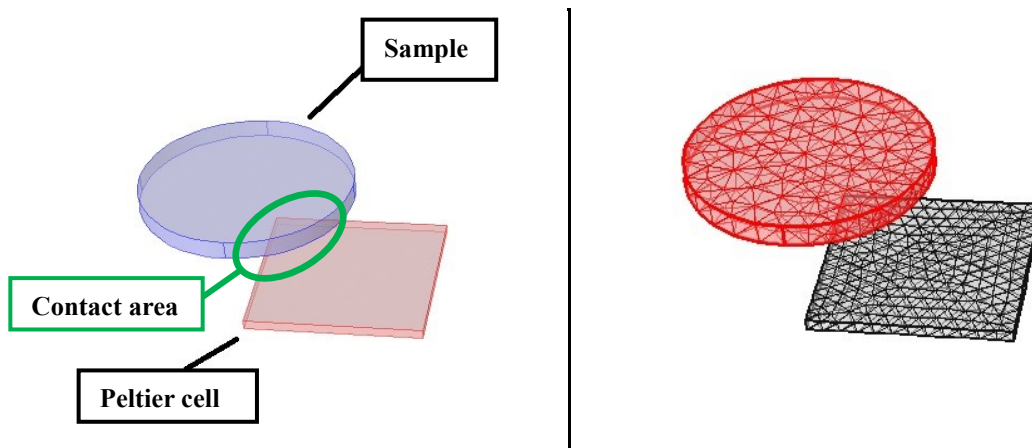


Figure 81: Finite element model geometry. On the left: domains constituting the model; on the right: mesh domain.

Through the contact area shown in Figure 81 there is an heat transfer by conduction from Peltier cell to sample. From sample to environment is set a heat transfer by not forced convection.



Boundary conditions are shown in Figure 82, and are contact area temperature between sample and Peltier cell and h for a horizontal surface with upper or lower warm face.

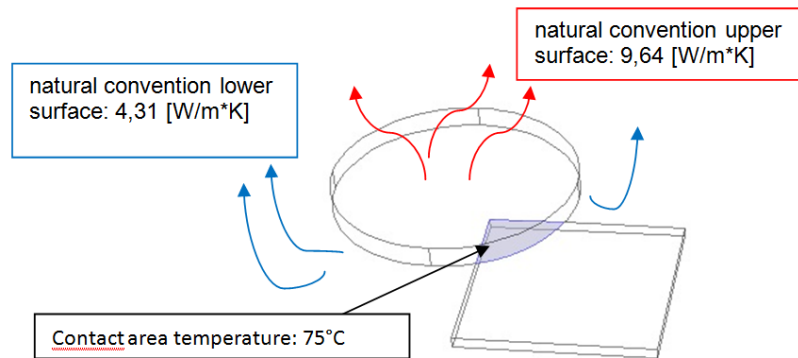


Figure 82: Boundary conditions (are relative to geometric dimensions of GO.33 tablet)

FEM analysis is preparatory to experimental data fitting previously obtained by scanning thermal determination. In Figure 83 are indicated four selected points (a, b, c, d) on GO.33 composite surface and measured temperature on them.

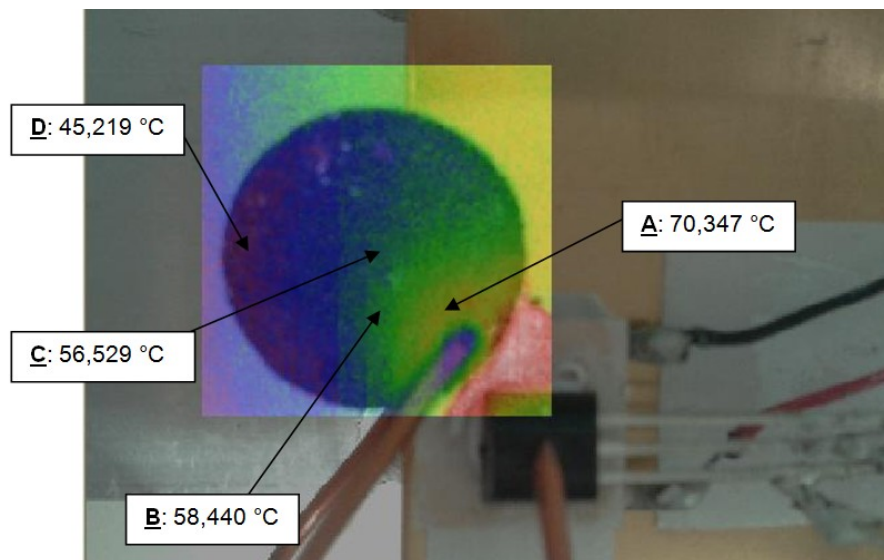


Figure 83: temperatures used to perform experimental data fitting

Moreover figure 84 reports simulated thermal map on which it is possible to obtain thermal conductivity coefficient for analyzed sample (GO.33): 0,88314 W/(m*K).

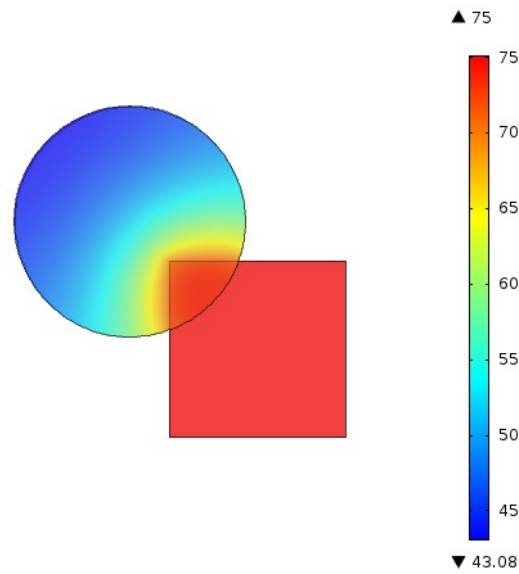


Figure 84: Finite element simulation. Conductivity coefficient is optimized by means of experimental temperatures best fitting.

Thermal method as until now described, has also been used for analysis of MO.33, obtained using DGEBA (as epoxy prepolymer), DETA (as curing agents), and Molibdenum Disolphure as filler.

Despite this thermal analysis has been more difficult, it is had a preliminary result of thermal conductivity, resulted to be about 15 W/mK.

5.6 Prototypes

In addition to thermal conductivity estimate of obtained composites, it is interesting to understand what are the local temperatures reached in composite, when placed on devices, when the latter, during operation, are subjected to the passage of current (Joule effect).

This allows to determine:

- ~ if these composites, during the work phase, are be able to dissipate product heat;
- ~ how vary thermal behavior of electronic device as “bare die” or "coated";
- ~ how the different fillers contribute to the dissipation of heat.

For these purposes, composites were synthesized directly on an electronic nude device, in particular it was a MOSFET.

In order to synthesize about 3 g of each composite, at first DGEBA (epoxy prepolymer) was weakly heating; then filler was added to it [poly(*p*-phenylen terephthalamide), poly(*p*-phenylen pyromellitimide), Silica or Graphene Oxide]. To crosslink mixture was added DETA (curing agent) and was homogenized by mixing vigorously with a spatula (N₂ flushing). The mixture, thus obtained, was casting on free-package device surrounded by a cardboard gasket (figure 95). The use of this gasket allowed to obtain a regular shape of known thickness and diameter for final composite.



Figure 85: Nude MOSFET, prepared to coating.

Also as gasket is insulating, did not interfere electrically with device. Finally, in order to promote composite polymerization, device is put in an oven for 4 h at a temperature of curing 80 °C. This temperature was chosen because precedent synthesis at 150 °C, gave breakdown device. All obtained sample are in Figure 86.



Figure 86: Several composite deposited on device; KAP.33 (A), KEV.33 (B); GO.33 (C) SIL.33 (D), Resine (E), bare die (F).

In order to evaluate composites behavior on device, infrared thermography analyzes were conducted for free-package (called DUT, device under test) and all coating devices. In particular, these analyzes were carried out in two steps. In the first, through 200000 scans per second, has recorded an heat map (Figure 87) of device subjected to a voltage pulse (10 V, 30 A) every 2.5 s. The time "dead" between a pulse and other, allowed DUT cooling to initial conditions. In fact, time necessary to complete cooling is only 16 msec.

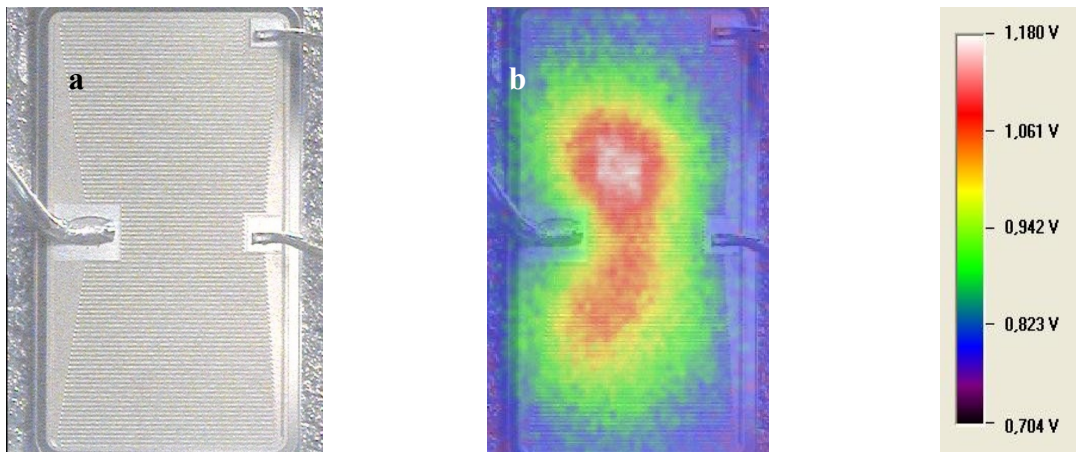


Figure 87: DUT in the absence of pulse (a); thermal map of DUT in presence of the pulse (b).

The obtained data from infrared thermography are reported below.

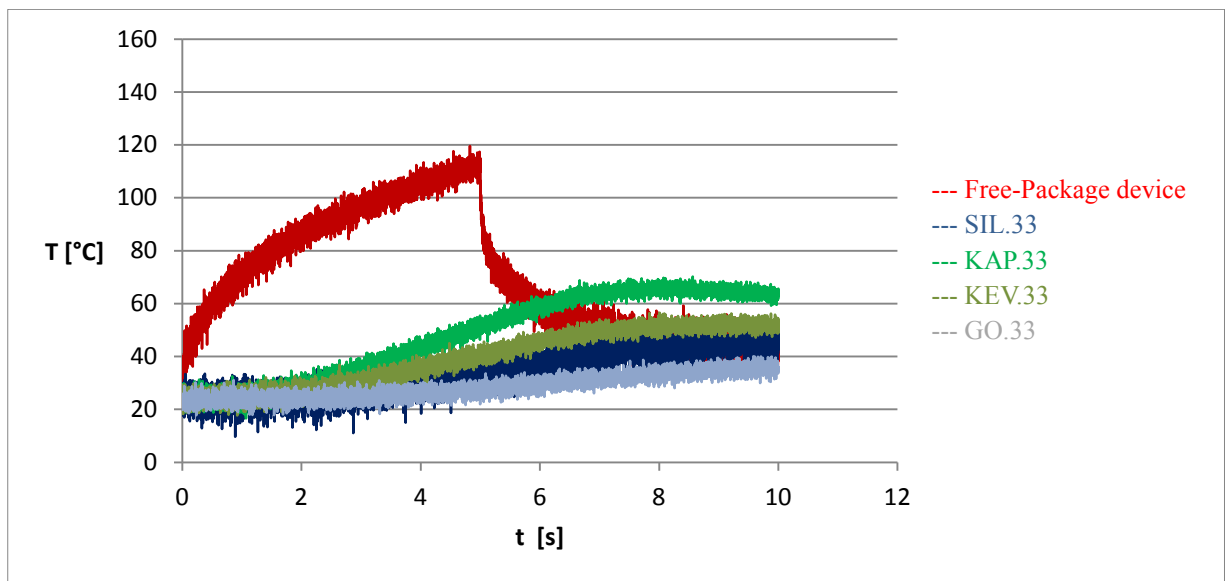


Figure 88: thermal temporal profiles of all analyzed composites

In Figure 88 reported the experimental curves obtained: it's possible to hypothesize that varying in maximum temperature values and the instant in time at which this value is reached, are a function of different thermal conductivity coefficient. In particular, as the coefficient of thermal conductivity, the temperature peak rises and the time instant in which it occurs is anticipated in time.

6. Conclusions and future perspectives

As devices evolve, it's necessary that also interconnections and all hardware circuits evolve, including packaging. Nowadays are required significant improvement in packaging properties: low resistance interconnections, less noise, less parasitic oscillations, increased reliability and improved thermal behavior.

For these purpose has designed a research activity for the synthesis of new materials capable to dissipating heat better in relation to the current ones. These materials, having to act both as a protective casing (eg. radiation, humidity) and as heat sinks, must also be equipped with a good thermal efficiency.

Thermal efficiency of a system depends on material degradation temperature and its thermal conductivity. Therefore, in the initial phase we proceeded with the investigation on the current materials used for commercial package characterizing their properties.

Particularly, thermogravimetric analysis allowed evaluation of filler percentage: from about 30% to 90% by weight; while FT-IR analysis revealed nature of polymeric matrix and that filler is silica, in fact was observed an intense and broad signal at 1106.94 cm^{-1} , due to Si-OH bond.¹⁰⁴

Later we moved to the synthesis of several epoxy resins and composites materials based on epoxy resin (as polymeric matrix) filled with synthetic or commercial techno-material to improve resin thermal efficiency.

These filler were chosen for their peculiar properties: aramides were chosen for their thermal stability and high thermal conductivity; polyimide has been chosen to solve the aramide hygroscopicity problems, graphene oxide and MoS₂ for their thermal conductivity.

Obtained composites are shown below (Table 29).

¹⁰⁴ R. M. Silverstein, F. X. Webster, D. J. Kiemle: "*Identificazione spettrometrica di composti organici*", CEA, 2006.

Table 29: Obtained composites based on epoxy resin

Composites	Filler (%)
1) NOM.10D	Poly(<i>m</i> -phenylen isophthalamide) (10 %)
2) NOM.10H	Poly(<i>m</i> -phenylen isophthalamide) (10 %)
3) NOM.10E	Poly(<i>m</i> -phenylen isophthalamide) (10 %)
4) NOM.33	Poly(<i>m</i> -phenylen isophthalamide) (33 %)
5) KEV.33	Poly(<i>p</i> -phenylen terephthalamide) (33%)
6) SIL.33	High Pressure Silica, diameter:0.04-0.63 μm (33%)
7) KAP.33	Poly(<i>p</i> -phenylen pyromellitimide) (33%)
8) GO.33	Graphenoxide (33%)
9) MO.33	Molybdenum disolphure (33%)
10) KEL.33	Kelin 130 ¹⁰⁵ (33%)

Some of obtained resins as is, showed, by DTA analysis, the presence of a glass transition (T_g). By making a comparison (figure 89) between DTA curves of composites having the same resins as polymeric matrix, and those of two resins for which it was previously observed a glass transition, it can be observed that filler determines, under the same polymerization conditions, the disappearance of glass transition. Therefore filler addition gives a structural improvement to final systems.

¹⁰⁵ Courtesy of “Spin Tech International s.r.l.” Via G. Galilei, 16 - 25030 Adro (BS) Italy.

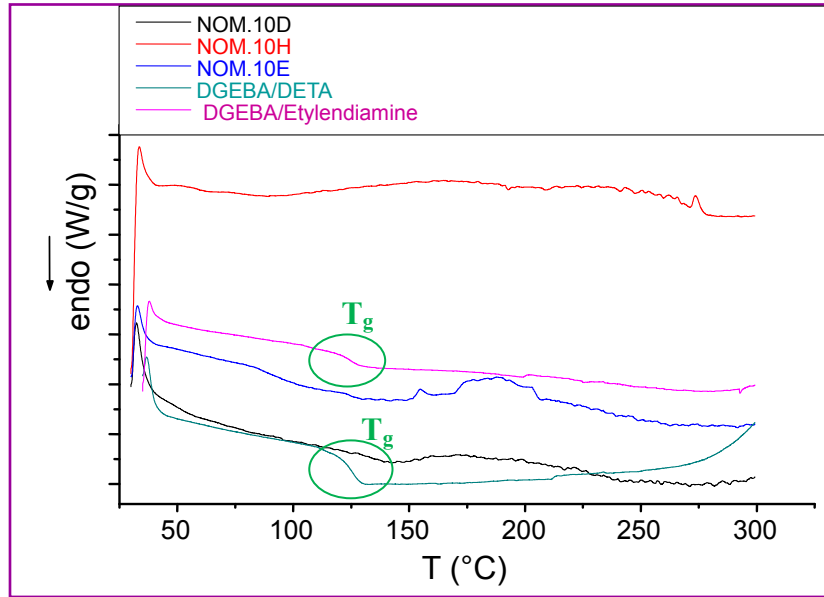


Figure 89: DTA curves of NOM.10 composites and two resins for which it was previously observed a glass transition

It was observed that also filler amount influenced, in a different way, thermal behavior of the final composites. Thermogravimetric data in Table 30 show as the presence of filler polymer, in air flow, lowers start degradation temperature if compared to resin as is; but with quantity of filler polymer increase from 10% to 33% by weight this temperature rises again.

Table 30: Thermogravimetric analysis relative to composites with different percentage of meta-aramidic filler, poly(*m*-phenylen isophthalamide) and resin alone

Samples	Atmosphere	T _{onset} (°C)	% Char
DGEBA/DETA	air	349,6	7,2
	N ₂	353	7,2
DGEBA/DETA/NOM.10	air	280,6	3
	N ₂	348,5	11
DGEBA/DETA/NOM.33	air	339,7	4,5
	N ₂	336	25,7
poly(<i>m</i> -phenylen isophthalamide)	air	530	0
	N ₂	434	31

In general, all obtained composites have a start degradation temperature, in air, higher than maximum reached by the latest generation devices ($250\text{ }^{\circ}\text{C}$)¹⁰⁶, this makes possible their use as microelectronic packaging.

Two methods for conductivity measurements were developed, direct and indirect; both were then verified by the application on some synthesized package.

In particular, indirect method has allowed to obtain thermal conductivity values by performing measurements of heat capacity by means of M-DSC calorimeter.

As can be seen data previously reported, almost all the composites obtained (with the exception of KEL.33), show a thermal conductivity higher than that of analyzed commercial package. In particular, KEV.33 showed the best behavior for purposes of this research. Both filler content in composites KEV.33 and KEL.33 are poly(*p*-phenylen terephthalamide), what differs them is their average molecular mass: the first is in oligomeric form, while the second is a commercial polymer. Probably the size of particles and/or macromolecules influence filler diffusion in the polymer matrix, interfering with the properties of the resin. It should also be noted that the Kelin 130 (filler of KEL.33) is as fiber and was difficult to make it into small parts.

Using the good thermal conductivity data of KEV.33, was made a FEM simulation of thermal transfer to a silicon chip enclosed within a package based on this composite, and placed on a circuit plate by means of pins. The chip is subject to a punctual internal heat source ($2 \times 10^8\text{ W/m}^3$) and is placed in the center of package and dissipating heat to the surrounding environment.

Simulations had shown that, when chip releases $2 \times 10^8\text{ W/m}^3$ power, it reaches a maximum temperature of $50\text{ }^{\circ}\text{C}$ if its package is made by common epoxy resin filled with about 70% of silica.

Vice versa, with a system where package material is KEV.33, it's possible to observe that chip does not exceed temperatures of $35\text{ }^{\circ}\text{C}$ (figure 90).

¹⁰⁶ www.st.com/st-web-ui/static/active/en/resource/technical/document/datasheet/DM00099968.pdf

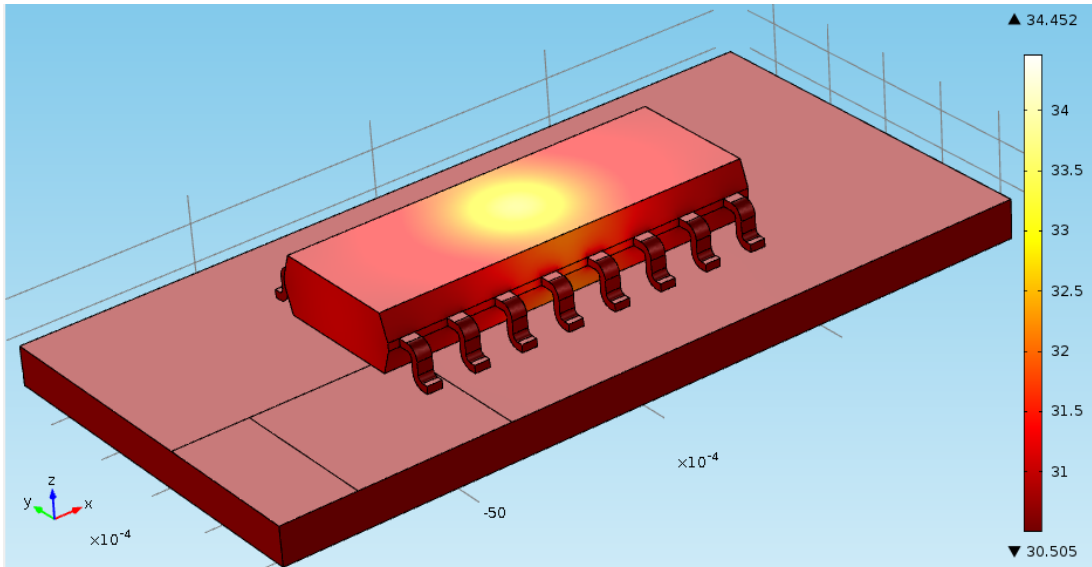


Figure 90: Simulation of thermal transfer of a device with package made of KEV.33 composite and having an internal punctual heat source equal to $2 \times 10^8 \text{ W/m}^3$

Whereas operation efficiency of a chip increases with decreasing temperature reached by it, the use of a package based on KEV.33 would also allow a considerable energy saving.

In order to evaluate composites thermal conductivity by means of a direct method, has been realized a measurement system composed of a temperature controller (Peltier cell) and an infrared microscope. Peltier cell is able to maintain temperature at a fixed value, a small portion of tested sample. In Figure 96 is shown system measurement: Peltier cell is in contact with the sample lower surface (approximately a quarter), maintaining it at $75 \text{ }^\circ\text{C}$.

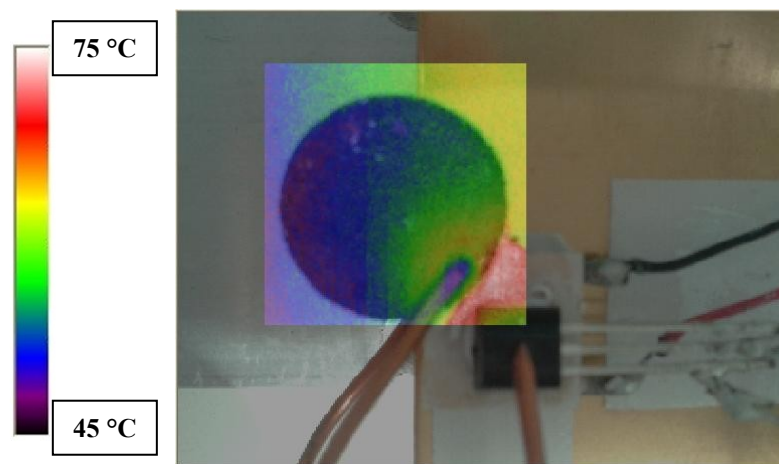
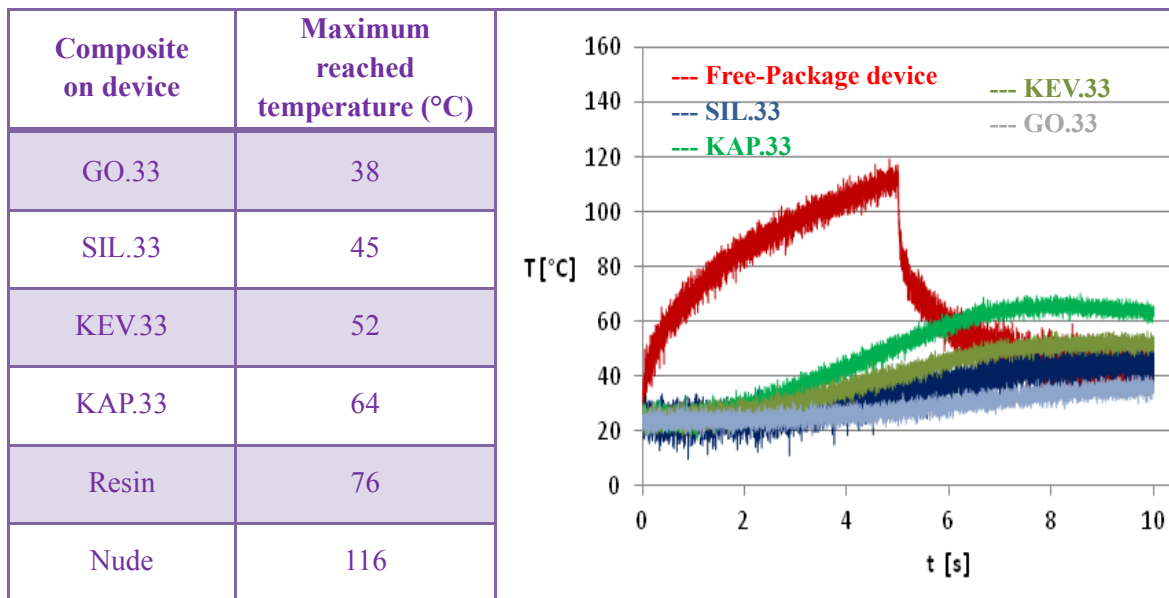


Figure 91: Test carried out on GO.33 composite

By means of FEM analysis was possible to obtain thermal conductivity.

In the end, it was considered interesting to understand what are the local temperatures reached in composite, when placed on devices in function. For these purposes, composites were synthesized directly on an electronic device, package-free; in particular it was a MOSFET. On this operating devices were carried on infrared thermography analyzes (data reported in Table 31) observing as, among the organic fillers, the polyimide shows better effect on the thermal conductivity of package, with respect to aramide filler, although both appear preferable to silica filler (currently used in commercial package).

Table 31: Data relative to infrared thermography



On the basis of collected data, almost all composites until now described, can be used as packaging having a better thermal efficiency than commercials. However, future perspective of this PhD work will see the synthesis of new composites using different fillers and / or in amounts varying percentages, also changing the curing agent. Also industrial polymers refuse could be used as fillers to lower production costs.

On composites thus obtained, may be made an evaluation of their thermal efficiency thanks to all assessment methods developed during the PhD work presented in this thesis.

Finally, prototypes obtainment, preliminarily presented here, will give a more real indications on the improved heat dissipation packaging.

Appendix

Instrumentation

Thermogravimetric Analysis (TGA)

Thermogravimetric analysis allows to observe materials degradation and sublimation processes, as a function of T. In this technique, sample weight is measured while it is subject to heating with controlled temperature growth. Heating can generate chemical modifications with bond breakings that usually produce volatile species.¹⁰⁷

Analysis can be carried out in nitrogen atmosphere, obtaining information on sample thermal stability, or in air, where occurs its thermo-oxidative degradation. Other information achievable by means of TGA concerns multicomponent systems or wet samples.¹⁰⁸

The instrumentation (figure 92a) is as follows:

- Analytical microbalance.
- Furnace, that can typically reach temperatures of 1500-2000 °C, is equipped with a thermocouple to monitor accurate measurements of the temperature.
- System purge gas.
- A reference sample placed in a separate chamber.
- Processor for instrument control, acquisition and data visualization.

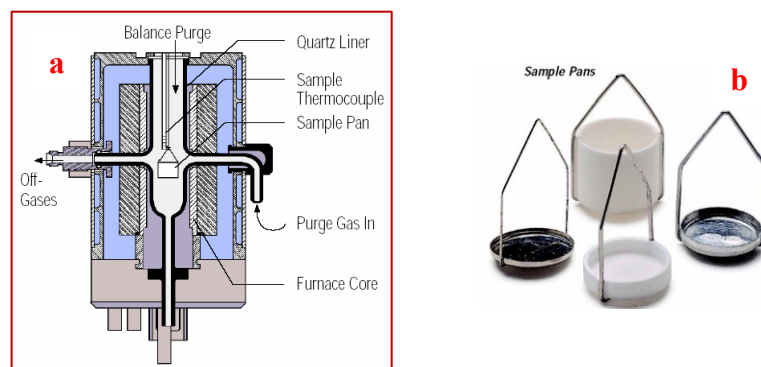


Figure 92: TGA strumentation (a) and crucibles (b)

¹⁰⁷ AIM, *Fondamenti di Scienza dei Polimeri*, Pacini Editore.

¹⁰⁸ A. W. Coats, J. P. Redfern: "Thermogravimetric Analysis: A Review", (1963), *Analyst* 88: 906–924.

Determination is carried out by placing the sample in a platinum (or ceramic) crucible (figure 97b), that is resistant to thermogravimetric temperatures. The balance is equipped with a platinum crucible-holder connected to the weight reading system by means of platinum wires.

When analyzed sample begins to lose weight, the instrument records this change and report it into a graph weight Vs temperature. This graph has a sigmoidal appearance and presenting an inflection point at a precise temperature, which corresponds to the maximum weight loss for the sample under examination. This maximum weight loss is more evident reporting the analysis as derivative Vs time (DTA curve); DTA curve allows to highlight processes with small changes in mass thus providing temperature at which the reaction has a maximum speed (PDT) and also allows to have more accurate values of start degradation temperature and weight loss at the end.¹⁰⁹

Experiments were carried on with a thermo balance TGA-7, Perkin Elmer (figure 93) in nitrogen or oxygen atmosphere (gas flow: 60ml/min); it measured a temperature range from 60 °C to 800 °C.

Calibration is carried out with paramagnetic samples, weighed with or without a magnetic field.



Figure 93: thermo balance TGA-7 (Perkin Elmer)

¹⁰⁹ A. W. Coats, J. P. Redfern: "*Thermogravimetric Analysis: A Review*",(1963), Analyst 88: 906–924.

FT-IR Spectroscopy

Fourier transform infrared spectroscopy is used to obtain infrared spectra of solid, liquid or gas samples. An FTIR spectrometer simultaneously collects spectral data in a wide spectral range, which provides higher performance because there is high availability of energy that results in a better signal/noise ratio than dispersive spectrometers.¹¹⁰ Furthermore the analysis time are significantly reduced. To convert collected data into the actual spectrum, is required Fourier Transform application.

Rather than shining a monochromatic beam of light at the sample (as in dispersive spectrometer), this technique shines a beam containing many frequencies of light at once, and measures how much of that beam is absorbed by the sample. Next, the beam is modified to contain a different combination of frequencies, by means of Michelson Interferometer (figure 94), giving a second data point. This process is repeated many times. Afterwards, a computer takes all these data and works backwards to infer what the absorption is at each wavelength.¹¹¹

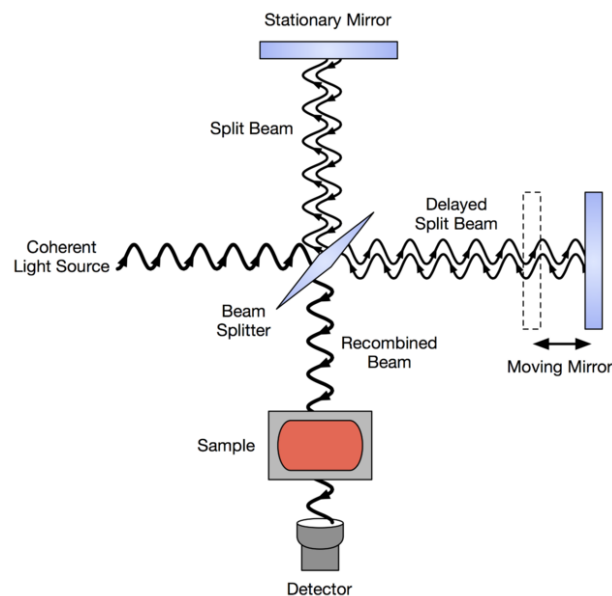


Figure 94: Schematic diagram of a Michelson interferometer, configured for FT-IR

¹¹⁰ P. Griffiths, J. A. de Hasseth: “Fourier Transform Infrared Spectrometry” (2007, 2nd ed.). Wiley-Blackwell.

¹¹¹ Banwell, C.N.; McCash, E.M. (1994). “Fundamentals of Molecular Spectroscopy” (4th ed.). McGraw-Hill.

When an infrared photon is absorbed by a molecule, this passes from its fundamental vibrational state to an excited vibrational state¹¹². A typical infrared spectrum reports Transmittance Vs Wavenumber (cm^{-1}) and can be divided into two different part: functional groups area ($3800\text{-}1300\text{ cm}^{-1}$) and fingerprints area ($1300\text{-}650\text{ cm}^{-1}$).

If analyzed sample isn't infrared transparent, absorption phenomena will occur, generating transitions between vibrational energy levels: the recorded spectrum will be characterized by a series of peaks, each one related to a transition. By means of FT-IR, it's possible to analyze both solid and liquid samples. Particularly, solid samples can be analyzed if reduced in film, or powdered and analyzed in nujol suspension or in KBr tablet.

Liquid samples are placed between two NaCl tablets, while gas sample into cylindrical cells having IR-transparent windows.

IR spectra reported in this PhD thesis, have been carried out using SPECTRUM ONE FT-IR, Perkin Elmer (figure 95). All samples were analyzed by means of KBr tablets, prepared under 5-7 ton pressure.



Figure 95: SPECTRUM ONE FT-IR, Perkin Elmer

The Perkin-Elmer Spectrum One FTIR Spectrometer is capable of data collection over a wavenumber range of $370\text{-}7800\text{ cm}^{-1}$. It can be configured to run in single-beam, ratio, or interferogram modes. The best resolution is 0.5 cm^{-1} . A mid-range Deuterated triglycine sulfate infrared detector processes signals with a 68340 integrated chip. The

¹¹² Douglas A. Skoog, James J. Leary, "*Chimica analitica strumentale*", EdiSES, 1995.

sample compartment is purgeable. Instrument are interfaced to Perkin Elmer Spectrum software, which gives the user the ability to extract both qualitative and quantitative data from the spectrum, and generate custom reports.¹¹³

MALDI-TOF Mass Spectrometry

In mass spectrometry¹¹⁴ the samples analyzed are converted into gaseous ions having high mobility, and then separated according to their mass/charge ratio.

The components of a typical mass spectrometer (Figure 96) are essentially five:

- an introduction system that allows to insert into spectrometer a very small amount of sample (ng) and, if necessary, also its volatilization;
- an ion source that converts sample into positive or negative ions by means of bombardment with photons, electrons, ions or molecules;
- a mass analyzer that disperses the ion beam as a function of the relationship m/z ;
- a detector which converts the ion beam into an electrical signal;
- a high vacuum system that maintains a very low pressure values (from 10^{-4} to 10^{-9} torr) avoiding interference between sample ions and residual air.

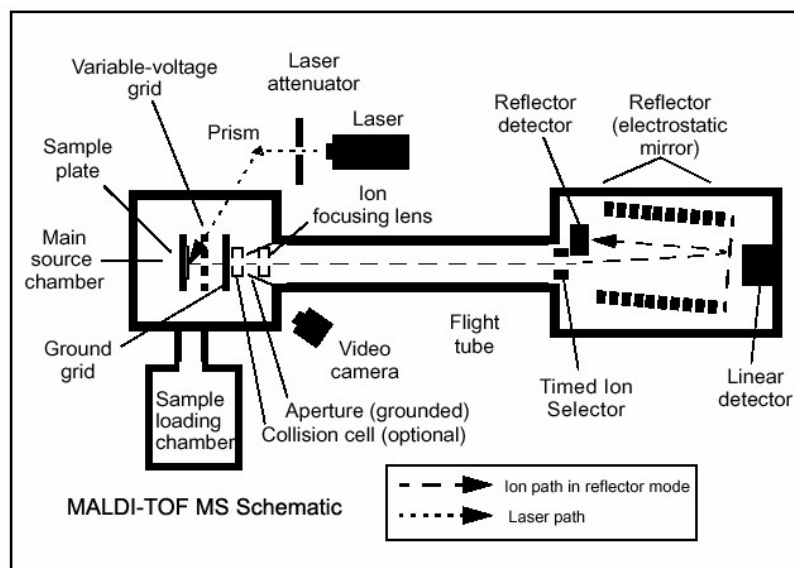


Figure 96: Typical MALDI-TOF components

¹¹³ www.perkinhelmer.com

¹¹⁴ Robert M. Silverstein, Francis X. Webster, David Kiemle, David L. Bryce : "Spectrometric Identification of Organic Compounds", 8th Edition, Wiley, 2014.

All the components are divided into further classes making unique the function of commercial mass spectrometers. The most important distinction concerns the type of source used for ions formation.

There are two different type of source¹¹⁵:

- ✓ "Hard", which provide high energy to generate ions accompanied by a high number of fragmentations, allows structural characterizations of the test compound.
- ✓ "Soft", which produce electronic excitation low enough not to generate any fragmentation allow an easy molecular weight determination of various compounds in a mixture. This kind of source includes MALDI.

MALDI-TOF (Matrix Assisted Laser Desorption/Ionization-Time of Flight) Mass Spectrometry was developed in the nineties by K. Tanaka¹¹⁶ and a few months later by M. Karas¹¹⁷.

The MALDI-TOF mass spectrometer has a source in soft desorption: without previous sample volatilization, that passes so directly from the condensed phase to the vapor phase as ionic species by means of a pulsed laser beam (with a specific λ).

Matrix has a very high ε at laser wavelengths: in fact it absorbs energy, desorbs and transfers energy to analyte which is thus ionized. Matrix/analyte molar ratio vary from 1: 50 to 1: 500, generally amount of analyte is in *pm*.

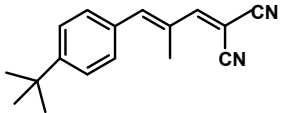
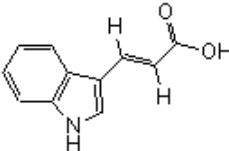
Matrix employed in present work are tabulated in table 32.

¹¹⁵ Skoog, D. A.; Leary, J. J.: "*Principles of Instrumental Analysis*", Saunders College Pub., 1992.

¹¹⁶ K. Tanaka, Y. Ido, S. Akita, Y. Yoshida, T. Yoshida, "*Proc. Second Japan-China Joint Symposium on Mass Spectrometry*". Editors H. Matsuda and L. Xiao-tian, Osaka, Japan, 1987, p. 185.

¹¹⁷ M. Karas, F. Hillenkamp, "*Laser desorption ionization of proteins with molecular masses exceeding 10,000 daltons*", *Anal. Chem.*, 60, 2299 (1988).

Table 32 : employed matrix for MALDI-TOF analysis¹¹⁸

Abbreviation	Name and Molecular Formula	Empirical Formula	MW
DCTB	2-[(2 E)-3-(4- <i>tert</i> -butylphenyl)-2-methylprop-2-enylidene] malonitrile	C ₁₇ H ₁₈ N ₂	250.35
			
IAA	3-Indoleacrylic acid	C ₁₁ H ₉ NO ₂	187.195
			

Matrix, generally, is mixed to analyte following a particular method:

- **Dried-Droplet Method:** sample and matrix are pre-mixed in solution in a microtube, deposited on the "Sample plate" and dried;
- **Thin Layer Method:** matrix is previously deposited on "Sample plate" and dried, then sample solution is deposited on the thin film matrix and dried;
- **Sandwich Method:** matrix solution is deposited on "Sample plate" and to dried, then is added sample solution and matrix again.

Sample-plates are dimples located on a metal plate, called repeller (figure 97) because during ionization has the same charge of sample ionized.

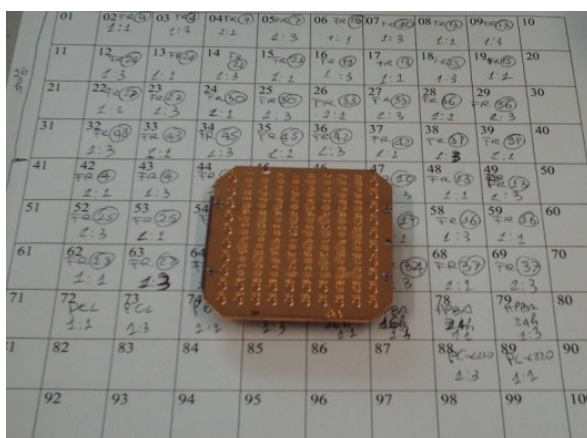


Figure 97: repeller having 100 dimples

¹¹⁸ R. M. Silverstein, F. X. Webster, D. J. Kiemle: "Identificazione spettrometrica di composti organici", CEA, 2006.

Analyzer is TOF (time of flight): it is constituted by a high vacuum tube ($10^{-7} \div 10^{-8}$ Torr) connected to MALDI source and to detector. The ions produced by the source are accelerated by an electric field of about 10^4 V and sent in this tube (1m long), in which electric field is zero; ions kinetic energy depends on acceleration potential: ions will move with different speeds in function of their mass. Unfortunately, because Maxwell-Boltzmann speed distribution, ions having the same mass can arrive at detector with different times. To solve this problems have been developed specific devices time-lag focusing:

- * **Delayed extraction**, is the application of a delay time (50-1000 ns) between the laser pulse and the instant at which acceleration potential is turned on: in this period the collision between the various ions creates an energy distribution more homogeneous.
- * **Reflectron** is constituted by plates having a growing ddp of the ions same sign: in this way, ion faster will cross larger space than ion slower with the result to correct differences

Particularly, Voyager DE-STR (PerSeptive Biosystem) MALDI-TOF spectrometer was used to analyzed some obtained compounds. This Spectrometer nitrogen laser source had a 337nm wavelength, a 3ns impulse and a 500 MHz ADC. Two different method were used to prepare samples: a phase liquid method and phase solid method too (REG method¹¹⁹) using two different matrix such as trans-Indole-3-acrylic acid (IAA) and trans-2[3-(4-tert-Butylphenyl)-2-methyl-2-propenylidene]-malononitrile (DCTB). The ratio matrix/analyte was 25:1. Furthermore, two different acquisition methods were used; CDXM method, for low mass, and ARRAY method for higher mass.^{120 121} For instrument calibration have been used appropriate standards prepared and characterized by work group lab, where these PhD took place.¹²²

¹¹⁹ Anthony P. Gies, William K. Nonidez: “A Technique for Obtaining Matrix-Assisted Laser Desorption/Ionization Time-of-Flight Mass Spectra of Poorly Soluble and Insoluble Aromatic Polyamides”, Anal. Chem.2004,76,1991-1997

¹²⁰ D. Vitalini, P. Mineo, E. Scamporrino. *Macromolecules* 1997, 30, 5285–5289.

¹²¹ E. Scamporrino, P. Maravigna, D. Vitalini, P. Mineo. *Rapid Commun. Mass Spectrom.*1998,12, 646–650

¹²² G. Montaudo, P. Mineo, E. Scamporrino, D. Vitalini, *Rapid Communication in Mass Spectrometry*, 1996, 10, 1551-1559.

Differential Thermal Analysis (DTA)

Differential Thermal Analysis allows to carry out evaluations of first and second order thermal transitions: Glass Transition Temperature, Melting Point, Cold Crystallization Temperature. In particular, knowing sample mass, by means heat flow differences between this and a reference, as the temperature increases, it's possible to evaluate endothermic or exothermic processes that take place.

The result of DTA analysis is a graph, which shows the speed of the heat flow (dQ/dT) as a function of T. It's possible to observe¹²³:

- ◆ glass transition (T_g) temperature of semicrystalline or amorphous materials and therefore their C_p (specific heat). Thermogram is an endothermic sigmoidal curve (figure 98, a);
- ◆ For semi-crystalline materials, as well as a glass transition, will be present typically crystalline materials processes: melting, evaporation, sublimation that give endothermic curves (figure 98, b); while crystallization and condensation give exothermic curves (figure 98, c); it's also possible to determine latent heat of these processes (λ).
- ◆ chemical reactions ΔH ;
- ◆ Assessment materials purity of the under examination.

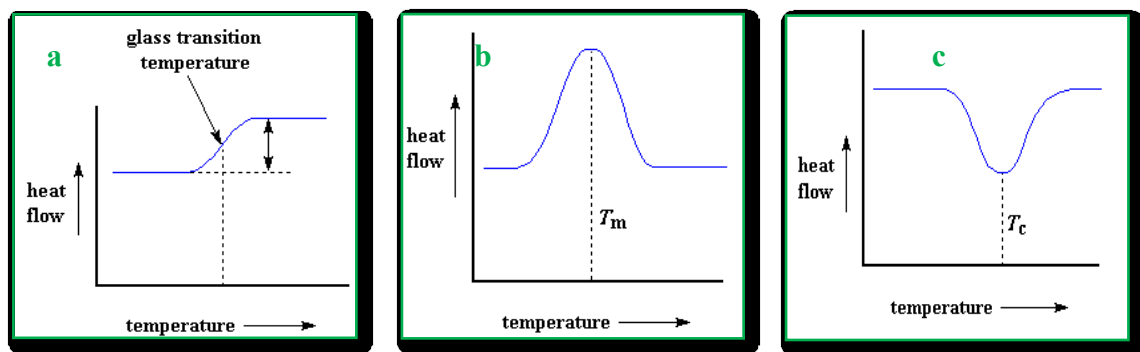


Figure 98: DTA event, Glass Transition (a), endothermic event (b), exothermic event (c)

DTA instrument records the difference between sample and reference heat flows, by means of thermocouples placed under samples, both in the same oven. For DTA determinations, samples are placed in an aluminum pan and then injected into instrument. Generally, experiments are carry on under nitrogen atmosphere.

¹²³ H.K.Bhadeshia: "Thermal analyses techniques. Differential thermal analysis". University of Cambridge, Material Science and Metallurgy

Nowadays there are calorimeters that allow determinations on a wide range of temperature: $-90\text{ }^{\circ}\text{C}$ to $500\text{ }^{\circ}\text{C}$.

DTA calorimeter, used in this PhD work, was Mettler TA3000 TC11 (figure 99).

Instrument calibration was carry on by using standard Indium.



Figure 99: Mettler TA3000 TC11 calorimeter

NMR Spectroscopy

NMR spectroscopy is based on the consideration that atom nucleus are, such as electrons, rotating particles and cause their positively charge, have an angular momentum p and also a magnetic moment μ : $\mu = \gamma \cdot p$, where γ is gyro-magnetic ratio and

$$p = \frac{h}{2\pi} I$$

In NMR spectroscopy atom nucleus most analyzed are those having $I = 1/2$ as the ^1H and ^{13}C . When these atom are immersed in a magnetic field, they have two possible orientations $m = -1/2; +1/2$ (figure 100).¹²⁴

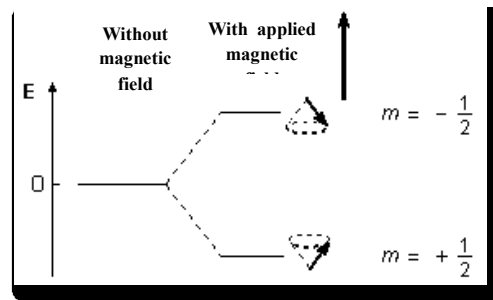


Figure 100: Energy states in absence or presence of a magnetic field

Energy gap between the levels increase proportionally to B_0 . There is a population prevalence for the state at low energy, which causes a magnetization vector \vec{M}_0 directed along \vec{z} axis (figure 101a). After that a transmitter gives a pulse of radiofrequency at 90° , magnetization vector \vec{M}_z moves on \vec{xy} plane, and subsequently tends to return to its initial position, in a relaxation time t , by a “spiral-like” movement (figure 101b).

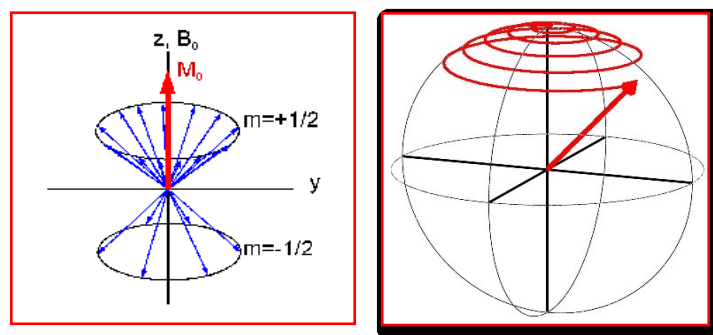


Figure 101: magnetization vector (a) and its movement during relaxation time

¹²⁴ AAVV. *Nuclear magnetic resonance imaging-Technology for the 21st century*, Oilfield Review, 1995.

When radiofrequency transmitter is turned off, the receiver (coaxial to \vec{y} axis) begins to acquire the signal that, at the end, will be a complex decay curve (FID = Free Induction Decay, figure 102) in time domain; subsequently Fourier transform application allows to obtain the signals in frequency domain, ie the NMR spectrum.

NMR spectrum shows intensity Vs frequency, expressed in ppm or δ (Chemical Shift, 0-12ppm for ^1H -NMR). Zero value is assigned to TMS (tetra-methyl silane).

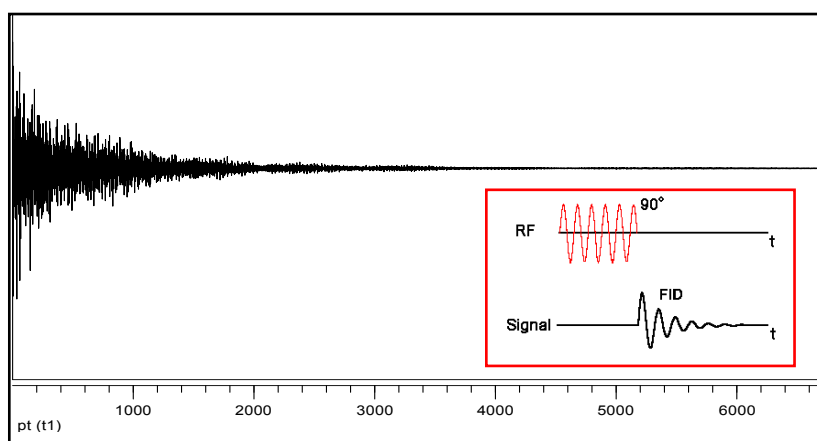


Figure 102: Free Induction Decay (FID) curve

^1H -NMR spectrum shows several factors that allow the analysis of the sample tested: the number of groups of signals (singlet or multiplet) constituting the spectrum, represent number of equivalent protons groups (having the same chemical environment); the position or chemical-shift of these lines suggest functional group to which that equivalent proton group could belong; the area under the peaks is an index of relative abundance of equivalent protons; the number of signals belonging to each multiplet gives information about number of adjacent protons to those determined by the signal itself.¹²⁵

Magnetic fields are generated by an electric current that runs in the wire loop of a superconductor, maintained at the temperature of liquid helium (4 K). Sample (about 7mg for ^1H -NMR and 20 mg for ^{13}C -NMR), dissolved in a deuterated solvent, is inserted in a glass NMR tube up to a volume of about 500-700 μL ; the tube is inserted into *probe* inside the instrument (figure 103) and interacts with the radio-frequencies

¹²⁵ R. M. Silverstein, F. X. Webster, D. J. Kiemle: “*Identificazione spettrometrica di composti organici*”, CEA, 2006.

and with magnetic field generated by the solenoid, placed into liquid He Dewar vessel, placed in a second Dewar containing liquid N₂ (77 K).

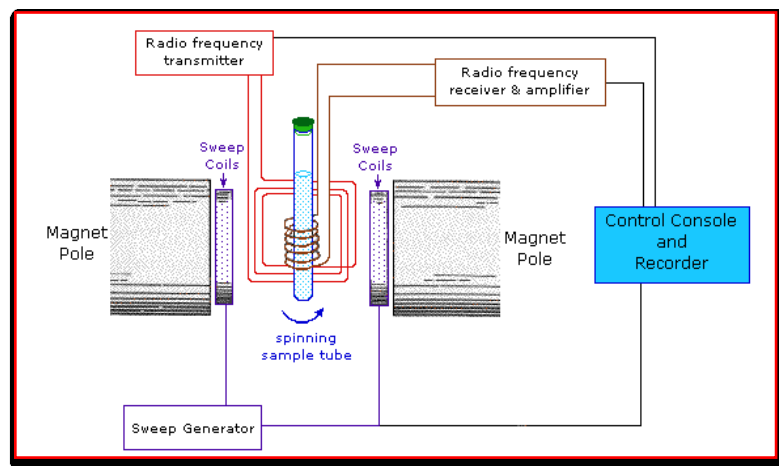


Figure 103: NMR spectrometer components

Said “one-dimensional” NMR spectrum, or 1D-NMR, is a graph of intensity Vs frequency (ν). It is also possible to implement NMR spectra in which the intensity is a function of two frequencies (indicated with ν_1 & ν_2 or, often, F1 and F2), called “two-dimensional” NMR, or 2D-NMR. In a 2D spectrum, correlation peaks appear as concentric circles having as coordinates Chemical-Shift of correlated atoms.

When 2D NMR spectrum report the same nucleus, it is said homonuclear: ¹H-¹H COSY and ROESY are typical homonuclear experiments. In these experiments there are peaks of correlation to F1 = F2, called diagonal (red and blue signals in figure104); peaks outside of diagonal peaks are called cross peaks (yellow signals).¹²⁶

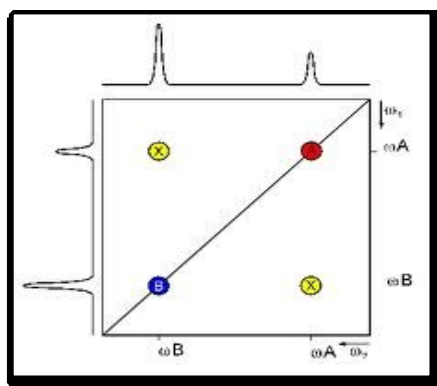


Figure 104: 2D-NMR spectrum

¹²⁶ G. E. Martin, A. S. Zekter,; “Two-Dimensional NMR Methods for Establishing Molecular Connectivity”. New York: VCH Publishers, Inc. (1988) p. 59.

Instrument acquires a series of one-dimensional experiments different from each other for the *time of evolution*, which is the time between sending the pulse and the start of FID acquisition, thus generating a second time-variable. Applying Fourier Transform in these experiments the two time variables are so converted in two variables of frequency which, with the third dimension that is signals intensity, they give three-dimensional peak (*stacked plot*, figure 105).

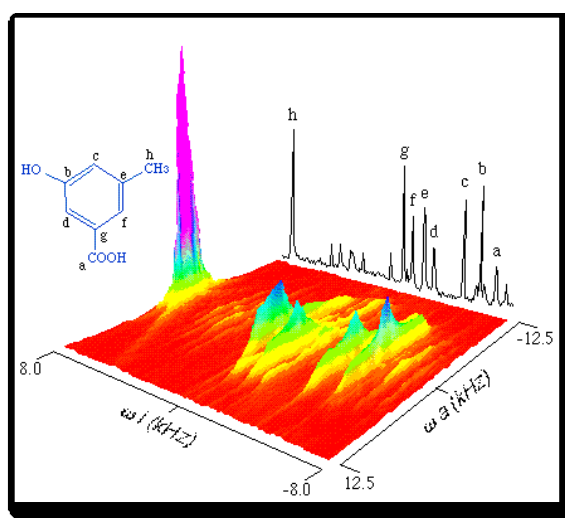


Figure 105: Stacked plot

Spectrum thus obtained can be presented in the form of two-dimensional map (*contour plot*), obtained by stacked plot sections at different heights.¹²⁷

NMR spectra reported in this PhD work, were recorded at 500 MHz on a Varian UNITY INOVA Spectrometer. The solutions were made with different solvents: CD₂Cl₂ 99.5Atom% D (Merk); Dimethylsulphoxide-d₆ 99.9Atom% D (Merk) and were placed in tubes Norell 5 mm (model S-5-400-7) and the spectra recorded at 323 K and 370 K, respectively. The chemical shifts are expressed in ppm using as calibrating the residual signal of the deuterated solvent. The two-dimensional COSY and ROESY experiments were acquired using Varian standard pulse sequences.

¹²⁷ Nakanishi, Koji: “*One-dimensional and two-dimensional NMR Spectra by Modern Pulse Techniques*”. Mill Valley, California: University Science Books (1990).

Modulated Differential Scanning Calorimeter (M-DSC)

DSC analysis, generally, uses isothermal conditions or a constant temperature change over entire measurement range. In these conditions, interpretation or energy quantification of some transformations is complex. To overcome these limitations, it's possible use thermal analysis techniques in which, overlapped on classic temperature profile, there is a variation in function of time. Principal difference between classic DSC and Modulated-DSC¹²⁸ is a modulated temperature profile overlapped on linear temperature variation (Figure 106), with a consequent continuous variation of instantaneous heating speed.

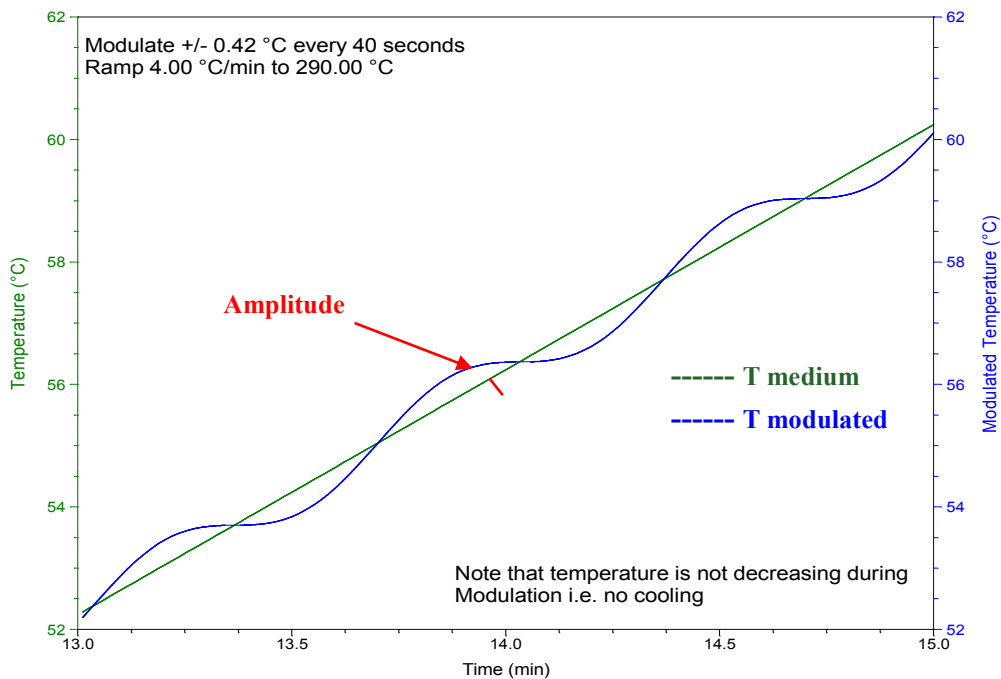


Figure 106: Medium and modulated temperature profiles

This allows to identify several contributes to heat flux: phenomena function of heating rate variation or C_p ("reversing" signal - the first term of Equation 9). Difference between total heat flux at constant speed heating and "reversing", it's possible to separate the contribution of phenomena that are not specific heat (C_p) function ("not reversing" signal - the second term in equation 10).

$$dH / dt = C_p (dt / dt) + f(T, t) \quad \text{Equation 9}$$

¹²⁸ TA-Instrument: "Thermal Analysis Review Modulated DSCTM Theory", available at http://www.eng.uc.edu/~beaucag/Classes/Characterization/ModulatedDSC_TAinst.pdf

In particular the dH/dt is relative to the total heat flow, relative to all thermal events. $C_p (dt/dt)$, relative to the "reversing" signal, takes into account heat capacity C_p , glass transition and melting. The last term of Equation 9, belong to "non-reversing" signal, regards events such as evaporation, crystallization, curing, denaturation, decomposition and fusion. In addition, with signals deconvolution it's possible the distinction of processes that normally occur in the same temperature range, for example, the glass transitions and the fusions are typically a function of the C_p .

Calorimeter used for heat capacity measurement during this PhD work, was M-DSC Q20 TA Instruments (figure 107). Calibration was carried out by means of indium and sapphire standards.



Figure 107: M-DSC Q20 TA Instruments

Infrared thermography

There is a direct correlation between body temperature and diseases. Infrared (IR) thermography is a non-contact and non-intrusive temperature analysis approach, with the important advantage of no alteration in the surface temperature and the capability of a real-time measure of the surface temperature distribution¹²⁹.

This kind of Thermography uses the physical principle that each body having a temperature above the absolute zero emits energy in the form of electromagnetic radiation in frequencies ranging in the infrared spectrum region, not visible for human eyes. The blackbody theory establishes that when it is in a thermal equilibrium, it radiates according to the Plank's law (figure 108) and the spectrum is determined only by the temperature.

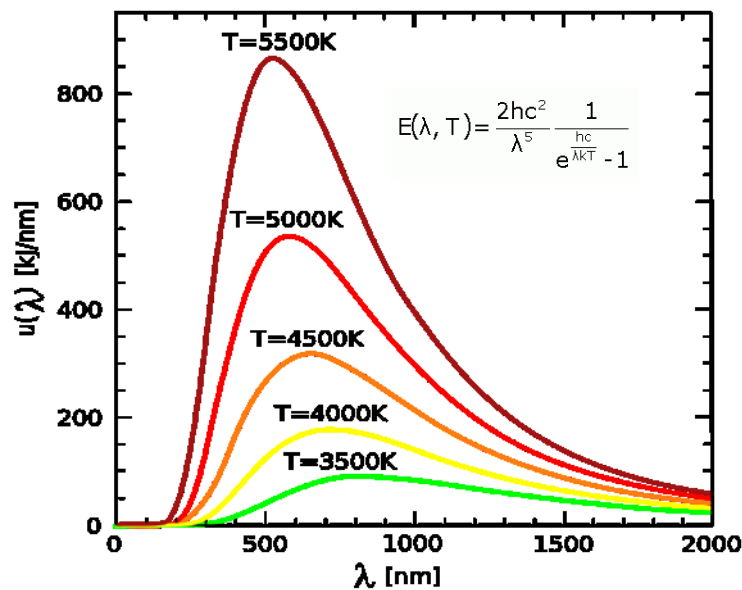


Figure 108: distribution of the curves related to the radiation emitted by a blackbody

As regards the spectral radiation intensity, the value of the overall radiation emitted by the body is given by the Stefan Boltzmann's correlation: $q = \sigma \times T^4$, where q is the thermal emittance, T the absolute temperature and σ is the Stefan-Boltzmann constant. Through this formula, the technique gives the possibility to obtain thermal images from infrared radiations in a non-invasive way. The radiation emitted by the sample is revealed by optical sensors, which employ a photocell in order to convert the infrared emission in electric signals (which in turn are amplified and sent to a monitor).

¹²⁹ J Med Phys. 2009 Jan-Mar; 34(1): 43–47

Obviously, the camera must be sensitive to the infrared radiations and so it is important to choose them in agreement with the temperatures that are expected from the tested materials. There are many different kind of thermocamera, depending on the sensor employed in order to reveal the radiation: it is possible to distinguish between photovoltaic quantum detectors and photoconductors ones.

Therefore, if the user wants to perform the analysis of fast thermal transients, he needs an enhancement of the temporal resolution of the measuring setup. This improving can be reached by means of the “scanning mode” thermal imaging. In this case, a single sensor is employed but the entire image is not acquired at the same time. The detector analyzes a smaller area and collect each point of the image separately and the thermal map is the result of the convolution of each point of the image separately.

The signal coming from every point of the analyzed surface is processed by a computer and then registered. The elaboration of all the collected enables the operator to achieve the alteration of the scanned spot temperature and finally the overall thermal map for each analyzed time.

Nevertheless, the captured images is affected by a contrast due to the different emissivity value of each tested point in addition to different intensity of the radiation coming from every one of them. Indeed, the emissivity is a properties depending on the nature of the species and since that the surface of the tested materials is generally constituted of different, this characteristic may be different for different points¹³⁰.

Figure 109 is a picture of measurement system used in this PhD work with the aim of obtaining infrared thermal characterization of different composites materials. The temperature is calculated simply by analyzing the electromagnetic radiation coming from the surface of the sample while it is dissipating power.

¹³⁰ Energy and Buildings 35 (2003) 663–667

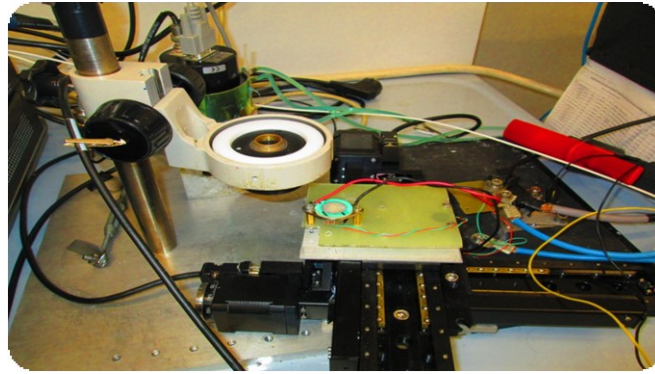


Figure 109: measurements system

These instruments are applied in power electronics, in order to study the capability of the integrated circuits of supporting thermal stresses due to the strong electric pulses. In this thesis it is discussed the effect of different composite constituent package of devices warmed with an electric pulse.

The equipment is made of the following element:

- * a 2D mechanical displacement system,
- * a wide optical bandwidth reflective objective,
- * an infrared optical,
- * an acquisition board; it generates the driving signal for the stepper motors, the power pulses supplied to the devices under test and the acquisition of the signals coming from the optical detector,
- * a proper software code that collects or produces the signals listed above, acquiring and saving the data and the synchronizing all the needed activities for the correct running of the instrument,
- * a temperature check apparatus built in the sample-holder,
- * a software that makes the thermal maps and reconstructs the films.

The displacement system is made of two fixed mechanized legs that allow moving the sample on a two-dimensional grid performing a linear translation up to 12 mm .These stages are coupled with two stepper motors. The lateral resolution of the obtained thermal maps is associated with the minimum translation that the motors can perform. The stepper motors employed in are the KP4M4-001.

Communications in Congress

4th EuChems Chemistry Congress

August 26-30, 2012,

Prague

P. Mineo, E. Scamporrino, F. Spitaleri*: *“Synthesis of nano-clip and nano-box compounds having free base porphyrins as wall”*

p 1060

XXXIV Convegno Nazionale Divisione di Chimica Organica

Pavia, 10-14

Settembre 2012

E. Scamporrino, P. Mineo, F. Spitaleri*, S. Dattilo, E. Spina, D.Vitalini: *“Copolyacrylates containing porphyrin units as pendant groups: synthesis, characterization and their use as sensors”* p 159

European Polymer Congress EPF2013

June 16-21, 2013,

Pisa

P. Mineo, F. Spitaleri*, E. Scamporrino, *“Synthesis and characterization of Composites for High Power Electronic Packaging”* P5-31

P. Mineo, F. Spitaleri*, E. Scamporrino: *“A Water Soluble Macromolecular Nanobox Having Porphyrinic Walls as a Large Host for Giant Guests”*. P3-105

The Italian meeting on Porphyrins and Phthaloyanines

Roma, 1-3 Luglio 2013

P. Mineo, F. Spitaleri*, E. Scamporrino: *“Macromolecular probe based on non-ionic water soluble porphyrines: suitable tools in molecular recognition”* p 19

Publications

Placido Mineo, Fabiola Spitaleri*, Emilio Scamporrino: *“A Water Soluble Macromolecular Nano-Box having Porphyrinic Walls as a Large Host for Giant Guests”*, Journal of Polymer Science, part A: Polymer Chemistry 2013, 51, 1428–1435

Research products

Placido Mineo, Barbera Vincenzina, Giovanni Romeo, Fabrizia Ghezzi, Emilio Scamporrino, Fabiola Spitaleri* and Ugo Chiacchio: “*Thermally reversible highly cross-linked polymeric materials based on furan/maleimide Diels-Alder adducts*”, Journal of Polymer Science, part A: Polymer Chemistry, Submitted.

Placido Mineo, Fabiola Spitaleri*, Salvatore Patanè, and Emilio Scamporrino: “*Synthesis and characterization of Organic Composites for High-Power Microelectronic Devices Packaging*”.

Manuscript in preparation, to be submitted to Journal of Polymer Science Part A: Polymer Chemistry

Acknowledgment in papers

Placido Mineo, Norberto Micali, Valentina Villari, Maria Grazia Donato, Emilio Scamporrino: “*Reading of Protein Surfaces in the Native State at Micromolar Concentrations by a Chirogenetic Porphyrin Probe*” Chem. Eur. J.2012, 18, 12452 – 12457

Acknowledgments

*Signore Dio Amore,
Ti rendo grazie perché
hai sempre voluto porre accanto a me splendide persone,
con cui condividere la Vita in ogni sua sfaccettatura:*

*Marco, per l'Amore Infinito condiviso, da sempre e per sempre,
dal quale è nata il nostro gioiello: la mia piccola Amata.*

*Mamma e Papà,
Dario e Noemi,
per i Valori che ho in cuore e che ci legano indissolubilmente.*

*Il Prof. Mineo,
per la passione per la Scienza, che sapientemente ha saputo arricchire in me,
e perché mi ha accompagnata, essendo un riferimento costante, in tanti anni di crescita
professionale.*

*Carolina, ,Giusy,
Nadia, Ylenia,
Salvuccia, Valentina,
Davide, Renato,
per l'Amicizia Infinita che ci lega.*

*Simona, Stefania,
Valentina e Sofia,
per tutto il Bene che ci vogliamo.*

*Collegghi/amici "dottorandi"
Collegghi/amici di laboratorio,
per aver condiviso molto di quest'avventura.*

*Tutte le persone che amo, e quelle che ho perso di vista, lungo la strada...
per l'amore fraterno che ci legherà sempre.*

Grazie Dio Amore, per ognuno di loro, preziosissimo ai tuoi occhi, ed anche ai miei...

Fabiola

